# A review on recent advances and trends in symmetrical electrodes for solid oxide cells

Javier Zamudio-García[1,*], Leire Caizán-Juanarena[2], José M. Porras-Vázquez[1], Enrique R. Losilla[1], David Marrero-López[2,*]

[1] Universidad de Málaga, Dpto. de Química Inorgánica, Cristalografía y Mineralogía, 29071-Málaga, Spain.

[2] Universidad de Málaga, Dpto. de Física Aplicada I, 29071-Málaga, Spain.

**Keywords:** solid oxide cells; symmetrical electrodes; perovskite; exsolution; $CO_2$ electroreduction; electrolysis cell

**Abstract**

Symmetrical solid oxide cells (SSOCs) with identical air and fuel electrodes have gained significant scientific interest in the last decade because they offer several advantages over conventional cell configurations. Among other features, simpler fabrication, better chemical and thermo-mechanical compatibility between cell layers, and electrode reversibility, make them attractive for electricity generation, $H_2$ production and $CO_2$ electroreduction. This review offers an overview of the most recent advances in the field of SSOCs, paying special attention to the relationship between electrode composition, crystal structure and properties. With that aim, symmetrical electrodes are classified in four groups according to their redox stability, i.e. single phases, composites, electrodes with exsolved metal particles and those that suffer a drastic phase transformation under reducing conditions, known in the literature as quasi-symmetrical electrodes. Furthermore, an outlook of other cell configurations with increased scientific interest are also discussed, i.e. symmetrical protonic fuel cells (H-SSOCs) and solid electrolyzers for $CO_2$ electroreduction. With this overview in mind, the authors would like to highlight the challenge ahead of finding electrode materials that optimally work under both oxidizing and reducing conditions in terms of redox stability and electrochemical properties, and further conclude on the future development of SSOCs.

* Corresponding author.
E-mail address: marrero@uma.es (David Marrero-López); zamudio@uma.es (Javier Zamudio-García)
Current address: Dpto. de Física Aplicada I, Facultad de Ciencias, Campus de Teatinos, Universidad de Málaga, 29071-Málaga, Spain.
Tel: +34 952137057, Fax: +34 952132382

## Contents

## 1. Introduction

Given the need for clean and renewable energy sources, new technologies are being explored to substitute conventional fuel combustion processes with low energy conversion efficiencies as well as to reduce the emission of greenhouse gases that are harmful to the environment [1,2]. In this context, fuel cells are a promising technology for fuel-to-power conversion with an efficiency up to 80% and a low carbon footprint [3–5]. Among the different fuel cells, solid oxide fuel cells (SOFCs) are among the most promising ones due to their capability of working with a wide variety of fuels, including hydrogen, natural gas, coal gas and other renewable fuels (*e.g.* methanol, ethanol and CO) [6–8]. In addition, SOFCs can operate in reverse mode as Solid Oxide Electrolysis Cell (SOEC) to produce hydrogen gas from renewable energy sources.

The main components of a Solid Oxide Cell (SOC) are: (i) the air electrode (oxidizing atmosphere) for the oxygen reduction reaction (ORR) and oxygen evolution reaction (OER); (ii) the fuel electrode (reducing atmosphere) for the hydrogen oxidation reaction (HOR) and hydrogen evolution reaction (HER); and (iii) the electrolyte through which oxide ions or protons are transported. Since research on SOCs started in the early 1980s, most of the focus has been put on the synthesis and characterization of new materials that can be used as any of the aforementioned cell components [9–12]. The most commonly used fuel electrode material is a composite made of a mixture of NiO and YSZ (yttria-stabilized zirconia) powders, which under reducing conditions form a Ni-YSZ cermet, showing excellent catalytic activity, mixed ionic-electronic conductivity and good current collector properties. The traditional air electrode is $La_{0.8}Sr_{0.2}MnO_{3-\delta}$ (LSM) due to its better phase stability, high electrical conductivity and electrocatalytic activity towards oxygen reduction reactions at elevated temperatures (T> 800 ºC) [13,14]. Alternative mixed ionic-electronic conductors (MIECs) have also been investigated for intermediate temperature applications (500-800 ºC), such as $La_{0.6}Sr_{0.4}Co_{0.2}Fe_{0.8}O_{3-\delta}$, $Ba_{0.5}Sr_{0.5}Co_{0.8}Fe_{0.2}O_{3-\delta}$, $Sm_{0.5}Sr_{0.5}CoO_{3-\delta}$ and (Gd,Pr)$BaCo_2O_{5+\delta}$ [15–18]. Among the electrolytes, $Zr_{0.84}Y_{0.16}O_{2-\delta}$ (YSZ), $La_{0.8}Sr_{0.2}Ga_{0.8}Mg_{0.2}O_{3-\delta}$ (LSGM) and $Ce_{0.8}Gd_{0.2}O_{1.9}$ (GDC) are the standard oxide ion conductors, while doped-Ba(Ce,Zr)$O_{3-\delta}$ are the most widely used proton conductors [9,19–21].

Non-identical materials with specific properties are usually used for the air and fuel electrodes, as they exhibit different properties in oxidizing and reducing atmospheres in terms of electrical conductivity, phase stability and electrocatalytic activity [9,22]. However, the use of two different electrodes increases the production cost of the cells as a consequence of the different fabrication and thermal treatment steps needed. Therefore, an increasing effort has been devoted to developing alternative electrode materials that can potentially be used as both air and fuel electrodes in an alternative cell configuration known as symmetrical solid oxide cells (SSOCs) [23,24]. The advantages of SSOCs over conventional SOCs rely not only on their simplified cell fabrication process, as both electrodes have the same composition, but also on their improved chemical and thermo-mechanical compatibility between the different cell components [25]. Special attention is paid to the electrode/electrolyte interface, minimizing thermal and lattice expansion mismatch between the cell layers and avoiding the formation of non-desired reaction products [26]. Another relevant property of SSOCs

relies on their reversibility, meaning that the oxidizing and reducing atmospheres to which electrodes are exposed can be reversed [27,28]. This confers important advantages to prevent detrimental effects associated with sulfur poisoning and carbon deposition in the electrodes by simply switching the gas flow or alternating operation between fuel and electrolysis modes, making possible the implementation of this technology for power generation (SOFC), hydrogen production (SOEC) and $CO_2$ electroreduction processes [28–32]. This feature gives a great flexibility of use to these electrochemical devices, as the stored chemical energy can be delivered under demand as electrical energy.

The field of SSOCs have thereby aroused a great interest among the scientific community in the last 15 years, with 115 publications and over 2900 citations registered in 2020 (data source: Scopus database). Pioneer studies in SSOFC technology started in 2006 when Bastidas *et al.* and Ruiz-Morales *et al*. revealed promising results for La(Cr,Mn)$O_3$-based electrodes, becoming a real alternative to the traditional approach based on Ni-cermet anode supported cells [12,33]. From this point onwards, great efforts have been made to implement MIECs derived from perovskite-type compounds, such as $LaMnO_3$, (La,Sr)$FeO_3$ and (La,Sr)$CoO_3$; however, they exhibit low redox stability to be used under reducing atmospheres. In order to overcome this drawback, much investigation has been devoted to modifying the electrode composition by doping with elements with better redox stability in the B-site of the perovskite structure (*e.g.* Sc, Ti, Mo, W, Nb and Zr) [34]. Alternatively, layered perovskites with compositions of $Sr_2Fe_{1.5}Mo_{0.5}O_{6-\delta}$, $PrBaMn_2O_{5+\delta}$ and $La_2MnO_{4\pm\delta}$ have also been proposed for SSOC electrodes due to their inherent phase stability and good electrical conductivity in both oxidizing and reducing environments. In addition, they possess faster ionic conduction than single-perovskites, thereby showing high activity for ORR [35–37].

Although improved symmetrical electrodes have been reported in the last few years, their low electronic conductivity and poor electrocatalytic activity in fuel conditions, compared to the conventional Ni-YSZ cermets, are the main drawbacks for their potential application [38]. In order to overcome this issue, the direct infiltration of active metals, such as Ru, Pd, Ni, onto the electrode surface has proven to be a good approach to enhance the overall electrode performance. Alternatively, these active metals can be directly incorporated as dopants within the crystal structure. They stay in the crystallographic phase in oxidizing conditions, while they are exsolved as metal nanoparticles on the surface in a reducing atmosphere without phase transformation and little lattice volume variation, which is beneficial for the mechanical stability of the cell [39]. In some cases, traditional air electrodes such as $La_2NiO_{4+\delta}$ (LNO), $La_{0.6}Sr_{0.4}Co_{0.2}Fe_{0.8}O_{3-\delta}$ (LSCF) and $Ba_{0.5}Sr_{0.5}Co_{0.8}Fe_{0.2}O_{3-\delta}$ (BSCF) have been tested for applications in SSOCs, suffering a severe phase transformation under reducing atmosphere into multiple phases, including metal particles that improved their electrocatalytic properties. These materials are known in the literature as quasi-symmetrical electrodes because the phase composition of the fuel and air electrodes is different. Nevertheless, it is important to highlight that this phase decomposition should be reversible in air, being possible to regenerate the original electrode composition by switching the gas feed [40–42].

With this in mind, the present review aims to give an overview of the latest advances in the field of SSOCs, paying special attention to the relationship between material composition and properties. In the last few years, new trends and perspectives in symmetrical electrode materials have been implemented for potential application in SSOFC and symmetrical solid electrolysis cell (SSOEC) systems with both oxide-ion and proton conducting electrolytes, as shown in **Fig. 1a** and **b**. Protonic cells have increasingly gained ground on the field of SSOCs, as they can operate at relatively low temperatures (500-800 ºC), thereby offering benefits such as improved performance and durability [43–46]. Similarly, SSOECs in the context of $CO_2$ electroreduction have increasingly become of interest due to its impact on global warming [47–49]. **Fig. 1c-f** presents an overview of the main electrode compositions that are discussed here, and summarize the outline of the present review: (c) single phases, (d) composite electrodes, (e) electrodes with exsolved nanoparticles and (f) quasi-symmetrical electrodes.

Apart from focusing on the intrinsic properties and reversibility of the electrode materials, other aspects such as microstructure, morphology and electrode architecture design will be also addressed, as they are crucial to increase the electrocatalytic activity and extend the durability of SSOCs [10,50]. Special attention will be given to alternative synthesis methods and electrode deposition techniques, such as sol-gel, freeze-drying, templating method, infiltration technique and spray-pyrolysis deposition, which improves the electrode microstructure and electrochemical properties in comparison to materials prepared by the traditional solid state reaction method at high sintering temperatures [51–58]. These strategies have proven to be more cost-effective by providing optimized properties for all cell components, although special consideration should be paid to possible detrimental reactions between the different layers of the cell.

We believe that this study provides insightful information to keep up to date the state-of-the art of SSOCs and, consequently, boost their most immediate development. To this aim, not only the latest findings are discussed but also the main drawbacks of the technology are pointed out in order to identify the main challenges ahead and future perspectives, including new electrode compositions and alternative preparation methods in order to obtain efficient and durable electrodes at low operating temperatures.

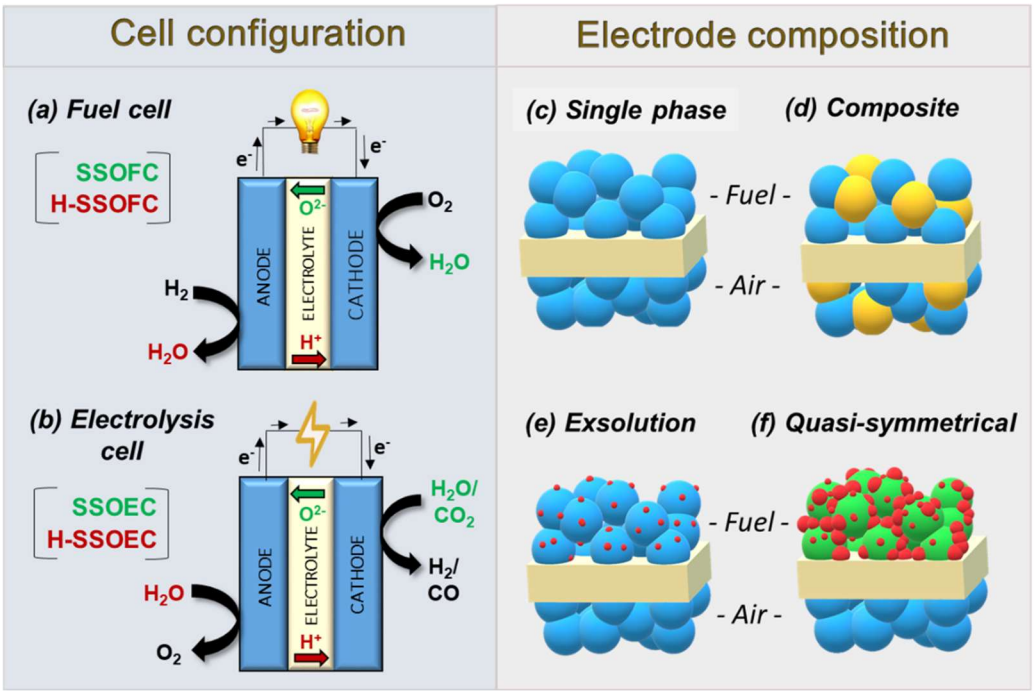


**Figure 1.** The two main application of symmetrical electrodes: (a) fuel cell and (b) electrolysis cell, including both oxide-ion and proton conducting electrolytes. Most studied electrode compositions in SSOCs: (c) single phases, (d) composites, (e) electrodes with exsolved nanoparticles and (f) quasi-symmetrical electrodes.

## 2. Symmetrical electrodes with single perovskite-type structure

### 2.1. La(Cr,Mn)$O_3$-based electrodes

Lanthanum chromites, widely employed as interconnect materials for SOFCs due to their remarkable stability at high temperatures in a wide range of oxygen partial pressures (1-$10^{-24}$ atm), were the first electrodes considered for SSOFCs [59]. Traditionally, a co-doping approach on both A- and B-sites of the perovskite has been employed in order to enhance their conductivity and electrocatalytic activity in both oxidizing and reducing conditions. In general, A-site doping with $Sr^{2+}$, $Ca^{2+}$ and $Ba^{2+}$ is used to increase the concentration of oxygen vacancies and to improve the ionic and electronic conductivity. However, the introduction of cations with better redox stability in the B-site, such as Sc, Ti, Mo, W, Nb and Zr, improves the phase stability under reducing conditions and diminishes the thermal expansion coefficients. In the following paragraphs, a summary on the electrochemical performance of La(Cr,Mn)$O_3$-based electrodes in SSOCs is presented, and the most relevant compositions and properties are given in **Table 1.**

The partial incorporation of Mn in $LaCrO_3$-based electrodes enhances the catalytic activity towards hydrocarbon oxidation without detrimental effects on the redox stability in a $H_2$ atmosphere [60,61]. In 2003, Irvine *et. col.* proposed a Sr- and Mn- co-doping strategy to develop the $La_{0.75}Sr_{0.25}Cr_{0.5}Mn_{0.5}O_{3-\delta}$ (LSCM) anode material [62,63], which rendered a promising performance when fueled with $H_2$ and $CH_4$, achieving area specific resistance (ASR) values of 0.2 and 0.9 Ω $cm^2$ at 900 ºC, respectively [62]. Later, the properties of LSCM for ORR were predicted by density functional theory (DFT) [64] and confirmed by electrochemical measurements

[65]. In this way, the first SSOFC based on LSCM electrode on YSZ electrolyte, proposed in 2006 by Bastidas *et al.,* rendered a maximum power density (MPD) of 300 and 230 mW $cm^{-2}$ at 900 ºC in $H_2$ and $CH_4$, respectively [33]. Simultaneously, Ruiz-Morales *et al.* prepared the LSCM-YSZ composite electrode by mixing the powders with poly(methyl-methacrylate) (PMMA) microspheres as pore formers to tailor the porosity. The LSCM-YSZ|YSZ(250µm)|LSCM-YSZ cell rendered an improved MPD of 546 and 347 mW $cm^{-2}$ at 950 ºC when fueled with $H_2$ and $CH_4$, respectively [12]. The addition of GDC to LSCM-YSZ was also tested with the aim of improving the ionic conductivity; however, the power output was not improved (400 mW $cm^{-2}$ at 950 ºC in $H_2$) because the electrode microstructure was not optimized with PMMA templates, demonstrating the great importance of the electrode design on the cell performance [66]. In this context, several efforts have been made to tailor the microstructure and boost the electrochemical performance of LSCM symmetrical electrodes. Among them, the implementation of an aqueous gel-casting method [67], combustion synthesis [68], infiltration of LSCM into a highly porous YSZ scaffold [69] and the infiltration of $Ce_{0.8}Gd_{0.2}O_{1.9}$ (GDC)/$Ce_{0.8}Sm_{0.2}O_{1.9}$ (SDC) particles into LSCM-YSZ composite [66,67,69,70], have demonstrated to improve the electrochemical properties for both ORR and HOR. However, the MPD values were still modest, ranging from 250 to 450 mW $cm^{-2}$ at 850 ºC, due to the low electrocatalytic activity of the electrodes for ORR as well as the high temperatures needed for the synthesis of LSCM (above 1200 ºC), increasing drastically the grain size of the powders, and consequently worsening the electrochemical properties (**Table 1**).

In order to enhance the electrochemical activity, several B-site doping strategies have been deeply investigated. For instance, Peña-Martínez *et al.* studied the $La_{0.75}Sr_{0.25}Cr_{0.5}B_{0.5}O_{3-\delta}$ (B= Fe, Mn and Al) series. The lowest ASR values in air in contact with LSGM electrolyte were obtained for Al-doped electrode, 1 Ω $cm^2$ at 800 ºC, compared to 20 Ω $cm^2$ for LSCM [71]. In another study, Rath *et al.* explored the doping effects of several aliovalent transition metals on $La_{0.7}Ca_{0.3}Cr_{0.8}B_{0.2}O_{3-\delta}$ (B= Ti, Mn, Fe, Co and Ni). In all cases, minor segregations of $Cr_2O_3$ were detected after calcination in air at 800 ºC although this impurity was removed after treating the electrodes in a hydrogen atmosphere at 800 ºC for 2 h. ASR values in $H_2$ ranged from 0.36 to 0.12 Ω $cm^2$ at 800 ºC, increasing the catalytic activity for HOR in the following order: Ti< Co< Fe≈ Ni< Mn [72].

Chen *et al.* studied the $La_{0.75}Sr_{0.25}Cr_{0.3}Fe_{0.7}O_{3-\delta}$ symmetrical electrode, which showed low ASR values of 0.10 and 0.40 Ω $cm^2$ in oxidizing and reducing conditions at 800 ºC, respectively [73]. An LSGM electrolyte supported cell with a $La_{0.4}Ce_{0.6}O_{2-\delta}$ (LDC) protective interlayer achieved a stable MPD of 300 mW $cm^{-2}$, operating with $H_2$ at 800 ºC. Interestingly, the cell showed a remarkable phase stability against carbonation and sulfur poisoning in an atmosphere of 50% $H_2$-CO and 10 ppm $H_2S$. A related A-site deficient electrode, $(La_{0.8}Sr_{0.2})_{0.95}Cr_{0.7}Fe_{0.3}O_{3-\delta}$, was also investigated, revealing a small segregation of $FeO_x$ in reducing environments [74]. However, the ASR values were relatively elevated, *i.e.* 3.8 and 12 Ω $cm^2$ in air and 5% $H_2$-$N_2$, respectively, at 950 ºC. Recently, Skinner *et col.* studied the electrical conductivity and oxygen diffusion behavior of A-site deficient $(La_{0.8}Sr_{0.2})_{0.95}Cr_xFe_{1-x}O_{3-\delta}$ (x= 0.3, 0.5 and 0.7) electrodes [75,76]. The conductivity increased with the Cr-content, while the surface exchange coefficients decreased up to two order of magnitudes, *i.e.*

$1.1\times10^{-10}$ and $8.6\times10^{-13}$ cm$^2$ s$^{-1}$ at 950 ºC for x= 0.3 and 0.7, respectively, revealing that great efforts are needed to deeply understand the properties of these materials under oxidizing conditions.

A-site doping strategies have also been explored in order to improve the electrochemical properties of LSCM. One of the first attempts was proposed by Zhang *et al.* by testing different compositions of the $La_{0.7}A_{0.3}Cr_{0.5}Mn_{0.5}O_{3-\delta}$ (LACM, A= Ca, Sr and Ba) series [70]. The materials exhibited similar conductivity values, *i.e.* 26.5 and 29.9 S cm$^{-1}$ for LSCM and LCCM in air, respectively, at 800 ºC, as well as comparable ASR values, ~0.5 Ω cm$^2$ in air at 900 ºC.

Ca-doped $LaCrO_3$ has also been widely studied as symmetrical electrodes due to its higher electronic conductivity compared to LSCM under reducing atmosphere *i.e*. 0.3 and 3 S cm$^{-1}$ for LSCM and $La_{0.7}Ca_{0.3}CrO_{3-\delta}$ (LCC), respectively, in 10% $H_2$-$N_2$ at 700 ºC [77,78]. Zhang *et al.* investigated LCC-GDC composite electrodes by both the physical mixing powder method [79] and the infiltration technique [80], showing the infiltrated electrodes higher MPD values of 400 and 200 mW cm$^{-2}$ at 800 ºC in $H_2$ and city gas containing $H_2S$, respectively. In another study, the Cr-deficient composite electrode, $La_{0.7}Ca_{0.3}Cr_{0.97}O_3$-YSZ, showed higher conductivity values, 62 S cm$^{-1}$ at 850 ºC in air, but modest values of MPD were achieved, 50.7 mW cm$^{-2}$ at 800 ºC using $H_2$ [81].

In 2020, Wan *et al.* prepared a symmetrical composite electrode based on Bi-doped lanthanum chromite, $La_{0.65}Bi_{0.1}Sr_{0.25}Cr_{0.5}Fe_{0.5}O_{3-\delta}$-SDC [82]. High ASR values were obtained in air, 2.90 Ω cm$^2$ at 800 ºC, attributed to the inherent poor activity of these materials for ORR. In contrast, competitive ASR values were achieved working as anode, 0.32 Ω cm$^2$ at 800 ºC in $H_2$, rendering MPDs of 280, 260 and 240 mW cm$^{-2}$ using $H_2$, syngas and ethanol as fuels, respectively (**Fig. 2 a-d**). It has to be commented that the redox stability of these materials was not studied, despite the high reducibility of Bi and Fe, which could be partially reduced to Bi-Fe metal, explaining the improved efficiency of the anode.

The incorporation of Ce in LSCM was similarly investigated due to the high catalytic activity of $Ce^{4+}/Ce^{3+}$ species for hydrocarbon oxidation [83,84]. $La_{0.75-x}Ce_xSr_{0.25}Cr_{0.5}Mn_{0.5}O_3$ (x= 0-0.375) series showed better electrochemical performance in $H_2$ with increasing Ce-doping [85]. Similarly, Song *et al.* confirmed the better catalytic activity of $La_{0.75}Sr_{0.25-x}Ce_xCr_{0.5}Mn_{0.5}O_{3-\delta}$ (x= 0-0.15) from $O_2$-temperature programmed desorption (TPD) and $H_2$-temperature programmed reduction (TPR) [86,87]. Highly Ce-doped samples (x>0.15) showed poor resistance to sulfur poisoning. The optimal composition in terms of performance and stability, $La_{0.75}Sr_{0.125}Ce_{0.125}Cr_{0.5}Mn_{0.5}O_{3-\delta}$, showed a modest MPD of 33.12 mW cm$^{-2}$ at 900 ºC in wet $H_2$ and 1% $H_2S$ as a consequence of the thick YSZ electrolyte.

The classical $La_{0.8}Sr_{0.2}MnO_{3-\delta}$ (LSM) cathode was also investigated as a potential candidate for symmetrical electrode. No phase transformation was observed under reducing conditions up to at 800 ºC; however, modest ASR values were obtained for the LSM-GDC composite electrodes, 1.44 and 5.19 Ω cm$^2$ in air and $H_2$, respectively, at 800 ºC. The MPD of the symmetrical LSM-GDC electrode on a YSZ-supported cell rendered 150.8 mW cm$^{-2}$ at 800 ºC with negligible degradation for 140 h of stability test at 700 ºC [88]. A Sc-doping

strategy was also explored, $La_{0.8}Sr_{0.2}Sc_{0.2}Mn_{0.8}O_{3-\delta}$ (LSSM) showed greater electrical conductivity than the typical LSCM under both anode and cathode operating conditions, as well as excellent chemical and structural stability. A symmetric cell with scandium-stabilized zirconia electrolyte showed a stable MPD of 310 and 130 mW $cm^2$ at 900 °C, respectively, when operating on wet $H_2$ and wet $CH_4$ [89].

Alternative chromite-based compounds have also been proposed as highly efficient fuel electrode materials, such as $Pr_{0.7}Ca_{0.3}Cr_{1-x}Mn_xO_{3-\delta}$ [90], $La_{0.70}Sr_{0.3}Cr_{0.85}Ni_{0.15}O_{3-\delta}$ [91], $Y_{0.9}Sr_{0.1}Cr_{0.9}Fe_{0.1}O_{3-\delta}$ [92], $Y_{0.7}Ca_{0.3}Cr_{1-x}Cu_xO_{3-\delta}$ [93] and $La_{0.65}Bi_{0.1}Sr_{0.25}Cr_{0.5}Mn_{0.5}O_{3-\delta}$ [94], but their application in SSOCs is restricted due to their low ORR activity. Further efforts in microstructural optimization is needed to consider them as promising symmetrical electrodes, despite their remarkable and stable performance under reducing conditions.

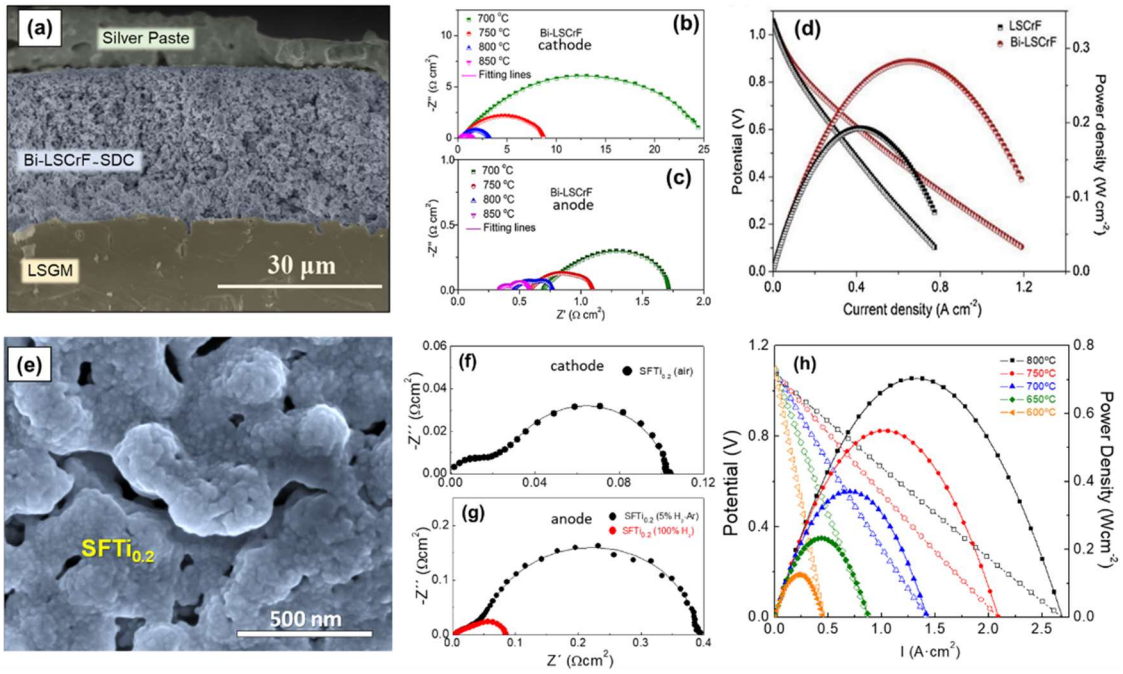


**Figure 2.** (a) SEM image of the $La_{0.65}Bi_{0.1}Sr_{0.25}Cr_{0.5}Fe_{0.5}O_{3-\delta}$–SDC symmetrical electrode on LSGM electrolyte. Impedance spectra in (b) air and (c) $H_2$ at different temperatures and (d) Voltage and power density curves of the symmetrical cells in $H_2$ at 800 ºC. Reprinted with permission, Elsevier [82]. (e) SEM images of the $Sr_{0.98}Fe_{0.8}Ti_{0.2}O_{3-\delta}$ (SFT) by spray-pyrolysis deposition. Impedance spectra in (f) air and (g) $H_2$ at 700 ºC. (h) Voltage and power density curves of the symmetrical electrode on LSGM electrolyte. Reprinted with permission, Royal Society of Chemistry [95].

## 2.2. (La,Sr)$FeO_3$-based electrodes

Most of the highly efficient air electrodes for classical SOCs are based on doped-$LaFeO_{3-\delta}$ and $SrFeO_{3-\delta}$ perovskites [96,97]. However, these materials usually present poor redox stability to be used as fuel electrodes due to phase transformation or decomposition under reducing conditions. As previously mentioned, the redox stability of these electrodes could be enhanced by adequate doping in the B-site of the perovskite with less reducible cations, such as Mo, W, Ta, Nb, Zr, Ti and Sc. In this section, doping and microstructural strategies used on (La,Sr)$FeO_3$-based electrodes for SSOCs are discussed (**Table 1**).

It is well known that $SrFeO_{3-\delta}$ exhibits different crystal structures depending on the lattice oxygen stoichiometry. In particular, $SrFeO_{3-\delta}$ crystallizes in a cubic perovskite in oxidizing atmospheres with disordered oxygen vacancies, and it transforms in reducing atmospheres into a brownmillerite-type structure with oxygen-vacancy ordering, which is detrimental for the electrochemical properties due to the reduced oxide ion mobility [98,99]. Moreover, the easy reduction of $Fe^{4+}$ to $Fe^{3+}$ causes an excessive oxygen deficiency and a decrease of the electron hole charge carriers, and as a consequence the electronic conductivity is drastically reduced, limiting its potential application as fuel electrodes [100,101]. In order to improve the redox stability of $SrFeO_{3-\delta}$, different studies have adopted a doping strategy in the B-site of the perovskite. In 2014, Fernández-Ropero *et al.* investigated the $SrFe_{0.75}B_{0.25}O_{3-\delta}$ (B= Cr, Mo, W, Ti, Zr, V and Nb) electrodes for their application in SSOFCs [102]. All doped materials crystallized with a cubic perovskite-type structure in both air and hydrogen atmosphere, contrary to the undoped one. The lowest ASR values were reported for Ti-doped electrodes, *i.e.* 0.25 and 1.5 Ω $cm^2$ at 700 ºC in air and 5%-$H_2$, respectively.

Later, the electrochemical properties of $Sr_{0.98}Fe_{0.8}Ti_{0.2}O_{3-\delta}$ were further improved by using a spray-pyrolysis deposition technique to obtain nanostructured electrodes [95]. The spray-pyrolysis deposition was carried out at 250 ºC on LSGM electrolyte and the electrodes were sintered at only 800 ºC, obtaining a particle size of 50 nm compared to 500 nm for the screen-printed electrodes with the same cation composition at 1100 ºC (**Fig. 2e-f**). This resulted in higher TPB density for the electrochemical reactions, achieving ASR values as low as 0.1 and 0.07 Ω $cm^2$ at 700 ºC in air and wet $H_2$, respectively, much better than those reported for a screen-printed electrode, *i.e.* 0.25 Ω $cm^2$ in air at 700 ºC [102]. A cell with LSGM electrolyte (300 μm) achieved a remarkable MPD of 700 mW $cm^{-2}$ at 800 ºC. Great MPD values of 700 mW $cm^{-2}$ at 800 ºC were also found for $SrFe_{0.8}Ti_{0.2}O_{3-\delta}$ (SFT)-$La_{0.8}Sr_{0.2}Ga_{0.8}Mg_{0.18}Zn_{0.02}O_{2.8}$(LSGMZ) (2:1) composite electrode [103].

Mo-doped $SrFeO_3$ are among the most studied symmetrical electrodes in the last few years; however, there exist discrepancies in the literature regarding the real crystal structure of these compounds. In general, electrodes with low Mo-content, *i.e.* $SrFe_{1-x}Mo_xO_{3-\delta}$ ($x<0.2$), exhibit a single cubic perovskite-type structure [104,105], but it is not completely clear if the electrodes with $x\geq0.25$ crystallize as a $SrFe_{0.75}Mo_{0.25}O_{3-\delta}$ single or a $Sr_2Fe_{1.5}Mo_{0.5}O_6$ double perovskite [24]. Recently, Merkulov *et al.* studied $SrFe_{0.7}Mo_{0.3}O_{3-\delta}$ by electron diffraction and weak superstructure reflections, corresponding to an ordered double perovskite, were observed [106,107]. Since many authors have considered that the most studied composition, i.e. $Sr_2Fe_{1.5}Mo_{0.5}O_{6-\delta}$, has a double perovskite-type structure, the Mo-doped $SrFeO_3$ electrodes are discussed in the next section.

Further research on W-doped $SrFeO_{3-\delta}$ single perovskite symmetrical electrodes showed a phase transformation on W-doping from a single cubic perovskite for $SrFe_{0.9}W_{0.1}O_{3-\delta}$ to tetragonal phase for $SrFe_{0.8}W_{0.2}O_{3-\delta}$. The chemical stability and electrochemical properties of the electrodes improved with increasing W-doping, meanwhile the thermal expansion coefficient decreased ($17.9\times10^{-6}$ $K^{-1}$ for $SrFe_{0.8}W_{0.2}O_{3-\delta}$) [108]. The same composition, investigated by Cao *et al.* [109], achieved very low ASR values of 0.084 and 0.20 Ω $cm^2$ in air and $H_2$, respectively, at 800 ºC and a MPD of 931 mW $cm^{-2}$ at 850 ºC (**Fig. 3a-d**).

Composite symmetrical electrodes of $SrFe_{1-x}Zr_xO_{3-\delta}$-GDC (x= $0 \leq x \leq 0.35$) were also tested, showing good phase stability in reducing conditions for Zr-content $x \geq 0.1$ [110]. One of the main benefits of Zr-doping was a reduction of the thermal expansion coefficient (TEC) in air, from $44 \times 10^{-6}$ $K^{-1}$ for the pristine material to $32 \times 10^{-6}$ $K^{-1}$ for x= 0.25. However, these values are larger than those observed for $Mo^{6+}/W^{6+}$-doped $SrFeO_{3-\delta}$ (~ 15-$20 \times 10^{-6}$ $K^{-1}$), indicating that high valence transition metals are more suitable to lower the TEC of these materials and to improve the mechanical compatibility with the electrolytes [108,111]. The best results were found for the composition $SrFe_{0.75}Zr_{0.25}O_{3-\delta}$-GDC, achieving a MPD of 425 mW $cm^{-2}$ at 800 ºC in $H_2$ [110]. A similar composition, $BaFe_{0.9}Zr_{0.1}O_{3-\delta}$, achieved ASR values of 0.005 and 1 Ω $cm^2$ at 800 ºC in air and $H_2$, respectively, with good stability in $H_2$ for 100 h [112]. Si-doping in $SrFeO_3$ was also investigated; the conductivity of $SrFe_{1-x}Si_xO_{3-\delta}$ ($x \leq 0.15$) series reached its maximum for x= 0.1, with a value of 35.3 S $cm^{-1}$, compared to 26.3 S $cm^{-1}$ for x= 0 at 700 ºC in air [113]. Moreover, the Si-doping avoided the transformation of $SrFeO_3$ perovskite into $Sr_2Fe_2O_5$ brownmillerite phase in reducing conditions. The ASRs were also improved after Si-doping with values of 0.25 and 0.08 Ω $cm^2$ for x= 0 and x= 0.1, respectively, at 800 ºC in air (**Table 1**).

Similarly, $La_{1-x}Sr_xFe_{1-y}B_yO_{3-\delta}$ electrodes, where B is a transition metal, have been widely investigated as symmetrical electrodes. In general, the substitution of $La^{3+}$ by $Sr^{2+}$ creates oxide-ion vacancies in the lattice, increasing the ionic conductivity, whereas B-site doping is used to improve the redox stability [114,115]. However, Traversa *et. col.* have proposed the conventional $La_{0.8}Sr_{0.2}FeO_{3-\delta}$ (LSF) cathode as a stable symmetrical electrode without phase transformation after annealing in $H_2$ at 800 ºC for 10 h. In order to avoid the well-known reaction between $LaFeO_3$-based materials and the YSZ electrolyte, a GDC protective interlayer was deposited by screen-printing, enhancing the performance of the single cell up to 387 mW $cm^{-2}$ at 800 ºC in $H_2$ [116]. A related composition, $Sm_{0.95}Ce_{0.05}FeO_{3-\delta}$ (SCFO), also showed a good stability in reducing conditions [117], suggesting that B-site doping is not needed to achieve sufficient redox stability at temperature lower than 800 ºC.

Moreover, the commonly used $La_{0.6}Sr_{0.4}Co_{0.2}Fe_{0.8}O_{3-\delta}$-$Ce_{0.9}Gd_{0.1}O_{1.95}$ (LSCF-GDC) air electrode was also tested as symmetrical electrode in SOEC mode, showing no phase transformation in reducing conditions. The current density reached 0.5 A $cm^{-2}$ at 850 ºC and 1.3 V, while the hydrogen production rate was up to 3.5 $cm^3$ $min^{-1}$ $cm^{-2}$ [118]. However, recent studies have reported that LSCF transforms under reducing atmosphere into a Ruddlesden-Popper type structure with Fe-Co metal segregation [119]. Other studies have also reported low phase stability for the same electrode materials under reducing conditions. For instance, Kulkarni *et al.* observed by synchrotron X-ray powder diffraction a severe decomposition of LSCF into multiple phases: $La_2O_3$, SrO, $LaSrFeO_4$, $La(OH)_3$ and Fe-Co nanoparticles in $H_2$ at 800 ºC for 50 h [120]. Such differences could be explained by the different reduction kinetics of these materials, which depend on several factors such as temperature, gas composition and oxygen partial pressure, but also morphological characteristics, *i.e.* grain size and porosity. Hence, the discrepancies between these studies are possibly related to insufficient annealing time under reducing atmosphere. Thus, further research is needed to reach more solid conclusions on this matter.

Niu *et al.* reported an enhancement of the electrochemical performance for the Nb-doped and A-site deficient $(La_{0.6}Sr_{0.4})_{0.9}Co_{0.2}Fe_{0.6}Nb_{0.2}O_{3-\delta}$ symmetrical electrode in comparison with the stoichiometric material, attributed to an increase of the oxygen vacancy concentration [121]. Other Nb-doped ferrites have been investigated. For instance, Kong *et al.* impregnated $La_{0.9}Ca_{0.1}Fe_{0.9}Nb_{0.1}O_{3-\delta}$-SDC composite electrode into a $Zr_{0.8}Sc_{0.2}O_{2-\delta}$ (SSZ) scaffold, reaching a MPD of 528 mW $cm^{-2}$ in $H_2$ at 850 ºC, and interestingly comparable values were found when CO or syngas were used as fuel [122]. Promising results were also obtained for $Pr_{0.4}Sr_{0.6}Co_{0.2}Fe_{0.7}Nb_{0.1}O_{3-\delta}$ electrodes impregnated with GDC nanoparticles, which achieved ASR values as low as 0.04 and 0.31 Ω $cm^2$ at 800 ºC in air and $H_2$, respectively. Moreover, these electrodes were stable when operated with $CH_4$ fuel for 384 h [123].

Mo-doping has also been intensively investigated to enhance the redox stability of LSF electrodes. Bian *et al.* reported rather low ASR values of 0.08 Ω $cm^2$ in air and 0.09 Ω $cm^2$ in $H_2$ for $La_{0.5}Sr_{0.5}Fe_{0.9}Mo_{0.1}O_{3-\delta}$ and an excellent MPD value of 640 mW $cm^{-2}$ at 850 ºC, while a current of -1 A $cm^{-2}$ was obtained at 1.3 V in SOEC mode [124]. The same composition has been tested with CO fuel, obtaining a MPD of 474 mW $cm^{-2}$ at 750 ºC [125]. A similar composition, $La_{0.6}Sr_{0.4}Co_{0.2}Fe_{0.7}Mo_{0.1}O_{3-\delta}$, showed a good phase stability in reducing conditions with a remarkable MPD of 481 mW $cm^{-2}$ at 850 ºC, using ethanol as fuel; however, the possible Co-Fe exsolution at such high working temperature was not investigated [126]. Recently, W-doping was also explored in $La_{0.5}Sr_{0.5}Fe_{0.9}W_{0.1}O_{3-\delta}$, achieving low ASR values of 0.08 and 0.16 Ω $cm^2$ at 800 ºC in air and $H_2$, respectively, and a remarkable MPD of 617 mW $cm^{-2}$ at the same temperature [127].

An alternative Ga-doping strategy was also tested for LSF, the $La_{0.7}Sr_{0.3}Fe_{0.7}Ga_{0.3}O_{3-\delta}$ symmetrical electrode showed good stability in wet $H_2$ up to 800 ºC [128]. The conductivity values were 47.5 S $cm^{-1}$ in air and 0.42 S $cm^{-1}$ in 5%-$H_2$ at 800 ºC. A LSGM-supported cell rendered an MPD of 489 mW $cm^{-2}$ in wet $H_2$ at 800 ºC. Similar findings were observed for Sc-doped LSF, the $La_{0.6}Sr_{0.4}Fe_{0.9}Sc_{0.1}O_{3-\delta}$ symmetrical electrode exhibited decent electrochemical properties, *i.e.* 0.015 Ω $cm^2$ in air and 0.29 Ω $cm^2$ in $H_2$ at 800 ºC [129].

Other Fe-containing single perovskites have been reported in the literature as potential candidates for symmetrical electrodes. Yang *et al.* successfully incorporated Mo in the highly efficient $Ba_{0.5}Sr_{0.5}Co_{0.2}Fe_{0.8}O_{3-\delta}$ (BSCF) SOFC cathode for its implementation in SSOC (**Fig. 3e-g**). The $Ba_{0.5}Sr_{0.5}Co_{0.2}Fe_{0.7}Mo_{0.1}O_{3-\delta}$ (BSCFM) electrode showed improved redox stability over time and very low ASR values in $H_2$ (0.035 Ω $cm^2$ at 800 ºC). The power output of a YSZ-supported cell reached 418 mW $cm^{-2}$ at 700 ºC without any degradation for 115 h [130]. In another study, $Ba_{0.5}Sr_{0.5}Fe_{0.9}Mo_{0.1}O_{3-\delta}$ (BSFM) on a LSGM electrolyte showed surprising low ASR values, *i.e.* 0.007 Ω $cm^2$ and 0.047 Ω $cm^2$ at 800 ºC in air and humidified $H_2$, respectively [131]. In contrast, higher ASR values were obtained for the same electrode deposited onto a GDC electrolyte. The similar lattice cell parameters between BSFM and LSGM electrolytes have been suggested to be responsible for the improved electrochemical performance, obtaining an exceptional MPD of 2280 mW $cm^{-2}$ at 800 ºC in $H_2$. These results suggested the importance of tailoring and controlling the properties of the electrode/electrolyte interfaces [131].

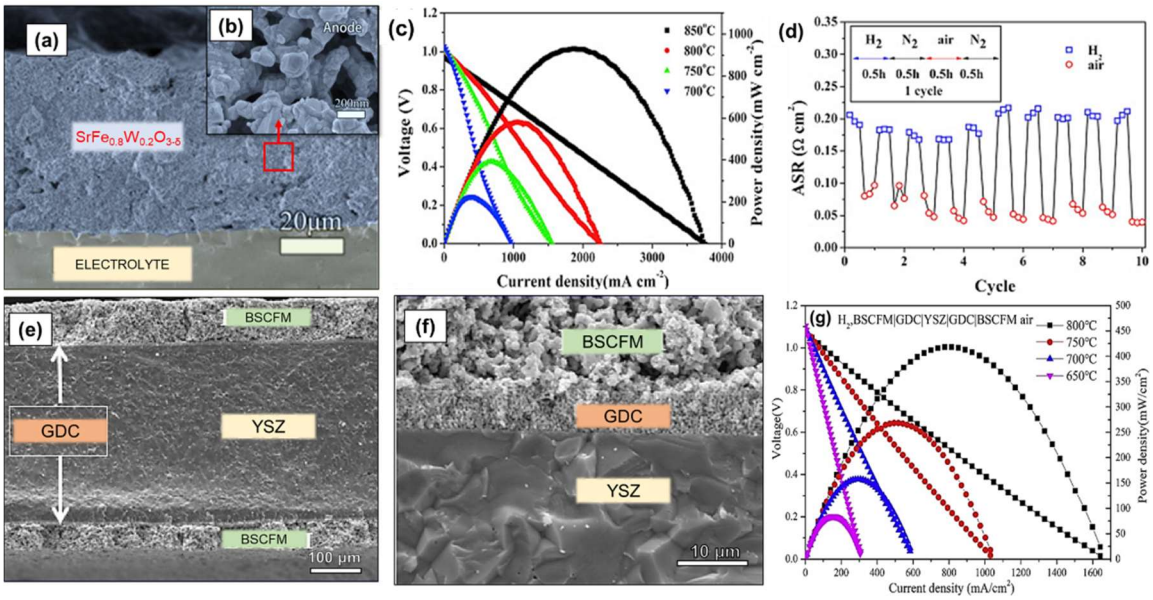


**Figure 3.** (a,b) SEM images at different magnifications of $SrFe_{0.8}W_{0.2}O_{3-\delta}$ electrode on LSGM electrolyte, (c) I-V-P curves of the electrolyte-supported SSOFC in $H_2$ at different temperatures and (d) redox stability of the symmetrical electrode over 10 cycles at 800 ºC. Reprinted with permission, Elsevier [109]. (e,f) SEM images of the BSCFM|GDC|YSZ|GDC|BSCFM singles cell at different magnifications and (g) I-V-P curves of the single cell in $H_2$ at different temperatures. Reprinted with permission, Elsevier [130].

## 2.3. (La,Sr)$TiO_3$-based electrodes

Titanates have been considered as one of the most promising alternative anode to conventional Ni-cermets because of their excellent stability under reducing atmospheres, high tolerance towards sulfur-containing fuels and low cost [132]. In particular, the high electronic conductivity of these materials in reducing conditions is due to the partial reduction of $Ti^{4+}$ to $Ti^{3+}$. On the contrary, their poor ionic-electronic conductivity in oxidizing atmosphere have made them unsuitable for air electrodes. $La_{1-x}Sr_xTiO_{3+\delta}$ (LST) are the most widely investigated fuel electrodes for SOFCs [132] and $CO_2$ electrolysis [133]. In order to improve the properties to work simultaneously as air and fuel electrodes, several doping strategies in the B-site of the perovskite have been explored by replacing Ti with other transition metals with variable oxidation states, such as Fe, Mn and Co. In this section, a summary of titanates-based symmetrical cells is presented together with some properties in **Table 1**.

Canales-Vazquez *et al.* studied the performance of Fe-doped LST, $La_{1/3}Sr_{2/3}Ti_{1-x}Fe_xO_{3+\delta}$ with different Fe-content (x= 1/8-0.5). The electronic conductivity in air increased notably with Fe-content, while minor changes were observed in reducing atmospheres [134]. In addition, the electrocatalytic activity under both oxidizing and reducing conditions was also improved, which makes these electrodes suitable for SSOFC applications. Other related compositions, such as $La_{0.3}Sr_{0.7}Ti_{0.3}Fe_{0.7}O_{3\pm\delta}$ (LSTF07) and LSTF07-$CeO_2$ composites, have also been investigated, but only as fuel electrodes [135–137].

Regarding the Co-doped $La_{0.2}Sr_{0.8}TiO_{3+\delta}$ (LST) electrodes, Napolitano *et al.* investigated the structural parameters and charge compensation mechanisms on Co-doping. The electronic conductivity increased with Co-content, making them suitable for SSOC applications [138–140]. A similar composition, $La_{0.5}Sr_{0.5}Co_{0.5}Ti_{0.5}O_{3-\delta}$, was tested by Martínez-Coronado *et al.* [141], not showing any phase transformation in reducing conditions despite the high Co-content of this electrode. The conductivity values were of 25 S $cm^{-1}$ in air and 0.05 S $cm^{-1}$ in 5% $H_2$ at 800 ºC. The MPD obtained by the LSCT|LDC|LSGM|LDC|LSCT cell in $H_2$ was 110 mW $cm^{-2}$ at 800 ºC [141]. The doping of (La,Sr)$TiO_3$ with other transition metals, such as Mo and Mn, has also been investigated. In particular, the increase of Mo-content in (La,Sr)$Ti_{1-x}Mo_xO_{3-\delta}$ reduced the bond energy between metal and oxygen ions in the perovskite and, consequently, the concentration of the $Mo^{5+/}Mo^{6+}$ redox couple increased, leading to higher electronic conductivity and lower ASR. Nevertheless, these materials were only tested as fuel electrodes [142,143].

In another study, the A-site deficient $La_{0.2}Sr_{0.25}Ca_{0.45}TiO_{3-\delta}$ (LSCaT) perovskite was proposed as a potential electrode/electrolyte material for SOFCs due to its different properties under both oxidizing and reducing atmospheres [144]. The success of this material at different redox conditions was attributed to its different conducting properties at low and high oxygen partial pressures ($pO_2$), as well as its high ionic conductivity at the intermediate $pO_2$ range. It has to be noted that excellent results have recently been reported for titanate-based fuel electrodes for $CO_2$ electrolysis, such as $Sr_{0.95}Ti_{0.8}Nb_{0.1}Mn_{0.1}O_3$ [145], $(La_{0.2}Sr_{0.8})_{0.85}Ti_{0.8}Cr_{0.1}Ni_{0.1}O_{3-\delta}$ [146], $(La_{0.2}Sr_{0.8})_{0.9}Ti_{0.5}Mn_{0.4}Cu_{0.1}O_{3-\delta}$ [147] and $La_{0.43}Ca_{0.37}Rh_{0.06}Ti_{0.94}O_3$ [148].

As previously mentioned, most of the research about (La,Sr)$TiO_3$-based perovskites is focused on their application as fuel electrodes for SOFC and SOEC applications, and rarely as symmetrical electrodes. This is because of the difficulty to synthesize titanate-based electrodes with high mixed ionic-electronic conductivity in both air and fuel environments, therefore a trade-off should be found between the conductivity and catalytic activity in each electrode condition. To overcome this problem, further research should not only be focused on electrode composition, but also on the microstructure optimization. One of the main limitations of titanates is the low reduction kinetic, which could be improved by obtaining electrodes with nanometric particle size. Another approach is the incorporation of noble metals and active interlayers to improve their properties [51,132].

**Table 1.** Most relevant symmetrical electrodes with single perovskite-type structure. Area specific resistance (in air and $H_2$) and power/current density are given at 800 ºC. In those case, where not data are available at 800 ºC, the temperature is included.

| Electrode | Abbreviation | $ASR^{air}$ ($\Omega$ cm$^2$) | $ASR^{H_2}$ ($\Omega$ cm$^2$) | P (mW cm$^{-2}$) | Electrolyte | Ref. |
|---|---|---|---|---|---|---|
| $La_{0.75}Sr_{0.25}Cr_{0.5}Mn_{0.5}O_{3-\delta}$ | LSCM | $0.35^{900ºC}$ (wet $O_2$) | $0.30^{900ºC}$ | $300^{900\,ºC}$ ($H_2$)<br>$230^{900\,ºC}$ ($CH_4$) | YSZ | [33] |
| $La_{0.75}Sr_{0.25}Cr_{0.5}Mn_{0.5}O_{3-\delta}$ -YSZ | LSCM-YSZ | $0.27^{900ºC}$ | $0.34^{900ºC}$ ($H_2$)<br>$0.67^{900ºC}$ ($CH_4$) | $546^{950\,ºC}$ ($H_2$)<br>$347^{950\,ºC}$ ($CH_4$) | YSZ | [12] |
| $La_{0.75}Sr_{0.25}Fe_{0.7}Cr_{0.3}O_{3-\delta}$ | LSFCr | 0.105 | 0.40 | 300 ($H_2$) | LSGM/LDC | [73] |
| $Pr_{0.7}Ca_{0.3}Cr_{0.6}Mn_{0.4}O_{3-\delta}$ | PCaCM | 4 | 30 (5% $H_2$) | $250^{950\,ºC}$ ($H_2$)<br>$160^{950\,ºC}$ ($CH_4$) | YSZ | [90] |
| $La_{0.65}Bi_{0.1}Sr_{0.25}Cr_{0.5}Fe_{0.5}O_3$ -SDC | BiLSCrF-SDC | 2.90 | 0.32 | 280 ($H_2$)<br>260 (syngas)<br>240 ($C_2H_5OH$) | LSGM | [82] |
| $La_{0.7}Ca_{0.3}CrO_3$-GDC | LCaCr-GDC | - | - | 400 ($H_2$)<br>200 (city gas) | LSGM | [80] |
| $La_{0.8}Sr_{0.2}MnO_{3-\delta}$-GDC | LSM-GDC | 1.44 | 5.19 | 150.8 | YSZ | [88] |
| $La_{0.8}Sr_{0.2}Sc_{0.2}Mn_{0.8}O_{3-\delta}$ | LSSM | $0.18^{850\,ºC}$ | - | $310^{900\,ºC}$ ($H_2$)<br>$130^{900\,ºC}$ ($CH_4$) | SSZ | [89] |
| $La_{0.8}Sr_{0.2}FeO_{3-\delta}$ | LSF | 0.31 | 0.58 | 387 ($H_2$) | YSZ | [116] |
| $Sr_{0.98}Fe_{0.8}Ti_{0.2}O_{3-\delta}$-GDC | SFT-GDC | $0.1^{700\,ºC}$ | $0.07^{700ºC}$ | 700 ($H_2$) | LSGM | [95] |
| $SrFe_{0.8}Ti_{0.2}O_{3-\delta}$-LSGMZ | SFT-LSGMZ | - | - | 700 ($H_2$) | LSGMZ | [103] |
| $SrFe_{0.8}W_{0.2}O_{3-\delta}$ | SFW | 0.084 | 0.20 | $931^{850\,ºC}$ ($H_2$) | LSGM | [109] |
| $SrFe_{0.75}Zr_{0.25}O_{3-\delta}$-GDC | SFZ-GDC | $0.10^{750ºC}$ | $0.17^{750ºC}$ | 425 ($H_2$) | LSGM | [110] |
| $BaFe_{0.9}Zr_{0.1}O_{3-\delta}$ | BFZ | 0.005 | 1 | 1097 ($H_2$) | LSGM | [112] |
| $SrFe_{0.9}Si_{0.1}O_{3-\delta}$ | SFS | 0.08 | $0.17^{600\,ºC}$ (5% $H_2$) | - | GDC | [113] |
| $Pr_{0.4}Sr_{0.6}Co_{0.2}Fe_{0.7}Nb_{0.1}O_3$-GDC | PSCFN-GDC | 0.04 | 0.31 | - | LSGM | [123] |
| $La_{0.5}Sr_{0.5}Fe_{0.9}Mo_{0.1}O_{3-\delta}$ | LSFM | $0.08^{850ºC}$ | $0.09^{850ºC}$ | $640^{850ºC}$ ($H_2$) | LSGM | [124] |
| $La_{0.7}Sr_{0.3}Fe_{0.7}Ga_{0.3}O_{3-\delta}$ | LSFG | - | - | 489 ($H_2$) | LSGM | [128] |
| $La_{0.6}Sr_{0.4}Fe_{0.9}Sc_{0.1}O_{3-\delta}$ | LSFS | 0.015 | 0.29 | 560 ($H_2$) | LSGM | [129] |
| $Ba_{0.5}Sr_{0.5}Mo_{0.1}Fe_{0.9}O_{3-\delta}$ | BSMF | 0.007 | 0.047 | 2280 ($H_2$) | LSGM | [131] |
| $La_{0.5}Sr_{0.5}Co_{0.5}Ti_{0.5}O_{3-\delta}$ | LSCT | - | - | 110 ($H_2$) | LSGM | [141] |
| $CaFe_{0.4}Ti_{0.6}O_{3-\delta}$ | CaFT | 1 | 1 | 58 ($H_2$) | YSZ | [149] |

## 3. Symmetrical electrodes with layered perovskite structure

### 3.1. $Sr_2Fe_{1.5}Mo_{0.5}O_{6-\delta}$-based double perovskites

Since Liu *et al.* implemented the $Sr_2Fe_{1.5}Mo_{0.5}O_{6-\delta}$ (SFM) double-perovskite for SSOFCs, great efforts have been dedicated to the development of related compositions as both air and fuel electrodes **(Table 2)** [24]. This

symmetrical electrode is highly promising because it exhibits high electrical conductivity in both air (550 S $cm^{-1}$) and $H_2$ (310 S $cm^{-1}$) atmospheres, as well as excellent redox stability, electrocatalytic activity in $H_2$ and $CH_4$ and high sulfur tolerance. However, recent reports have shown somewhat lower conductivity values in the range of 10-50 S $cm^{-1}$ [150–153]. In addition, density functional theory (DFT) calculations revealed that the good catalytic activity for ORR is due to the high ionic conductivity induced by the elevated concentration of oxygen vacancies.

Recently, several approaches have been proposed to improve the electrochemical properties of the pristine SFM for its implementation in SSOCs. Osinkin *et al.* proposed to mix SFM with $Ce_{0.8}Sm_{0.2}O_{1.9-\delta}$ (SDC), which was then topped with SFM as current collector. This cell configuration achieved power densities of 250-500 mW $cm^{-2}$ at 800 ºC in $H_2$ in a LSGM supported cell [154,155]. The same authors studied the CO oxidation kinetics and redox cycling stability of SFM, showing no changes in the polarization resistance after fast gas cycling [156]. Liu *et al*. prepared SFM electrodes by infiltration onto a LSGM porous scaffold obtained by tape-casting, and the cells were subjected to a fast heating/cooling rate of 200 ºC $min^{-1}$ in order to avoid the formation of insulating $SrMoO_4$ scheelite as secondary phase [157]. No interfacial crack formation was detected due to the similar thermal expansion coefficients between both materials. SFM was also infiltrated into a porous LSGM scaffold, obtained by phase inversion tape-casting [158]. This optimized porosity of the electrodes resulted in a high power density of 703 mW $cm^{-2}$ at 800 ºC compared to 390 mW $cm^{-2}$ for a cell fabricated by traditional tape-casting method. Bernadet *et al.* also studied $Sr_2Fe_{1.5}Mo_{0.5}O_{6-\delta}$ electrodes on zirconium-based electrolytes with a GDC interlayer to avoid reactivity between the materials, achieving -1.4 A $cm^{-2}$ at 1.3 V and 900 ºC in SOEC mode [159].

Numerous doping strategies have also been explored to further improve the electrochemical properties of SFM. Firstly, Song *et al.* partially substituted Fe by Co in $Sr_2Fe_{1.5-x}Co_xMo_{0.5}O_{6-\delta}$ (SFCM, $0 \leq x \leq 1$) series. The electrodes were structurally stable in both air and 5% $H_2$, despite the high Co-content of these materials. The values of power density in a symmetrical cell with LSGM electrolyte increased with Co-doping from 25 mW $cm^{-2}$ for x= 0 to 42.6 mW $cm^{-2}$ for x= 0.5 at 800 ºC in 3% $H_2$ [160]. These values were surprisingly low despite the thin LSGM electrolyte used ~200 μm (**Table 2**). In contrast, the $Sr_2Fe_{1.3}Co_{0.2}Mo_{0.5}O_{6-\delta}$-GDC composite electrode showed surprisingly low ASR values of 0.036 and 0.047 Ω $cm^2$ at 850 ºC in air and $H_2$, respectively, and a MPD of 986 mW $cm^{-2}$ at the same temperature [161]. $Sr_2FeCo_{0.5}Mo_{0.5}O_{6-\delta}$ also showed a high conversion of $H_2S$ into $SO_2$ and no obvious degradation was observed when the cell was fueled with 0.05% $H_2S$-$N_2$ gas at 800 ºC [162]. A complete substitution of Fe by Co was also tested, $Sr_2Co_{1+x}Mo_{1-x}O_{6-\delta}$ (x= 0.1, 0.15 and 0.2) [163], although dos Santos *et al.* reported decomposition of $Sr_2CoMoO_{6-\delta}$ into a mixture of double-perovskite, $Sr_3MoO_6$ and Co-metal above 800 ºC in 5% $H_2$ atmosphere [164].

Gou *et al.* also studied the influence of Nb-doping in SFM; the composition $Sr_2Fe_{1.4}Nb_{0.1}Mo_{0.5}O_{6-\delta}$ showed slightly higher conductivity values in both air and $H_2$, as well as ASR values of 0.098 Ω $cm^2$ in air and 1.5 Ω $cm^2$ in 5% $H_2$-Ar at 800 ºC, which were relatively lower than those observed for the undoped SFM, 0.134 and 2.0 Ω $cm^2$, in air and 5%-Ar [153]. In another study, a related Sr-deficient electrode, $Sr_{1.9}FeNb_{0.9}Mo_{0.1}O_{6-\delta}$, was

prepared and impregnated with Pd nanoparticles to improve its electrocatalytic activity [165]. The ASR values decreased from 0.469 to 0.097 Ω $cm^2$ in air at 800 ºC after Pd-impregnation (Table 2). An LSGM- electrolyte supported cell achieved an MPD of 935 and 196 mW $cm^{-2}$ at 850 ºC in $H_2$ and $CH_4$, respectively

Ca-doping has also been proposed to enhance the electronic conductivity of SFM in reducing conditions, [166]. The conductivity of $Sr_{2-x}Ca_xFe_{1.5}Mo_{0.5}O_{6-\delta}$ ($x \leq 0.5$) series in wet $H_2$ increased from 39.9 S to 55.68 S $cm^{-1}$ for x=0 and x=0.25, respectively. The best electrochemical properties were found for x= 0.25 with very low ASR values at 800 ºC of 0.094 and 0.198 Ω $cm^2$, in air and $H_2$, respectively (**Fig. 4a-c**).

Fe was also substituted by Mn in SFM, the $Sr_2MnMoO_{5+\delta}$ (SMM) symmetrical electrode was infiltrated into a porous NiO-SDC scaffold, showing *in-situ* exsolution of $SrMoO_4$ nanoparticles. The symmetrical cell SMM-NiO-SDC|SDC|NiO-SDC-SMM rendered an MPD of 245 mW $cm^{-2}$ in $CH_4$ and 183 mW $cm^{-2}$ in $C_2H_5OH$ at 800 ºC. However, a long-term stability test during 320 h revealed an increase of the cell resistance due to detrimental carbon deposition [167].

### 3.2. $K_2NiO_4$-type, $PrBa(Mn,Fe)_2O_{5+\delta}$ and other layered perovskites

In recent years, several double perovskites and Ruddlesden-Popper (RP) type electrodes such as $GdBaCo_2O_{5+\delta}$, $PrBaCo_2O_{5+\delta}$, and $La_2NiO_{4+\delta}$ have demonstrated excellent electrochemical properties for ORR but poor redox stability to be used as fuel electrodes [36,168,169]. In the same way as single perovskite-type electrodes, the redox stability of these materials has been improved through adequate doping to be used in SSOCs (**Table 2)**.

The Ruddlesden-Popper structure (RP), with a general $A_{n+1}B_nO_{3n+1}$ (n= 1, 2…) structure, is composed of perovskite layers ($ABO_3$) and rock salt layers (AO) alternately ordered along the c-axis, where *n* represents the number of consecutive perovskite layers that are sandwiched between two rock-salt layers [170]. Among the different electrodes with this structure, $La_{0.6}Sr_{1.4}MnO_{4\pm\delta}$ (n= 1) has demonstrated good redox stability up to 900 ºC in diluted $H_2$ for application in SSOCs [171]. However, the first studies reported high ASR values of 0.87 Ω $cm^2$ in air and 2.07 Ω $cm^2$ in 5% $H_2$. Sandoval *et al.* further studied the $La_xSr_{2-x}MnO_{4\pm\delta}$ series ($0.25 \leq x \leq 0.6$) and the highest values of conductivity were found for $La_{0.5}Sr_{1.5}MnO_{4\pm\delta}$, *i.e.* 35.6 S $cm^{-1}$ in air and 1.9 S $cm^{-1}$ in 3% $H_2$-Ar at 800 ºC [172]. Later on, the same group concluded that a protective GDC barrier layer is needed to avoid the formation of reaction products at the electrode/electrolyte interface when YSZ or LSGM are used as electrolytes due to interdiffusion of Sr [173,174].

Shen *et al.* proposed two different infiltration methods to improve the electrochemical properties of $La_{0.6}Sr_{1.4}MnO_{4+\delta}$ symmetrical electrodes. In the first work, a $La_{0.6}Sr_{1.4}MnO_{4+\delta}$ porous scaffold was coated by SDC and NiO nanoparticles by infiltration. The $La_{0.6}Sr_{1.4}MnO_{4+\delta}$-SDC-NiO composite electrode showed excellent electrochemical activity in both oxidizing and reducing atmospheres with an MPD of 614 and 378 mW $cm^{-2}$ at 800 ºC with $H_2$ and $CH_4$ fuels, respectively [175]. In a second report, a SDC scaffold was infiltrated

with $La_{0.6}Sr_{1.4}MnO_{4+\delta}$ and NiO nanoparticles [176], obtaining an MPD of 714 mW $cm^{-2}$ at 800 ºC. The improved MPD achieved for $La_{0.6}Sr_{1.4}MnO_{4+\delta}$-NiO impregnated into SDC was attributed to the higher oxide-ion conductivity of the SDC scaffold compared to the $La_{0.6}Sr_{1.4}MnO_{4+\delta}$ skeleton with predominant electronic conductivity, as well as the higher electrocatalytic activity of $La_{0.6}Sr_{1.4}MnO_{4+\delta}$ nanoparticles for both ORR and fuel oxidation.

A related composition with Fe instead of Mn, $La_{0.8}Sr_{1.2}FeO_{4+\delta}$, revealed a good stability in both oxidizing and reducing atmospheres. Unfortunately, high ASR values of 1.85 and 5.82 Ω $cm^2$ were found in air and 5%-$H_2$-Ar at 800 ºC, respectively, presumably attributed to the high synthesis temperatures ~1380 ºC, resulting in excessive grain growth and poorer performance [177]. In another study, Ling *et al.* studied the influence of La-doping in an oxygen-deficient RP-type structure, $Sr_3Fe_2O_{7+\delta}$ (n= 2), obtaining new electrodes for SSOFCs with $La_xSr_{3-x}Fe_2O_{7-\delta}$ (x= 0, 0.25 and 0.5) composition. The partial substitution of Sr with La improved both the electrical conductivity and electrochemical performance, obtaining the best MPD for x= 0.5 with a value of 480 mW $cm^{-2}$ at 800 ºC in $H_2$ on YSZ/GDC electrolyte [178].

Other RP-type electrodes have been reported in recent years. For instance, Durán *et al*. studied the $La_4BaMn_5O_{13+\delta}$ (n= 4) electrode, which showed good redox stability and chemical stability with barium zirconate proton-based conductor electrolytes [179]. Preliminary results showed high conductivity values at 800 ºC, *i.e.* 178 and 33 S $cm^{-1}$ in air and $H_2$, respectively.

Double perovskites have traditionally been tested as air or fuel electrodes independently [180–182], but recently some compositions have also been implemented in SSOCs. Among them, $PrBaMn_2O_{5+\delta}$ (PBMO) is one of the most promising symmetrical electrodes due to its remarkable redox stability and high tolerance to carbon coking and $H_2S$ poisoning. Furthermore, an excellent catalytic activity has been demonstrated when fueled with hydrocarbons [182]. It has to be noted that $PrBaMn_2O_{5+\delta}$ double perovskite is typically obtained after reduction of $Pr_{0.5}Ba_{0.5}MnO_{3-\delta}$ single perovskite [182,183]. Preliminary results on PBMO infiltrated into LSGM revealed that BaO and $Pr_2O_3$ secondary phases appeared when calcined in air at 1000 ºC but not reaction was observed at lower temperatures [183]. Recently, $Pr_6O_{11}$ nanoparticles were infiltrated into a PBMO scaffold and the ASR values decreased significantly from 0.25 to 0.016 Ω $cm^2$ in air and from 0.46 to 0.20 Ω $cm^2$ in $H_2$ at 800 ºC [184].

An alternative composition with Ca-doping, $PrBa_{0.8}Ca_{0.2}Mn_2O_{5+\delta}$, was proposed as a highly efficient and fuel versatile electrode for SSOC [185]. In order to improve the electrode performance, a 15 wt.% of $Co_{0.5}Fe_{0.5}$ catalyst was infiltrated in both air and fuel electrodes. No secondary phases were found after annealing the electrodes in air and $H_2$ at 800 ºC. A LSGM supported cell with a $CeO_2$-based protective layer rendered MPDs of 1101, 740 and 470 mW $cm^{-2}$ in $H_2$, $CH_4$ and $C_8H_{18}$, respectively, at 800 ºC; and an excellent carbon coking tolerance was observed after 250 h of stability test.

In another study, Chen *et al.* tested the layered perovskites $PrBaFe_2O_{5+\delta}$ and $PrBaFe_{1.6}Ni_{0.4}O_{5+\delta}$ as symmetrical electrode [186]. The Ni-doped electrode showed surprisingly low ASR values of 0.034 Ω $cm^2$ at

650 ºC in $H_2$, possibly due to Ni-exsolution, which was not confirmed by additional experiments such as XRD and SEM. A Mo-doping strategy was also tested in $(PrBa)_{0.95}(Fe_{0.9}Mo_{0.1})_2O_{5+\delta}$, rendering a high and stable MPD of 1050 and 400 mW $cm^{-2}$ in $H_2$ and $CH_4$, respectively, at 800 ºC for 1060 h [187]. Zhang *et al.* observed similar results with W-doping, $(PrBa)_{0.95}(Fe_{0.95}W_{0.05})_2O_{5+\delta}$, achieving ASR values of 0.031 and 0.12 Ω $cm^2$ in air and $H_2$, respectively, at 800 ºC (**Fig. 4d-f**). In addition, high power outputs were achieved when fueled with hydrocarbons: 610, 624 and 448 mW $cm^{-2}$ at 800 ºC for syngas, ethane and propane, respectively [188]. Other similar compositions such as $PrBa(Fe_{0.8}Sc_{0.2})_2O_{5+\delta}$ [189] and $(PrBa)_{0.95}(Fe_{0.9}Mo_{0.1})_2O_{5+\delta}$-SDC [190] have also demonstrated promising results as SSOC electrodes (**Table 2**).

The $GdBaFe_2O_{5+\delta}$ double perovskite also showed excellent phase stability in both oxidizing and reducing conditions up to 900 ºC, as well as a remarkable resistance to carbon deposition [191]. The ASR values were 0.073 Ω $cm^2$ in air and 1.91 Ω $cm^2$ in $H_2$ at 800 ºC on a LSGM electrolyte supported cell with SDC protective inlayer. Power outputs of 858, 696 and 101 mW $cm^{-2}$ using $H_2$, wet syngas and wet $CH_4$, respectively, were measured at 800 ºC.

Recently, $SmBaMn_{1.9}Mg_{0.1}O_{5+\delta}$ electrodes with orthorhombic and tetragonal symmetry in air and $H_2$ atmosphere, respectively, were tested as symmetrical electrodes rendering ASR values of 0.296 and 0.67 Ω $cm^2$ in air and $H_2$, respectively, at 800 ºC. Redox tests revealed that the Mg-doping considerably reduced the chemical-induced expansion, improving the thermomechanical compatibility with the LSGM electrolyte. The LSGM-supported cell showed a MPD of 317 mW $cm^{-2}$ at 800 ºC [192].

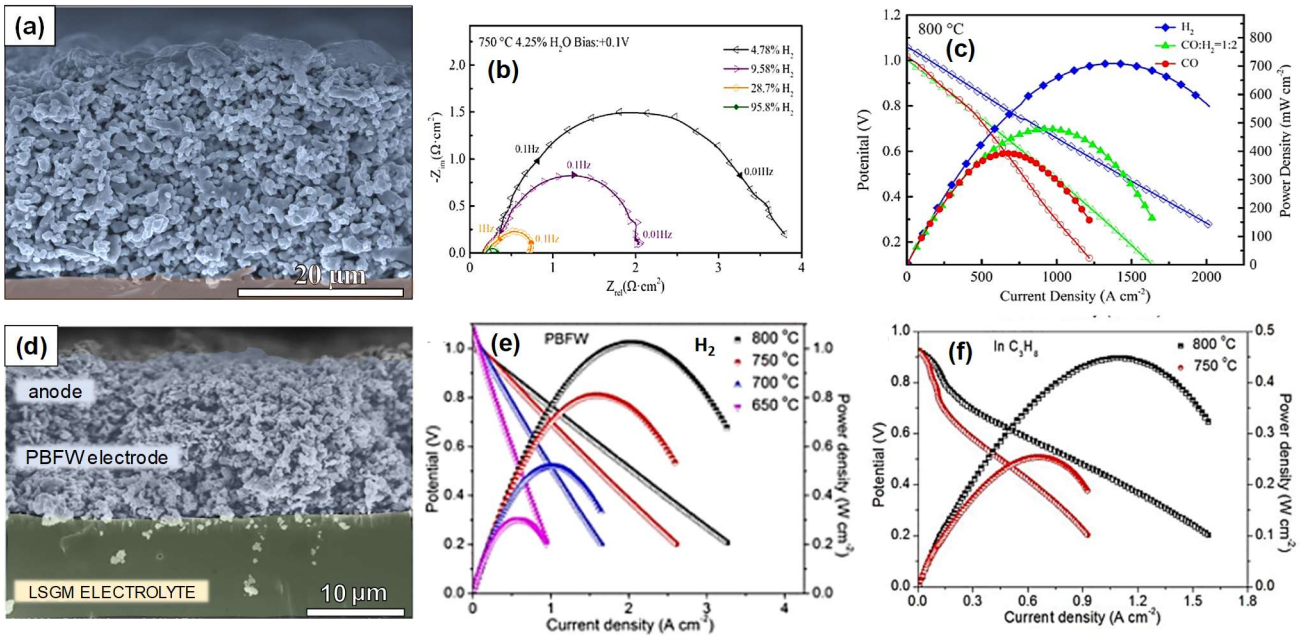


**Figure 4.** (a) SEM image of $Sr_{1.75}Ca_{0.25}Fe_{1.5}Mo_{0.5}O_{6-\delta}$ electrode on LSGM electrolyte, (b) Nyquist spectra under different hydrogen partial pressures ($pH_2$) and (c) I-V-P curves of the LSGM-supported symmetrical cell at 800 ºC with different fuels. Reprinted with permission, Elsevier [166]. (d) SEM image of the PBFM electrode on LSGM, (e,f) I-V-P curves of the symmetrical cell at different temperatures when $H_2$ and $C_3H_8$ were used as fuels, respectively. Reprinted with permission, Elsevier [188].

**Table 2.** Most relevant symmetrical electrodes within layered perovskite-type structure. Area specific resistance (in air and $H_2$) and power/current densities are given at 800 ºC. In those case, where not data are available at 800 ºC, the temperature is included.

| Electrode | Abbreviation | $ASR^{air}$ ($\Omega$ cm$^2$) | $ASR^{H_2}$ ($\Omega$ cm$^2$) | P (mW cm$^{-2}$) | Electrolyte | Ref. |
|---|---|---|---|---|---|---|
| *$Sr_2Fe_{1.5}Mo_{0.5}O_{6-\delta}$-type* | | | | | | |
| $Sr_2Fe_{1.5}Mo_{0.5}O_{6-\delta}$ | SFM | 0.24 | 0.27 | $650^{850ºC}$ ($H_2$)<br>$100^{850ºC}$ ($CH_4$) | LSGM | [24] |
| $Sr_2Fe_{1.4}Nb_{0.1}Mo_{0.5}O_{6-\delta}$ | SFNM | 0.098 | 1.5 (5% $H_2$) | 531.5 ($H_2$) | LSGM | [153] |
| $Sr_2Fe_{1.5}Mo_{0.5}O_{6-\delta}$-SDC | SFM-SDC | 0.29 | 0.12 | 220 ($H_2$) | LSGM | [154] |
| $Sr_2Fe_{1.5}Mo_{0.5}O_{6-\delta}$ | SFM | 0.5 | 1 | 1.4 A cm$^{-2}$ $^{900ºC}$ (at 1.3V) | YbScSZ | [159] |
| $Sr_2FeCo_{0.5}Mo_{0.5}O_{6-\delta}$ | SFCM | - | - | 42.6 (3%-$H_2$) | LSGM | [160] |
| $Sr_2Fe_{1.3}Co_{0.2}Mo_{0.5}O_{6-\delta}$ -GDC | SFCM-GDC | 0.036 | $0.047^{850ºC}$ | 986 ($H_2$) | LSGM | [161] |
| $Ca_{0.25}Sr_{1.75}Fe_{1.5}Mo_{0.5}O_{6-\delta}$ | CaSFM | 0.094 | 0.198 | 709 ($H_2$)<br>480 (syngas)<br>392 (CO) | LSGM | [166] |
| $Sr_2MnMoO_{5+\delta}$ | $SMMO_5$ | - | - | 245 ($CH_4$)<br>183 ($C_2H_5OH$) | SDC | [167] |
| *$K_2NiO_4$-type and PrBa(Mn,Fe)$_2O_{5+\delta}$* | | | | | | |
| $La_{0.4}Sr_{1.6}MnO_{4\pm\delta}$ | $LSMO_4$ | 0.87 | 2.07 | 59 ($H_2$) | LSGM | [171] |
| $La_{0.4}Sr_{1.6}MnO_{4\pm\delta}$ – NiO-SDC | $LSMO_4$ | $0.17^{700\ ºC}$ | - | 614 ($H_2$)<br>378 ($CH_4$) | SDC | [175] |
| $La_{0.8}Sr_{1.2}FeO_4$ | $LSFO_4$ | 1.85 | 8 | 73 ($H_2$) | LSGM | [177] |
| $La_{0.5}Sr_{2.5}Fe_2O_{7-\delta}$- GDC | $LSFO_7$-GDC | - | - | 480 ($H_2$) | YSZ/GDC | [178] |
| $PrBaMn_2O_{5+\delta}$ - $Pr_6O_{11}$ | $PBMO_5$-$Pr_6O_{11}$ | 0.016 | 0.20 | 423 ($H_2$)<br>227 ($CH_4$) | YSZ | [184] |
| $PrBa_{0.8}Ca_{0.2}Mn_2O_{5+\delta}$ | $PBCaMO_5$ | - | - | 1101 ($H_2$)<br>740 ($CH_4$)<br>470 ($C_8H_{18}$) | LSGM | [185] |
| $(PrBa)_{0.95}(Fe_{0.9}Mo_{0.1})_2O_{5+\delta}$ | $PBFMO_5$ | 0.027 | 0.074 (5% $H_2$)<br>0.86($CH_4$) | 1050 ($H_2$)<br>400 ($CH_4$) | LSGM | [187] |
| $(PrBa)_{0.95}(Fe_{0.95}W_{0.05})_2O_{5+\delta}$ | $PBFWO_5$ | 0.031 | 0.12 | 1020 ($H_2$)<br>610 (syngas)<br>624 ($C_2H_6$)<br>448 ($C_3H_8$) | LSGM | [188] |
| $PrBa(Fe_{0.8}Sc_{0.2})_2O_{5+\delta}$ | $PBFSO_5$ | 0.05 | 0.18 | 713 ($H_2$)<br>$275^{900\ ºC}$ ($CH_4$) | LSGM | [189] |
| $(PrBa)_{0.95}(Fe_{0.9}Mo_{0.1})_2O_{5+\delta}$-SDC | $PBFMO_5$-SDC | - | - | 0.51 A cm$^{-2}$ $^{800ºC}$ (at 1.3V) | LSGM | [190] |
| $GdBaFe_2O_{5+\delta}$ | $GBFO_5$ | 0.073 | 1.911 | 858 ($H_2$)<br>696 (syngas)<br>101 ($CH_4$) | LSGM/SDC | [191] |
| $SmBaMn_{1.9}Mg_{0.1}O_{5+\delta}$ | $SBMMO_5$ | 0.296 | 0.67 | 317 ($H_2$) | LSGM | [192] |

## 4. Electrodes with exsolved metal nanoparticles

A wide variety of oxide materials decorated with active metal nanoparticles have exhibited improved catalytic performance for different energy applications [39,193]. In particular, metal exsolution is a promising approach to improve the fuel oxidation properties of SOFC electrodes [194]. Moreover, the bimetallic nanoparticles have recently demonstrated to be even more interesting than single-metal nanoparticles due to the synergistic effects of the different metals, being Fe-Ni and Fe-Co the most employed systems [195]. Several strategies have been implemented to promote metal exsolution in oxide materials, such as A-site deficiency in perovskites, a phase transformation during reduction, cation exsolution induced by lattice strain, and by applying a DC bias [39,196]. In general, the exsolution is a reversible process during the oxidation/reduction cycles, producing finer and higher dispersion of nanoparticles on the electrode surface in comparison to nanoparticles deposited by wet-infiltration, thereby exhibiting lower particle agglomeration and improved durability [197]. Moreover, the possible deactivation of the nanoparticles due to carbon and sulfur depositions could be reverted by oxidizing the fuel electrode, a fact that makes these materials potential candidates for SSOCs. The following three subsections are dedicated to study symmetrical electrodes with different exsolved metal particles, where the main compositions and properties are summarized in **Table 3**.

### 1.1. Symmetrical electrodes with Ni and Ni-Fe exsolution

Nickel-doped materials are among the most investigated fuel electrodes due to their ability to form Ni nanoparticles in reducing conditions with improved electrocatalytic activity for $H_2$ and hydrocarbon oxidation [198–200]. One of the first attempts was performed with the traditional LSCM symmetrical electrode by partially substituting Mn or Cr by Ni. For instance, $La_{0.75}Sr_{0.25}Cr_{0.5-x}Ni_xMn_{0.5}O_{3-\delta}$ (x= 0.06 and 0.2) and $La_{0.75}Sr_{0.25}Cr_{0.5}Mn_{0.5-x}Ni_xO_{3-\delta}$ (x= 0-0.3) series showed Ni-exsolved nanoparticles after reducing in $H_2$ [201,202] (**Table 3**).

The Ni-doped strategy has also been widely employed in (La,Sr)$FeO_3$-based SSOC electrodes, showing either Ni or Ni-Fe exsolved nanoparticles depending on the reducing conditions. For instance, Tian *et al.* reported *in-situ* exsolved Ni-Fe nanoparticles in $La_{0.6}Ca_{0.4}Fe_{0.8}Ni_{0.2}O_{3-\delta}$-$Ce_{0.9}Gd_{0.1}O_{1.95}$ composites, which greatly improved the electrochemical properties of the fuel electrode. The ASR values in air, $H_2$ and $CO_2$ were 0.24, 0.13 and 0.47 Ω $cm^2$ at 800 ºC, respectively. A YSZ-supported cell showed a MPD of 300 mW $cm^{-2}$ at 800 ºC in $H_2$ [203]. A related composition with Ce-doping, $La_{0.6}Ce_{0.1}Sr_{0.3}Fe_{0.9}Ni_{0.1}O_{3-\delta}$, showed a drastic enhancement of the performance in wet $CH_4$ compared to the undoped electrode, 522 and 221 mW $cm^{-2}$, respectively, on a LSGM electrolyte at 850 ºC [204]. This is one of the best results reported in the literature for hydrocarbon fueled SSOFCs, confirming the high catalytic activity of Ce-doped materials under $CH_4$ operation.

Different Ti-based perovskites have also been doped with Ni to combine the high redox stability of titanate based materials with Ni-exsolution. The conductivity of $La_{0.875}Sr_{0.125}Ti_{1-x}Ni_xO_3$ (LSTNx) series increased in air with increasing Ni-content, from $2.8\times10^{-3}$ S $cm^{-1}$ for LSTN0.1 to $3.5\times10^{-2}$ S $cm^{-1}$ for LSTN0.5 at 800 ºC, while

it drastically decreased in reducing conditions, from 0.7 S $cm^{-1}$ for LSTN0.1 to $2.6\times10^{-4}$ S $cm^{-1}$ for LSTN0.5 at 800 ºC [205]. The nickel exsolution was further studied by the same research group, concluding that this process was limited by the slow reduction kinetics at 800 ºC in diluted $H_2$ [206].

A related Ni-doped ferrite, $La_{0.7}Sr_{0.3}Ti_{0.1}Fe_{0.6}Ni_{0.3}O_3$, showed a maximum conductivity of 318 and 1.1 S $cm^{-1}$ at 700 ºC in air and $H_2$, respectively, and low ASR values of 0.05 and 0.20 Ω $cm^2$ in air and $H_2$, respectively; however, the authors did not find any signs of Ni exsolution after 24 h reduction at 800 ºC by XRD and X-ray photoelectron spectroscopy [207]. In another study, $La_{1-x}Sr_xFe_{0.7}Ni_{0.3}O_{3-\delta}$ (LSFNx) series (x= 0, 0.1 and 0.2) were reduced at 800 ºC and Ni-exsolution was not detected by XRD; however, high-resolution TEM revealed the presence of Ni-metal on the electrode surface [208]. Hence, the discrepancies between both works seem to be associated with the different characterization techniques employed, implying that high-resolution electron microscopy techniques are needed to identify these highly dispersed metal nanoparticles.

Recently, A-site deficient $(La_{0.7}Sr_{0.3})_{1-x}(Fe_{0.7}Ti_{0.3})_{0.9}Ni_{0.1}O_{3-\delta}$ (x= 0.1, 0.2 and 0.3) single perovskites were explored as symmetrical electrodes [209]. The best results were found for x= 0.3 with ASR values of 0.043 and 0.17 Ω $cm^2$ in air and $H_2$, respectively. The influence of Ca- and Ba-doping in $La_{0.7}A_{0.3}Ti_{0.5}Mn_{0.4}Ni_{0.1}O_3$ (A= Ca and Ba) was studied, where Ca-doped electrode showed $La_2O_3$ segregation and also higher performance than the corresponding Ba-doped electrode [210].

An improvement of the electrochemical properties has also been achieved in Ni-doped SFM double perovskite. Osinkin *et al.* observed a higher electrochemical activity in both oxidizing and reducing conditions for $Sr_{1.95}Fe_{1.4}Ni_{0.1}Mo_{0.5}O_{6-\delta}$ due to Ni-Fe exsolution after a heat treatment at 800 ºC in wet $H_2$ [211]. A LSGM supported cell showed an MPD of 500 mW $cm^{-2}$ at 800 ºC in $H_2$.

Xu *et al.* tested the influence of Ni-metal exsolution in the $La_{0.5}Sr_{1.5}(MnNi_{0.1})O_{4+\delta}$-SDC composite electrode [212] (**Fig. 5a,b**). The excess of Ni in the B-site of the RP-type structure slightly increased the activity for ORR and greatly enhanced the performance for HOR, although the ASR values in 5% $H_2$-Ar were rather high (**Table 3**).

### 1.2. Symmetrical electrodes with Fe and Fe-Co exsolution

Fe-Co nanoparticle exsolution has been extensively studied in fuel electrodes for SOCs, as it confers improved stability, coking/sulfur tolerance, as well as high electrocatalytic activity for fuel oxidation [195]. Electrode materials with high Fe-Co-content usually exhibit a phase transformation in $H_2$ from single perovskite to RP-type structure, which is accompanied by exsolution of metal nanoparticles [194,196]. Since no severe phase change occurs during this process, these electrodes are classified into electrodes with exsolved metal particles instead of quasi-symmetrical electrodes (Q-SSOC).

The first studies were performed in traditional air electrodes, such as LSCF, by adequate doping in the B-site of the perovskite to enhance the redox stability [213,214]. For instance, Song *et al.* studied the $La_{0.4}Sr_{0.6}Fe_{0.7}Ti_{0.3-x}Co_xO_{3-\delta}$ (LSFTC, x= 0-0.2) series, which transform into a mixture of perovskite, RP-type

phase and Fe-Co metallic nanoparticles in $H_2$ [214]. A similar behavior was observed for $La_{0.4}Sr_{0.6}Co_{0.2}Fe_{0.7}Nb_{0.1}O_{3-\delta}$ [213] and $Pr_{0.4}Sr_{0.6}Co_{0.2}Fe_{0.7}Nb_{0.1}O_{3-\delta}$ [215] (**Table 3**). Later on, A-site deficient $(Pr_{0.4})_xSr_{0.6}Co_{0.2}Fe_{0.7}Nb_{0.1}O_{3-\delta}$ ($x$= 0.9 ≤ x ≤ 1.1) was tested in SSOFCs, showing the composition of x= 1.05 the lowest ASRs in both air (0.025 Ω $cm^2$) and $H_2$ (0.2 Ω $cm^2$) at 800 ºC [216], fact that is attributed to the A-site nonstoichiometric facilitating metal particle exsolution.

Zhou *et al.* prepared a layered perovskite, $La_{0.8}Sr_{1.2}Fe_{0.9}Co_{0.1}O_{4\pm\delta}$ ($LSFCO_4$), by Co-doping the pristine $La_{0.8}Sr_{1.2}FeO_{4\pm\delta}$ electrode. The ASR in air drastically decreased due to an enhancement of the mixed ionic-electronic conductivity after Co-doping, which greatly improved the electrochemical properties in reducing conditions. The $LSCFO_4$-GDC composite electrode achieved ASR values of 0.21 Ω $cm^2$ in air and 0.93 Ω $cm^2$ in 5% $H_2$, while a MPD of 325 mW $cm^{-2}$ was obtained at 800 ºC in $H_2$ on a LSGM electrolyte supported cell [217]. $LaSr_3Fe_2CoO_{10-\delta}$ (n= 3) with RP-type structure was also studied, which showed negligible degradation during 100 h of operation at 700 ºC and reached a MPD of 351 mW $cm^{-2}$ at 800 ºC in $H_2$ in a YSZ-supported cell [218]. Another RP-type electrode was investigated by Chung *et al.*, $La_{1.2}Sr_{0.8}Mn_{0.4}Fe_{0.6}O_{4\pm\delta}$ -GDC, which transformed after reduction into $La_{0.6}Sr_{0.4}Mn_{0.2}Fe_{0.8}O_{3-\delta}$ single perovskite, a process that was fully reversible. The phase transformation was accompanied by Fe-exsolution, showing the LSGM-supported cell a MPD of 770 mW $cm^{-2}$ at 800 ºC in $H_2$ [219].

$Sr_2Co_{0.4}Fe_{1.2}Mo_{0.4}O_{6-\delta}$ double perovskite also showed a phase transformation after reduction into $Sr_3Co_{0.1}Fe_{1.3}Mo_{0.6}O_{7-\delta}$ (n= 2) RP-type phase with Co-Fe nanoparticles distributed on the electrode surface, being this process reversible after calcining at 900 ºC in an oxidizing environment [27] (**Table 3**). In contrast, $Sr_2Ti_{0.8}Co_{0.2}FeO_6$ double perovskite also showed Co-Fe nanoparticles in reducing conditions but without any phase transformation [220]. Recently, a similar double perovskite, $Sr_2ScTi_{0.5}Mo_{0.5}O_6$, presented excellent electrochemical activity for ORR and HOR, which the authors attributed to Ti-metal exsolution [221]. High stability was reported by employing *in-operando* gas switching between $CH_4$ and air, reaching an MPD of 218 mW $cm^{-2}$ at 800 ºC in $CH_4$.

Other highly reducible transition metals have been investigated for metal exsolution in SSOFC electrodes, the A-deficient $(La_{0.6}Sr_{1.4})_{0.95}Mn_{1-x}B_xO_4$ (x= 0 and 0.1, B= Co, Ni and Cu) Ruddlesden-Popper phases achieved Co, Ni and Cu nanoparticle exsolution after reduction [222]. Higher electrical conductivity with lower activation energy was achieved for the B-site doped materials, obtaining the lowest ASR values for $(La_{0.6}Sr_{1.4})_{0.95}Mn_{0.9}Cu_{0.1}O_4$-SSZ composite electrode (**Table 3**).

### 1.3. Symmetrical electrodes with exsolution of noble metals

Among the different noble metals for particle exsolution, Ru has demonstrated to be a promising alternative to Ni due to its higher catalytic activity towards hydrocarbon oxidation, better thermal stability and coking resistance [223,224]. In particular, Barnett *et col.* compared the influence of Ni- and Ru-doping on $La_{0.75}Sr_{0.25}Cr_{1-x}M_xO_{3-\delta}$, (M= Ni and Ru, x< 0.31) for their implementation as anode material [223]. After a stability test at 800 ºC for 300 h, Ru-doped samples showed higher nanoparticle concentration, better thermal

stability and finer grain size (5 nm diameter) compared to Ni-doped samples (~50 nm diameter), findings that explain the better electrochemical performance of Ru-doped electrodes. For that reason, Ru-doping strategy has been proposed to enhance the electrochemical properties of several SSOC electrodes in reducing conditions, despite its higher prize in comparison with Ni [224-230]. For instance, a Ru/Ce-codoped, $SrFeO_3$, was also investigated as symmetrical electrode [225]. $Sr_{0.8}Ce_{0.2}FeO_{3-\delta}$ was a single phase at 1250 ºC, but $CeO_2$ segregation was found during the cooling process in air. The Ru/Ce-codoping in $Sr_{0.8}Ce_{0.2}Fe_{0.95}Ru_{0.05}O_{3-\delta}$ stabilized the perovskite structure in air, but SrO, $CeO_2$ and Ru-metal nanoparticles were observed after reduction due to superficial electrode decomposition. The formation of multiple phases on the electrode surface limited the grain growth and was the responsible of the very small size of the Ru particles ~10 nm. Remarkable power densities were obtained in a symmetrical LSGM supported cell, *i.e.* 846 and 310 mW $cm^{-2}$ at 800 ºC for $H_2$ and $C_3H_8$, respectively (**Fig. 5c,d**). The authors concluded that the exsolution of Ru-metal was critical for $H_2$ oxidation, the $CeO_2$ helped the absorption of propane molecules, while SrO improved the coke resistance in hydrocarbon fuels.

The influence of Ru-doping in the A-deficient $(La_{0.8}Sr_{0.2})_{0.9}Mn_{0.8-x}Sc_{0.2}Ru_xO_{3-\delta}$ perovskite was also studied by Zhou *et al.* [226]. Despite Ru nanoparticles were only detected after reduction in the fuel electrode, the electrochemical performance was greatly improved in both air and 5% $H_2$, with ASR values of 0.23 and 0.52 Ω $cm^2$, respectively, at 800 ºC. Similarly, a Ru-doped strategy has been employed to promote the formation of oxygen vacancies in $SmFeO_3$ orthorhombic perovskite. The composition $Sm_{0.9}Sr_{0.1}Fe_{0.9}Ru_{0.1}O_{3-\delta}$ (SSFR) showed excellent redox stability, but the exsolution of Fe-Ru nanoparticles in reducing conditions was not investigated [227]. The MPD of the SSFR|SDC|SSFR cell was 119 mW $cm^{-2}$ at 800 °C in $H_2$. In contrast, a similar A-site deficient perovskite symmetrical electrode, $Sm_{0.70}Sr_{0.20}Fe_{0.80}Ti_{0.15}Ru_{0.05}O_{3-\delta}$, showed Ru exsolution in reducing conditions, contrary to that of the A-site stoichiometric composition, demonstrating the importance of A-site deficiency on the exsolution of metal particles in B-site. The Ru-exsolution was linked to the lower ASR values, *i.e.* 0.13 and 0.11 Ω $cm^2$ in air and 5% $H_2$ at 800 ºC, respectively, slightly lower than those observed for the stoichiometric electrode 0.24 and 0.37 Ω $cm^2$ in air and 5% $H_2$, respectively [228].

Pd-doping has also been investigated to enhance the electrochemical activity of SSOC electrodes in reducing conditions. Marcucci *et al.* studied the effect of Pd-doping in $La_{0.6}Sr_{0.4}Fe_{0.95}Pd_{0.05}O_{3-\delta}$ electrode (LSFPd). A reversible partial phase transformation was observed from a single perovskite to a mixture of phases, including a RP-type structure, Pd and Fe nanoparticles, upon switching between oxidizing and reducing conditions [229]. The influence of GDC addition on the electrochemical properties of LSFPd was also investigated; the ASR values in air increased from 0.21 Ω $cm^2$ for LSFPd to 0.91 Ω $cm^2$ for LSFPd-GDC composite at 750 ºC, while a drastic decrease was observed in $H_2$ from 5.69 to 0.08 for LSFPd and LSFPd-GDC, respectively. The main role of GDC was to provide morphological and microstructural stability under reducing conditions, as well as to improve the charge transfer and $H_2$ oxidation reactions due to its high ionic and electronic conductivity. The LSFPd-GDC/LSGM/LSFPd cell rendered an MPD of 350 mW $cm^{-2}$ in $H_2$ at 750 ºC, higher than those observed for the Pd-free symmetric cell (268 mW $cm^{-2}$) measured under the same

operating conditions. These findings confirmed that Pd-exsolution is a promising approach to promote the electrocatalytic properties in the anode.

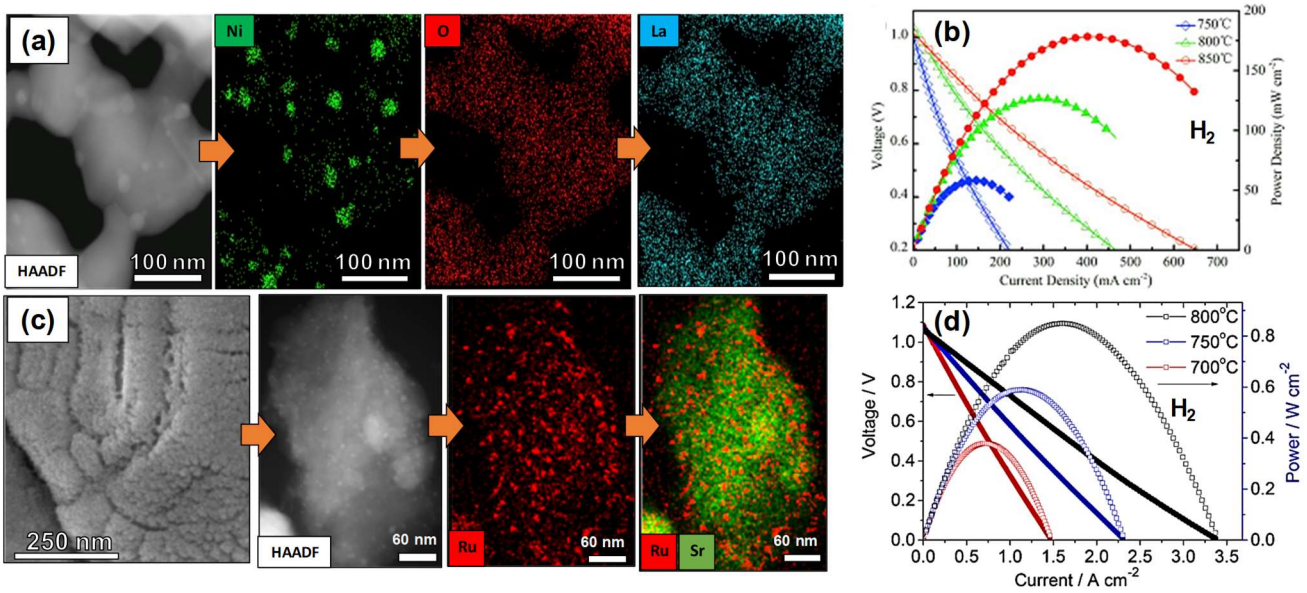


**Figure 5.** (a) STEM images of the reduced $(La_{0.5}Sr_{1.5}Mn)Ni_{0.1}O_{4+\delta}$ electrode, showing exsolution of Ni nanoparticles, and (b) I-V-P curves of the $(La_{0.5}Sr_{1.5}Mn)Ni_{0.1}O_{4+\delta}$-SDC symmetrical electrode on LSGM electrolyte at different temperatures in $H_2$ fuel. Reprinted with permission, Elsevier [212]. (c) SEM image of $Sr_{0.8}Ce_{0.2}Fe_{0.95}Ru_{0.05}O_3$ after annealing in $H_2$ at 800 ºC and HAADF-STEM and EDS images after reduction and (d) I-V-P curves of the symmetrical cell on LSGM electrolyte at different temperatures. Reprinted with permission, American Chemical Society [225].

**Table 3.** Most relevant symmetrical electrode with metal exsolved nanoparticles. Area Specific Resistance (in air and $H_2$) and power/current densities are given at 800 ºC. In those case, where not data are available at 800 ºC, the temperature is included.

| Electrode | Abbreviation | $ASR^{air}$ ($\Omega$ cm$^2$) | $ASR^{H_2}$ ($\Omega$ cm$^2$) | P (mW cm$^{-2}$) | Electrolyte | Ref. |
|---|---|---|---|---|---|---|
| *Ni exsolution* | | | | | | |
| $La_{0.75}Sr_{0.25}Cr_{0.5}Mn_{0.3}Ni_{0.2}O_{3-\delta}$ | LSCMN | 1.6 | 1.1 (5% $H_2$-Ar) | - | YSZ | [202] |
| $La_{0.6}Ca_{0.4}Fe_{0.8}Ni_{0.2}O_{3-\delta}$-GDC | LCaFN-GDC | 0.24 | 0.13 | 300 ($H_2$) | YSZ/GDC | [203] |
| $La_{0.6}Ce_{0.1}Sr_{0.3}Fe_{0.9}Ni_{0.1}O_{3-\delta}$ | LCSFN | - | - | 650 ($H_2$)<br>200 ($CH_4$) | LSGM | [204] |
| $La_{0.7}Sr_{0.3}Ti_{0.1}Fe_{0.6}Ni_{0.3}O_{3-\delta}$ | LSTFN | 0.047 | 0.201 | 402 ($H_2$) | LSGM | [207] |
| $La_{0.7}Sr_{0.3}Fe_{0.7}Ni_{0.3}O_{3-\delta}$ | LSFN | 0.1 | 0.06 | 540 ($H_2$) | LSGM | [208] |
| $(La_{0.7}Sr_{0.3})_{0.7}(Fe_{0.7}Ti_{0.3})_{0.9}Ni_{0.1}O_{3-\delta}$ | LSFTN | $0.043^{750\,°C}$ | $0.17^{750\,°C}$ | - | LSGM | [209] |
| $La_{0.6}Sr_{0.4}Fe_{0.9}Ni_{0.1}O_{3-\delta}$-YSZ | LSFN-YSZ | - | - | $400^{750°C}$ ($C_3H_8$)<br>$230^{750°C}$ ($CH_4$) | YSZ | [230] |
| $Sr_{1.95}Fe_{1.4}Ni_{0.1}Mo_{0.5}O_{6-\delta}$ | SFNM | 0.08 | 0.11 | 500 ($H_2$) | LSGM | [211] |

| | | | | | | |
|---|---|---|---|---|---|---|
| $(La_{0.5}Sr_{1.5}Mn)Ni_{0.1}O_{4+\delta}$-SDC | $LSMNO_4$-SDC | 0.6 | 3.51 | 126 ($H_2$) | LSGM | [212] |
| *Fe-Co exsolution* | | | | | | |
| $La_{0.4}Sr_{0.6}Co_{0.2}Fe_{0.7}Nb_{0.1}O_{3-\delta}$ | LSCFN | - | - | $500^{850\,°C}$ ($H_2$) | LSGM | [213] |
| $La_{0.4}Sr_{0.6}Fe_{0.7}Ti_{0.25}Co_{0.05}O_{3-\delta}$ | LSFTC | $0.1^{750\,°C}$ | $0.4^{750\,°C}$ | $450^{850\,°C}$ ($H_2$) | LSGM | [214] |
| $Pr_{0.4}Sr_{0.6}Co_{0.2}Fe_{0.7}Nb_{0.1}O_{3-\delta}$ | PSCFNb | 0.075 | - | 960 ($H_2$)<br>600 ($CH_4$)<br>940 ($C_3H_8$) | LSGM | [215] |
| $La_{0.8}Sr_{1.2}Fe_{0.9}Co_{0.1}O_{4\pm\delta}$-GDC | $LSFCO_4$-GDC | 0.21 | 0.93<br>(5% $H_2$-Ar) | 325 ($H_2$) | LSGM | [217] |
| $Sr_2Co_{0.4}Fe_{1.2}Mo_{0.4}O_{6-\delta}$ | $SCFMO_4$ | 0.055 | 0.14 | 802 ($H_2$)<br>271 ($CH_4$) | LSGM | [27] |
| $LaSr_3Fe_2CoO_{10-\delta}$ | $LSFCO_{10}$ | - | - | 351 ($H_2$) | YSZ/GDC | [218] |
| $La_{1.2}Sr_{0.8}Mn_{0.4}Fe_{0.6}O_4$ | $LSMFO_4$ | - | 0.59 | 770 ($H_2$) | LSGM | [219] |
| $Sr_2Ti_{0.8}Co_{0.2}FeO_6$ | $STCFO_6$ | 0.12 | 0.38 | 555 ($H_2$) | LSGM | [220] |
| $(La_{0.6}Sr_{1.4})_{0.95}Mn_{0.9}Cu_{0.1}O_4$-SSZ | LSMCu-SSZ | $0.12^{750°C}$ | $0.32^{750°C}$ | $623^{750\,°C}$ ($H_2$) | SSZ | [222] |
| *Noble metal exsolution (Ru and Pd)* | | | | | | |
| $Sr_{0.8}Ce_{0.2}Fe_{0.95}Ru_{0.05}O_{3-\delta}$ | SCFR | - | - | 846 ($H_2$)<br>310 ($C_3H_8$) | LSGM | [225] |
| $La_{0.6}Ce_{0.1}Sr_{0.3}Fe_{0.95}Ru_{0.05}O_3$-GDC | LCSFR-GDC | 0.11 | 0.32 | 904 ($H_2$) | LSGM | [231] |
| $(La_{0.8}Sr_{0.2})_{0.9}Sc_{0.2}Mn_{0.8-x}Ru_xO_{3-\delta}$ | LSSMR | x= 0<br>(0.23)<br>x= 0.05<br>(0.56) | x= 0<br>(3.6)<br>x= 0.05<br>(0.52)<br>(5%$H_2$-$N_2$) | 318 ($H_2$)<br>0.54 A $cm^{-2}$ $^{750\,°C}$<br>(1.5 V) | SSZ | [226] |
| $Sm_{0.70}Sr_{0.20}Fe_{0.80}Ti_{0.15}Ru_{0.05}O_{3-\delta}$ | SSFTR | 0.13 | 0.11 | 476 ($H_2$) | SDC | [228] |
| $La_{0.6}Sr_{0.4}Fe_{0.95}Pd_{0.05}O_{3-\delta}$-SDC | LSFPd-GDC | $0.91^{750\,°C}$ | $0.08^{750\,°C}$ | $350^{750\,°C}$ ($H_2$) | LSGM | [229] |
| $LaCo_{0.3}Fe_{0.67}Pd_{0.03}O_{3-\delta}$-SDC | LCFP-GDC | $0.02^{750°C}$ | - | $535^{750°C}$ ($H_2$) | SDC | [232] |

## 5. Electrode materials for quasi-symmetrical SSOCs

One of the limitations of traditional SSOCs, as the aforementioned studies have shown, is to find a material with sufficient electrical conductivity and electrocatalytic activity for simultaneous use as both air and fuel electrodes, especially at intermediate temperatures. A new approach based on Quasi-Symmetrical electrodes (Q-SSOC) is gaining increased attention in last few years, where the symmetrical electrode suffers a severe phase transformation in reducing atmospheres, accompanied with the formation of large amounts of metal particles that greatly enhance the electrical conductivity and electrochemical properties. In this context, several traditional MIECs have been tested as Q-SSOC, such as $Pr_{0.5}Ba_{0.5}Co_{0.25}Fe_{0.75}O_{3-\delta}$ [233], $La_{0.6}Sr_{0.4}Co_{0.2}Fe_{0.8}O_{3-\delta}$

[234] and $La_2NiO_4$, [235], which showed an improved performance compared to traditional SSOC approach based on redox stable electrodes.

In this section, only electrodes that show a complete or severe phase transformation in reducing conditions are discussed, excluding those that exhibit a single-phase transition (*i.e*. single to layered perovskite), which are classified as exsolved electrodes in the previous section. The most relevant Quasi-Symmetrical electrodes are summarized in **Table 4**, including the main properties.

In the attempt to stabilize the $Pr_{0.4}Sr_{0.6}Co_{0.2}Fe_{0.8}O_{3-\delta}$ air electrode for its implementation in SSOC, Zhang *et al*. incorporated different amounts of Mo in the B-site of the perovskite, $Pr_{0.4}Sr_{0.6}(Co_{0.2}Fe_{0.8})_{1-x}Mo_xO_{3-\delta}$ (PSCFMx) (x= 0-0.2) [236]. This new electrode underwent a partial decomposition into $SrFeLaO_4$, $Pr_2O_3$ and Co-Fe metal when reduced at 900 ºC for 2 h in $H_2$. It should be highlighted that the original oxidized phase was recovered after successive air/$H_2$ cycles, confirming the reversibility of the phase transformation. An LSGM-supported cell with PSCFM0.05 as symmetrical electrode reached an MPD of 493 and 160 mW $cm^{-2}$ in $H_2$ and $CH_4$, respectively, at 850 ºC. Similar findings were found by Lu *et al*. with $Pr_{0.6}Sr_{0.4}Fe_{0.7}Ni_{0.2}Mo_{0.1}O_{3-\delta}$ electrode [237] (**Table 4**).

In another study, Zhao *et al.* studied the $Pr_{0.6}Sr_{0.4}FeO_{3-\delta}$ single perovskite, the following phases were obtained after reduction process at 800 ºC: $(Pr_{0.6}Sr_{0.4})_3Fe_2O_7$ and $(Pr_{0.6}Sr_{0.4})_2FeO_4$ both with RP-type structure, as well as Fe-metal [238]. A YSZ-based cell generated an MPD of 502 mW $cm^{-2}$ at 800 ºC. The same electrode was recently tested by Yang *et al*., but different phases were identified after reduction: $Pr_{0.6}Sr_{0.4}FeO_{3-\delta}$ single perovskite and $(Pr_{0.6}Sr_{0.4})_3Fe_2O_7$ RP-type structure [239]. In addition, a remarkable current density under SOEC mode was achieved, *i.e*. -1.39 A $cm^{-2}$ at 800 ºC at 1.6 V. Tao *et al.* also tested the traditional $PrNi_{0.4}Fe_{0.6}O_{3-\delta}$ air electrode, prepared by infiltration method into a LSGM porous scaffold, for Q-SSOFC. The single perovskite suffered a phase transformation in fuel conditions into $Pr_2O_3$ and Fe-Ni nanoclusters that were quickly recovered to their initial phase after re-oxidation at 800 ºC with the presence of a little fraction of $Pr_6O_{11}$, reaching an excellent MPD of 663 mW $cm^{-2}$ with wet $CH_4$ at 800 ºC [240].

Cu-doping was implemented in the LSCF air electrode, $La_{0.5}Sr_{0.5}Fe_{0.8}Cu_{0.2}O_{3-\delta}$, which exhibited a reversible phase transformation from a single perovskite in air to a mixture of phases in reducing conditions: $SrFeLaO_4$ RP phase, $LaFeO_3$ single perovskite and Cu-metal, reaching power densities of 577 and 482 mW $cm^{-2}$ in $H_2$ and syngas at 800 ºC, respectively [241]. Duan *et al.* found that $LaCo_{0.6}Ni_{0.4}O_{3-\delta}$-$Ce_{0.9}Gd_{0.1}O_{1.95}$ composite electrode decomposed into multiple phases at 700 ºC in $H_2$, including $La(OH)_3$ and a Ni-Co alloy. Very low ASR values were obtained in both air and $H_2$ atmospheres, 0.046 and 0.037 Ω $cm^2$, respectively, with an MPD of 562 mW $cm^{-2}$ at 800 ºC in $H_2$ (**Fig. 6a-c**). A high current density of 2.32 A $cm^{-2}$ at 800 ºC and 2.0 V was also obtained in SOEC mode [41]. Similar results were observed by Han *et al.* in $LaNi_{0.82}Fe_{0.18}O_3$-NiO composite infiltrated into a LSGM scaffold, showing a complete decomposition into $La_2O_3$, $LaFeO_3$ and Fe-Ni nanoparticles, and a surprising high MPD of 928 mW $cm^{-2}$ at 650 ºC in a LSGM-electrolyte supported cell [40]. However, the

stability after successive oxidation/reduction cycles was not evaluated, which is an important issue due to the hydration/carbonation of lanthanum oxide in air atmosphere.

The traditional $La_2NiO_4$ RP-type phase was also tested for Q-SSOC, which presented a partial phase decomposition in $H_2$ atmosphere into a $La_2NiO_4$-related phase, $La_2O_3$ and Ni-metal. A MPD of 245 mW $cm^{-2}$ was obtained at 800 ºC in $H_2$ [235]. It is also worth noting that the segregation of $La_2O_3$ might lead to the formation of insulating $La_2Zr_2O_7$ at the electrode/YSZ interface at rather low temperature as 800 ºC [242], which was not investigated. Similar electrode decomposition was observed for the $Pr_2NiO_4$-SDC composite, showing $Pr_2O_3$ and Ni-metal in reducing conditions. The best electrochemical properties were found for $Pr_2NiO_4$-SDC (60:40 wt.%) with ASR values as low as 0.068 Ω $cm^2$ in air at 800 ºC. A SDC-supported cell (210 μm thickness) rendered an MPD of 375 mW $cm^{-2}$ at 800 ºC with almost negligible degradation in a long term stability test at 750 ºC for 168 h [243].

The $PrBaFe_{1.8}Co_{0.2}O_{5+\delta}$ double perovskite air electrode was also studied for Q-SSOFC with different fuels, achieving remarkable MPD values of 563, 439 and 221 mW $cm^{-2}$ in $H_2$, liquefied petroleum gas and $C_2H_5OH$, respectively, at 800 ºC [42]. $PrBaFe_{1.8}Co_{0.2}O_{5+\delta}$ decomposed into $PrBaFe_2O_{5+\delta}$, $Ba_6Pr_2Fe_4O_{15}$ and $Co_3Fe_7$ nanoparticles in reducing atmosphere, which was reversible after calcining in air at 800 ºC (**Fig. 6d-f**). However, the SEM image clearly showed a significant change of the electrode microstructure in air and $H_2$ atmospheres, which could be detrimental for the mechanical stability.

Chen *et al.* proposed a novel cell design consisting of a GDC electrolyte sandwiched between two Ni-foams current collectors, which were infiltrated with $Ni_{0.8}Co_{0.15}Al_{0.05}LiO_2$ electrode. During the cell operation, small amounts of $Li_2CO_3$ and NiO were formed on the air electrode surface, which presumably improved the ionic conductivity and lowered the activation energy for ORR. Furthermore, decent MPD was obtained at quite low temperature, *i.e.* 159 mW $cm^{-2}$ at 550 ºC, but no stability/cyclability tests were presented [244].

Other different Ni-based electrodes/cermets have been studied in recent years. Zhang *et al.* reported the performance of $Li_{0.3}Ni_{0.7}O$ as symmetrical electrode, showing power densities up to 503 mW $cm^{-2}$ at 600 ºC in $H_2$, with a relatively good stability over time [245]. It has to be noted that the original phase was not recovered during the re-oxidation process and diffraction peaks attributed to $Li_2O$ were not detected in the XRD patterns, explained by the amorphization or sublimation at high temperature. ZnO-NiO-SDC-$Na_2CO_3$ and $NiCuZnO_x$ (**Table 4**) electrodes were also tested with an oxide-ion-carbonate electrolyte (SDC–$Na_2CO_3$), showing a very high power output at low temperatures, *i.e.* 1257 mW $cm^{-2}$ at 520 ºC in $H_2$ for ZnO-NiO-SDC-$Na_2CO_3$ electrode [246,247]. These exceptional results could be explained by the implementation of the mixed electrolyte and the formation of Ni-metal in the fuel electrode. On the other hand, a $Ni_{0.7}Co_{0.3}O$-SDC cermet, which showed high redox reversibility, rendered a modest MPD of 200.2 mW $cm^{-2}$ at 800 ºC in $H_2$ [248].

Although the quasi-symmetrical electrodes exhibit improved electrochemical properties due to a significant segregation of metal particles, which increases the electronic conductivity in fuel conditions. The formation of multiple phases and the important microstructural change of electrodes during the oxidation/reduction cycles

could negatively affect the mechanical stability of the cell. For instance, lanthanides and alkaline earth-rare elements are susceptible to hydration and carbonation under the operation conditions of a SOFC. In addition, these phases could react with the electrolyte; hence further studies are need to confirm long-term stability and reversibility of these symmetrical electrodes.

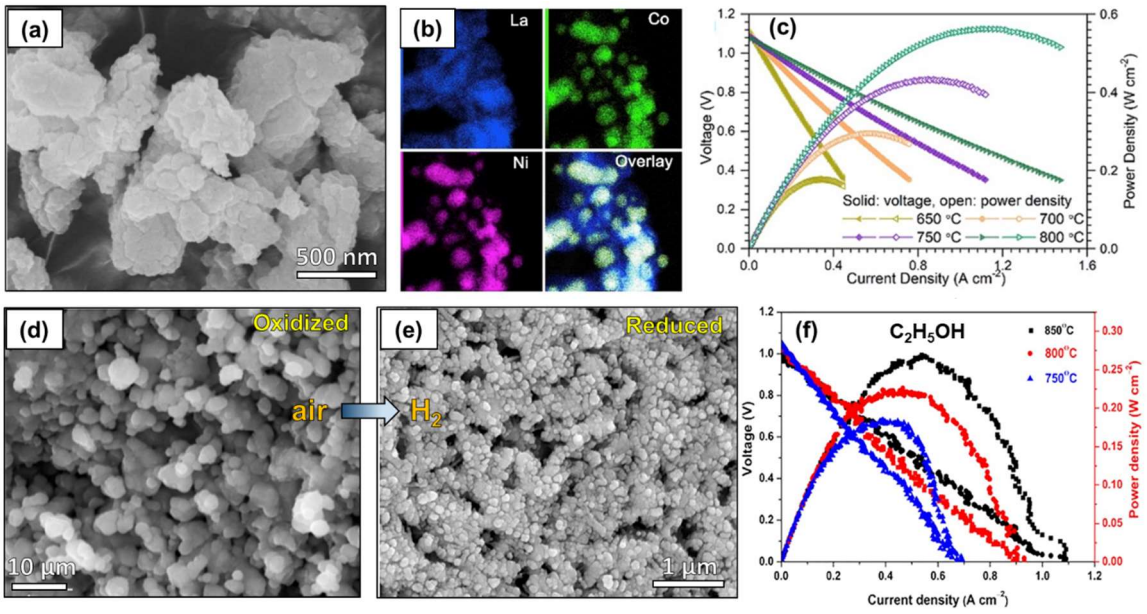


**Figure 6.** (a) SEM image of $LaCo_{0.6}Ni_{0.4}O_{3-\delta}$ (LCN) after successive air/$H_2$ redox cycles, (b) HAADF-STEM and EDS images after reduction; and (c) I-V-P curves of the LCN-GDC symmetrical electrode on YSZ electrolyte at different temperatures in $H_2$. Reprinted with permission, Elsevier, [41]. SEM images of $PrBaFe_{1.8}Co_{0.2}O_{5+\delta}$ in (d) air and (e) $H_2$; and (f) I-V-P curves of the symmetrical cell on LSGM electrolyte at different temperatures using $C_2H_5OH$ fuel. Reprinted with permission, Elsevier, [42].

**Table 4.** Properties of some quasi-symmetrical electrodes. Area specific resistance (in air and $H_2$) and power/current densities are given at 800 ºC. In those case, where not data are available at 800 ºC, the temperature is included.

| Electrode | Abbreviation | $ASR^{air}$ ($\Omega$ cm$^2$) | $ASR^{H_2}$ ($\Omega$ cm$^2$) | P (mW cm$^{-2}$) | Electrolyte | Ref. |
|---|---|---|---|---|---|---|
| $La_2NiO_4$ | LNO | 2.09 | - | 245 | YSZ-GDC | [235] |
| $Pr_{0.4}Sr_{0.6}(Co_{0.2}Fe_{0.8})_{0.95}Mo_{0.05}O_{3-\sigma}$ | PSCFM005 | 0.21 | 0.85 | $493^{850\,°C}$ ($H_2$)<br>$160^{850\,°C}$ ($CH_4$) | LSGM | [236] |
| $Pr_{0.6}Sr_{0.4}Fe_{0.7}Ni_{0.2}Mo_{0.1}O_{3-\delta}$ | PSFNM | 0.6 | 0.25 | 500 | LSGM | [237] |
| $Pr_{0.6}Sr_{0.4}FeO_{3-\delta}$ | PSF | 0.20 | 0.15 | 502 | YSZ-GDC | [238] |
| $Pr_{0.6}Sr_{0.4}FeO_{3-\delta}$ | PSF | 0.28 | 0.32 | 591<br>-1.39 A cm$^{-2}$ (1.6 V) | LSGM | [239] |
| $PrNi_{0.4}Fe_{0.6}O_{3-\delta}$ | PNF | 0.02 | 0.06 ($CH_4$) | 663 ($CH_4$) | LSGM | [240] |
| $La_{0.5}Sr_{0.5}Fe_{0.8}Cu_{0.2}O_{3-\delta}$ | LSFCu | - | - | 577 ($H_2$)<br>482 (syngas) | ScSZ-SDC | [241] |
| $LaCo_{0.6}Ni_{0.4}O_{3-\delta}$ | LCN-GDC | 0.046 | 0.037 | 562 ($H_2$) | YSZ | [41] |

| | | | | | | |
|---|---|---|---|---|---|---|
| | | | | 2.32 A $cm^{-2}$ (2.0 V) | | |
| $PrBaFe_{1.8}Co_{0.2}O_{5+\delta}$ | PBFC | 0.026 | 0.316 | 563 ($H_2$)<br>439 (L. petroleum)<br>221 ($C_2H_5OH$) | LSGM | [42] |
| $Pr_2NiO_4$-SDC | PNO-SDC | 0.06 | - | 375 | SDC | [243] |
| $Ni_{0.8}Co_{0.15}Al_{0.05}LiO_2$-Ni foam | - | $0.31^{550\,°C}$ | $0.39^{550\,°C}$ | $159.7^{550\,°C}$ | GDC | [244] |
| $Li_{0.3}Ni_{0.7}O$ | LNO | - | - | $503^{600\,°C}$ | $Ce_{0.8}(Gd,Y)_{0.2}O_{2-\delta}$ | [245] |
| $NiCuZnO_x$ | NCZO | - | - | $680^{600\,°C}$ | SDC-$Na_2CO_3$ | [247] |
| $Ni_{0.7}Co_{0.3}O$-SDC | NCO-SDC | 0.071 | - | 200.2 | YSZ-SDC | [248] |

## 6. Symmetrical electrodes for proton conducting solid oxide cells (H-SSOCs)

Proton conducting solid oxide cells (H-SOC) have attracted the attention of researchers in the last years due to their better electrochemical performance at intermediate temperatures (500-700 ºC) as a consequence of the higher mobility and lower activation energy of protons in comparison to oxide ions [43,249]. This lower operating temperature implies sluggish electrode kinetics but, in contrast, also brings several benefits for these devices, such as higher cell durability, lower operation costs and no dilution of fuels due to water formation [44,46]. The electrodes for H-SSOC require proton conduction to extend the TPB beyond the electrolyte/electrode interface. For this reason, the conventional SOC electrodes are mixed with a proton-conducting electrolyte. An alternative approach is to use triple-conducting electrodes with proton, oxide-ion and electron conductivity, such as $BaCo_{0.4}Fe_{0.4}Zr_{0.1}Y_{0.1}O_3$, $PrBa_{0.5}Sr_{0.5}Co_{1.5}Fe_{0.5}O_{5+\delta}$ and $PrNi_{0.5}Co_{0.5}O_{3-\delta}$ [250–252].

Most of the investigation carried out in the development of H-SOC has been mainly focused on the traditional Ni-anode-supported cell; however, recent promising advances on proton conducting symmetrical solid oxide cells (H-SSOC) are attracting a growing interest over this traditional anode-supported cell configuration due to the advantages previously commented. The most relevant electrodes are briefly discussed in the following paragraphs and included in **Table 5**.

In one of the first studies on these cells, Li *et al.* studied the $La_{0.6}Sr_{0.4}Fe_{0.8}Nb_{0.1}Cu_{0.1}O_{3-\delta}$ perovskite as symmetrical electrode to cogenerate ethylene and electricity in a proton conducting cell with $BaZr_{0.1}Ce_{0.7}Y_{0.1}Yb_{0.1}O_{3-\delta}$ (BZCYYb) electrolyte, achieving MPD values of 182 and 90 mW $cm^{-2}$ for $H_2$ and $C_2H_6$, respectively, at 750 ºC [253]. The results also revealed an enhancement of the phase stability in reducing atmospheres and a high coking resistance for the Cu-doped electrode. Similar findings in terms of power density were observed for the $SrMo_{0.8}Co_{0.1}Fe_{0.1}O_{3-\delta}$-$BaCe_{0.7}Zr_{0.1}Y_{0.2}O_{3-\delta}$ composite electrode (**Table 5**) [254].

$Nd_{1-x}Ba_xFe_{0.9}B_{0.1}O_{3-\delta}$ electrodes (x= 0.4 and 0.6; B= Cu and Ni) were tested in a proton conducting cell with $BaCe_{0.7}Zr_{0.1}Y_{0.2}O_{3-\delta}$ (BZCY) electrolyte, where $Nd_{0.6}Ba_{0.4}Fe_{0.9}Cu_{0.1}O_{3-\delta}$ showed exsolved Fe-Cu nanoparticles

in reducing conditions (**Table 5**) [255]. Fu *et al*. tested the $(LaSr)_{0.9}Fe_{0.9}Cu_{0.1}O_4$-$BaZr_{0.1}Ce_{0.7}Y_{0.2}O_{3-\delta}$ composite electrode on BZCY electrolyte, reporting Cu nanoparticle exsolution in reducing conditions [256]. This process was deeply studied by Density Functional Theory (DFT), concluding that the (100) orientation was the preferential surface orientation for the Cu-exsolution due to the lowest surface energy needed. In addition, MPDs of 573 and 396 mW $cm^{-2}$ were obtained in humidified $H_2$ and $CH_4$, respectively, at 800 ºC (**Fig. 7a-c**).

In 2021, Kim *et al.* studied the $PrBaFe_2O_{5+\delta}$ double perovskite on BZCY electrolyte, showing high redox stability and rather low ASR values both in air and $H_2$, 0.20 and 0.28 Ω $cm^2$, respectively, at 700 ºC and a MPD of 301 mW $cm^{-2}$ at the same temperature (**Fig. 7d-f**) [257].

The $SrCe_{0.9}In_{0.1}O_{3-\delta}$-$SrFe_{0.75}Mo_{0.25}O_{3-\delta}$ (SCI-SFM) symmetrical composite electrode achieved ASR values of 3.28 Ω $cm^2$ and 1.83 Ω $cm^2$ at 600 ºC in air and 5%-$H_2$, respectively, but a very low MPD of 32 mW $cm^2$ at 800 ºC was obtained due to the thick SCI electrolyte (0.4 mm) used [258].

Quasi-symmetrical electrodes with proton conductor electrolytes have also been investigated. For instance, Ba-doped $Pr_2NiO_4$ air electrode was tested with a $BaCe_{0.5}Zr_{0.3}Dy_{0.2}O_{3-\delta}$ (BCZD) electrolyte [259]. In reducing conditions, $Pr_{1.9}Ba_{0.1}NiO_{4+\delta}$ (PBN) decomposed into $(Pr,Ba)_2O_3$ and Ni nanoparticles. The PBN-BCZD|BCZD|PBN-BCZD cell rendered a MPD of 300 mW $cm^{-2}$ at 600 ºC [259]. More recently, Yu *et al.* proposed the implementation of $BaCo_{0.4}Fe_{0.4}Zr_{0.1}Y_{0.1}O_{3-\delta}$ (BCFZY), one of the most efficient air electrodes for classical H-SOCs up to date due to the triple-conducting properties, as a quasi-symmetrical electrode. In reducing conditions, a mixture of $Ba_2Fe_2O_5$, $YBa_4Fe_3O_{11}$, Co-Fe nanoparticles and zirconium-yttrium oxide phases was observed, but the BCFZY-SDC composition onto BZCY rendered good ASR values of 0.32 and 1.35 Ω $cm^2$ in air and 10% $H_2$ at 700 ºC, respectively [260].

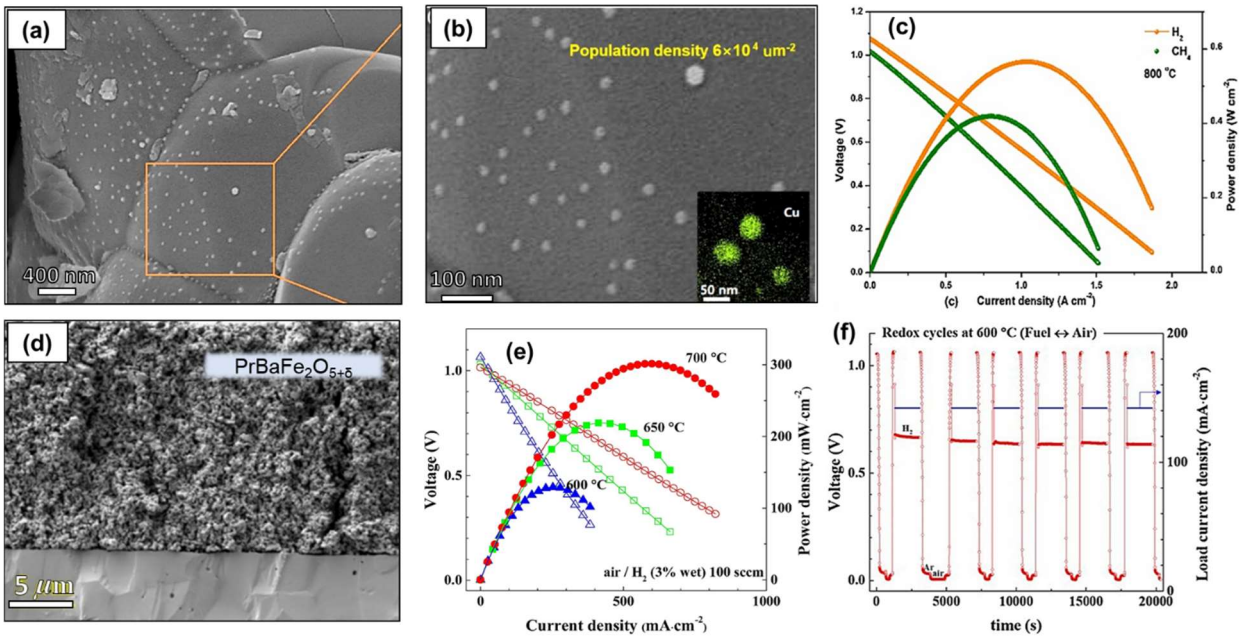


**Figure 7.** (a,b) SEM images of the reduced $(LaSr)_{0.9}Fe_{0.9}Cu_{0.1}O_4$ (LSFCu) electrode on BZCY electrolyte at different magnifications and (c) I-V-P curves of a single cell at 800 ºC using $H_2$ and $CH_4$ fuels. Reprinted with permission, Elsevier, [256]. (d) SEM image $PrBaFe_2O_{5+\delta}$ ($PBFO_5$) symmetrical electrode on BZCY electrolyte, (e) I-V-P curves of the single

cell at different temperatures with $H_2$ fuel, and (f) redox cycling test of the cell by switching from $H_2$ to air under 140 mA $cm^{-2}$ at 600 ºC. Reprinted with permission, Elsevier [257].

**Table 5.** Properties of several symmetrical electrodes employed in proton conducting fuel cells. Area specific resistance in air and $H_2$, and power/current densities are given at 750 ºC. In those case, where not data are available at 750 ºC, the temperature is included.

| Electrode | Abbreviation | $ASR^{air}$ ($\Omega$ $cm^2$) | $ASR^{H_2}$ ($\Omega$ $cm^2$) | P (mW $cm^{-2}$) | Electrolyte | Ref. |
|---|---|---|---|---|---|---|
| $La_{0.6}Sr_{0.4}Fe_{0.8}Nb_{0.1}Cu_{0.1}O_{3-\delta}$ | LSFNCu | - | - | 182 ($H_2$)<br>90 ($C_2H_6$) | BZCYYb | [253] |
| $SrMo_{0.8}Co_{0.1}Fe_{0.1}O_{3-\delta}$-BZCY | SMCF-BZCY | - | - | 377 ($H_2$)<br>268 ($CH_4$) | BZCY | [254] |
| $Nd_{0.6}Ba_{0.4}Fe_{0.9}Cu_{0.1}O_{3-\delta}$ | NBFCu | $1.1^{600\,ºC}$ | $15.1^{600\,ºC}$ | - | BZCYYb | [255] |
| $(LaSr)_{0.9}Fe_{0.9}Cu_{0.1}O_{4+\delta}$-BZCY | LSFCu-BZCY | 0.19 | 0.36 | $573^{800\,ºC}$ ($H_2$)<br>$396^{800\,ºC}$ ($CH_4$) | BZCY | [256] |
| $PrBaFe_2O_{5+\delta}$ | PBF | $0.20^{700\,ºC}$ | $0.28^{700\,ºC}$ | $301^{700\,ºC}$ ($H_2$) | BZCY | [257] |
| $SrFe_{0.75}Mo_{0.25}O_{3-\delta}$-SCI | SFM-SCI | $3.28^{600\,ºC}$ | $1.83^{600\,ºC}$ (5%$H_2$) | $32^{800\,ºC}$ ($H_2$) | $SrCe_{0.9}In_{0.1}O_{3-\delta}$ (SCI) | [258] |
| $Pr_{1.9}Ba_{0.1}NiO_{4+\delta}$-BCZD | PBN-BCZD | - | - | $300^{600\,ºC}$ ($H_2$) | BCZD | [259] |
| $BaCo_{0.4}Fe_{0.4}Zr_{0.1}Y_{0.1}O_{3-\delta}$-SDC | BCFZY-SDC | $0.32^{700\,ºC}$ | $1.35^{700\,ºC}$ (10%-$H_2$) | $114.8^{650\,ºC}$ | BZCY | [260] |

## 7. Symmetrical electrodes for electrochemical reduction of $CO_2$

Nowadays, the electroreduction of $CO_2$ is a promising technology for sustainable energy conversion and storage and likewise serves to mitigate the anthropogenic $CO_2$ emissions [47,261]. In this way, two mayor approaches based on ionic-liquid electrolytes at low operation temperature and solid oxide cells for high temperature applications have been proposed. Among them, high temperature solid oxide electrolyzer cells (SOEC) have had a much greater improvement in terms of redox reaction efficiencies, thereby achieving higher current density and stability than low temperature devices [7,48,262]. Most of the symmetrical electrodes proposed for $CO_2$ electroreduction are derived from similar compositions previously studied in SSOFC configuration [8], but alternative doping and microstructural strategies have been employed in order to enhance the efficiency. These are all discussed in this section and summarized in **Table 6**.

Lanthanum chromite electrodes were again the first symmetrical electrodes considered for $CO_2$ electroreduction in symmetrical solid oxide electrolyzer cells (SSOECs). In one of the first studies, Xu *et al.* tested the traditional LSCM-SDC composite electrode, achieving decent ASR values in air, *i.e.* 0.25 $\Omega$ $cm^2$ at 800 ºC. On the contrary, very high ASR values were obtained in a $CO_2$ atmosphere, 5-10 $\Omega$ $cm^2$, which were further lowered to 0.5 $\Omega$ $cm^2$ when a DC current of 200 mA $cm^{-2}$ was applied [263]. The LSCM electrode was also tested for the electrochemical reduction of $CO_2$/$H_2O$ into syngas (CO+$H_2$) in a proton conducting cell with

$BaCe_{0.5}Zr_{0.3}Y_{0.16}Zn_{0.04}O_{3-\delta}$ electrolyte [264]. Ru catalyst was also added by infiltration to enhance the electrochemical properties, and high chemical stability was observed in both oxidizing and reducing conditions. Addo *et al.* tested the $La_{0.3}Sr_{0.7}Fe_{0.7}Cr_{0.3}O_{3-\delta}$ electrode with a mixture $CO_2$/CO fuel, rendering an ASR of 0.94 Ω $cm^2$ when the feed ratio was 70:30 and a current density of -0.39 A $cm^{-2}$ at 1.5 V at 800 ºC [265].

In the same way, lanthanum ferrite based electrodes have demonstrated remarkable results for $CO_2$ electroreduction, *i.e.* $La_{0.6}Ca_{0.4}Fe_{0.8}Ni_{0.2}O_{3-\delta}$-$Ce_{0.9}Gd_{0.1}O_{1.95}$ symmetrical electrode on YSZ electrolyte demonstrated a current density at 800 ºC of -1.5 A $cm^{-2}$ at 2.0 V in $CO_2$ feed gas [203]. Later on, the same authors observed that these excellent results were linked to the synergetic effect of the phases formed after reduction, *i.e.* CaO, responsible for capturing the $CO_2$, and Ni-Fe nanoparticles, which highly boosted the electrocatalytic performance [266]. This hypothesis was confirmed when the results were compared to those reported by Tian *et al*. for $La_{0.6}Sr_{0.4}Fe_{0.8}Ni_{0.2}O_{3-\delta}$ (LSFN)-GDC electrodes, which showed a current density at 800 ºC of -1.03 A $cm^{-2}$ at 2.0 V and a CO formation rate of 6.35 mL $min^{-1}$ $cm^{-2}$ [267,268] (**Fig. 8a-c).**

$La_{0.5}Sr_{0.5}Fe_{0.9}Nb_{0.1}O_{3-\delta}$ (LSFN) [269] and $La_{0.4}Sr_{0.6}Co_{0.2}Fe_{0.7}Nb_{0.1}O_{3-\delta}$ (LSCFN) [270] also rendered high current density values for $CO_2$ electrolysis, showing that Co-doping led to exsolution of Co-Fe nanoparticles, improving the cell performance and preventing carbon deposition. In addition, the oxygen vacancies that were created as a result of the doping were also beneficial for the chemical absorption and activation of $CO_2$, fact that was confirmed by DFT calculations in another study with $La_{0.4}Sr_{0.6}Co_{0.2}Fe_{0.7}Mo_{0.1}O_{3-\delta}$-GDC [271]. The LSCFN-GDC|YSZ|LSCFN-GDC cell showed a current density at 800 ºC of 0.44 A $cm^{-2}$ at 1.5 V in pure $CO_2$. These results were further improved by the same group when $H_2O$ was incorporated into the steam feed [272] (**Table 6**).

The traditional LSCF-GDC air electrode was also tested as a symmetrical electrode in a SSOEC. A small amount of $SrCO_3$ was found after annealing in $CO_2$ at 800 ºC for 220 h. The SSOEC delivered a current density of -1.01 A $cm^{-2}$ at 1.4 V and 800 ºC and a Faraday efficiency of 98.8% [273]. Peng *et al*. evaluated a related composition, $La_{0.6}Sr_{0.4}Fe_{0.9}Mn_{0.1}O_{3-\delta}$-GDC, for $CO_2$ electrolysis, obtaining a current density at 800 ºC of -1.11 A $cm^{-2}$ at 2.0 V with a CO production rate of 6.4 mL $min^{-1}$ $cm^{-2}$ in the same conditions [274].

A Ti-doped LSCF air electrode, $La_{0.3}Sr_{0.7}Fe_{0.7}Ti_{0.3}O_3$, was also employed for $CO_2$ electrolysis with a current density of -0.51 A $cm^{-2}$ at 2 V and 800 ºC, although the performance was severely limited by the thick YSZ|SDC electrolyte (~700 μm) [275].

Kyriakou *et al.* employed a Rh-doping strategy in an A-deficient lanthanum titanate, $La_{0.43}Ca_{0.37}Rh_{0.06}Ti_{0.94}O_3$-GDC, showing highly distributed Rh nanoparticles after reduction on the electrode surface that played a key role in the syngas production ($CO+H_2$) from $CO_2$ co-electrolysis and methane partial oxidation. The ASR values at 850 ºC in air, $H_2$ and $CH_4$ were 5.89, 0.21 and 0.62 Ω $cm^2$, respectively. The current density was 1.57 A $cm^{-2}$ at 1.0 V using 40% $CH_4$-60% $N_2$ and 25% $H_2O$-25% $CO_2$-50% $N_2$ gas concentrations in the anode and cathode, respectively [148].

Regarding layered perovskites, most of the studies have been focused on $Sr_2Fe_{1.5}Mo_{0.5}O_{6-\delta}$ (SFM) due to its good stability in $H_2$, $CO_2$ and CO, as well as improved properties as both fuel and air electrodes. The SFM electrode infiltrated onto porous YSZ scaffold showed ASR values of 0.064 and 0.153 Ω $cm^2$ at 750 ºC in air and 50% CO-$CO_2$, respectively. The power output obtained was 265 mW $cm^{-2}$ in SOFC mode and the current density under electrolysis mode was -0.62 A $cm^{-2}$ at 1.5 V [276]. The SFM-SDC composite was also tested for syngas production, generating a current density at 850 ºC of -0.73 A $cm^{-2}$ at 1.3 V, and showing a good $CO_2$ conversion rate of 58% (**Fig. 8d-f**) [277]. In order to further increase the efficiency for $H_2O$-$CO_2$ electrolysis, Fe-overdoping in $Sr_2Fe_{1.6}Mo_{0.5}O_{6-\delta}$-SDC was investigated, showing Fe nanoparticles that improved the electrochemical performance [278]. Additionally, $Sr_2FeMoO_6$ was infiltrated into a LSGM porous scaffold. The symmetrical cell displayed a remarkable current density at 800 ºC of -1.24 A $cm^{-2}$ at 1.5 V when $CO_2$ was employed as feed gas, showing a high durability and no evidence of carbon deposition for 53 h of stability test [279].

A new $SrEu_2Fe_2O_7$ (n= 2) Ruddlesden-Popper-type electrode has also been proposed as a promising alternative to traditional layered perovskites, which showed excellent chemical and redox stability in $CO_2$ atmosphere, as well as high efficiency in air and $CO_2$-CO feed gas (**Table 6**). The LSGM-supported cell rendered a stable current density at 800 ºC of -1.27 A $cm^{-2}$ at 1.5 V for 260 h [280].

Quasi-symmetrical electrodes have also been investigated for $CO_2$ electroreduction. The $PrBaFe_{1.8}Co_{0.2}O_{5+\delta}$ double perovskite electrode showed improved performance for $CO_2$ electrolysis using 50% $CO_2$-$H_2O$ feed gas, achieving current densities at 850 ºC of -0.65 A $cm^{-2}$ at 1.3 V [42]. The $MnCo_2O_4$ spinel infiltrated into GDC scaffold in another quasi-symmetrical electrode for $CO_2$ reduction, achieving a current density at 800 ºC of -0.75 A $cm^{-2}$ at 1.5 V and a low degradation rate for 84 h of stability test [281].

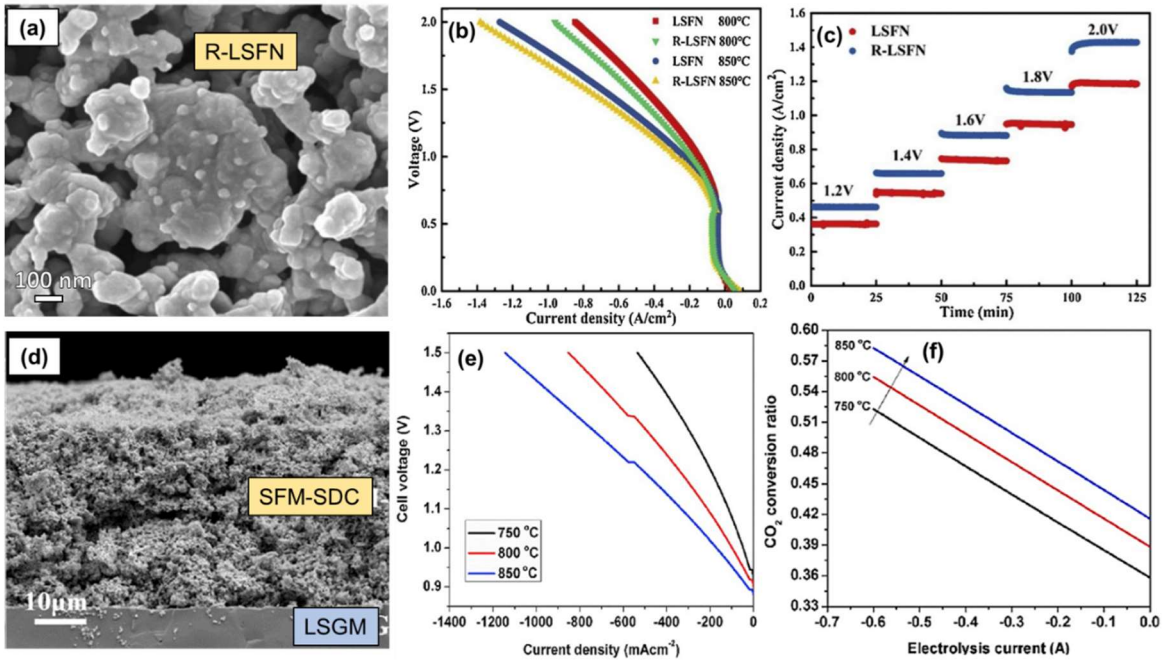


**Figure 8.** (a) SEM image of the reduced $La_{0.6}Sr_{0.4}Fe_{0.8}Ni_{0.2}O_{3-\delta}$ (R-LSFN) symmetrical electrode on GDC/YSZ electrolyte, (b) I-V curves of the SSOEC and (c) short-term stability of the cell for $CO_2$ electrolysis at different voltages. Reprinted with permission, Elsevier, [268]. (d) Cross section SEM image of the SFM-SDC symmetrical electrode on a LSGM electrolyte, (e) I-V curves of the SSOECs for $H_2O/CO_2$ electrolysis and (f) $CO_2$ conversion ratio at different temperatures. Reprinted with permission, Elsevier, [277].

**Table 6.** Properties of some symmetrical electrodes for $CO_2$ electroreduction. Area specific resistance (in air and $CO_2$) and current densities are given at 800 ºC. In those case, where not data are available at 800 ºC, the temperature is included.

| Electrode | Abbreviation | $ASR^{air}$ ($\Omega$ cm$^2$) | $ASR^{CO_2}$ ($\Omega$ cm$^2$) | Current (A cm$^2$) | Electrolyte | Ref. |
|---|---|---|---|---|---|---|
| $La_{0.75}Sr_{0.25}Cr_{0.5}Mn_{0.5}O_{3-\delta}$-SDC | LSCM-SDC | 0.25 | 0.50 | -0.18 A cm$^{-2}$ (2.0 V) | YSZ | [263] |
| $La_{0.3}Sr_{0.7}Fe_{0.7}Cr_{0.3}O_{3-\delta}$ | LSFCr | 0.5 | 0.94 $CO_2$-CO (70:30) | -0.39 A cm$^{-2}$ (1.5 V) | YSZ/GDC | [265] |
| $La_{0.6}Ca_{0.4}Fe_{0.8}Ni_{0.2}O_{3-\delta}$-GDC | LCaFN-GDC | - | - | -1.5 A cm$^{-2}$ (2.0 V) | YSZ/GDC | [203] |
| $La_{0.4}Sr_{0.6}Co_{0.2}Fe_{0.7}Nb_{0.1}O_{3-\delta}$-GDC | LSCFN-GDC | - | - | -0.638 A cm$^{-2,\ 850\ ºC}$ (1.3 V) $CO_2$:$H_2$:$H_2O$ (75:10:15) | YSZ/GDC | [272] |
| $La_{0.4}Sr_{0.6}Co_{0.2}Fe_{0.8}O_3$-GDC | LSCF-GDC | - | - | -1.01 A cm$^{-2}$ (1.4 V) | YSZ | [273] |
| $La_{0.6}Sr_{0.4}Fe_{0.9}Mn_{0.1}O_{3-\delta}$-GDC | LSFM –GDC | 0.24 | 0.58 | -1.11 A cm$^{-2}$ (2.0 V) | YSZ/GDC | [274] |
| $La_{0.3}Sr_{0.7}Fe_{0.7}Ti_{0.3}O_3$ | LSFT | - | - | -0.51 A cm$^{-2}$ (2.0 V) | YSZ/SDC | [275] |
| $Sr_2Fe_{1.5}Mo_{0.5}O_{6-\delta}$-YSZ | SFM-YSZ | $0.064^{750\ ºC}$ | $0.153^{750\ ºC}$ CO-$CO_2$ (1:1) | -0.62 A cm$^{-2,\ 750\ ºC}$ (1.5 V) 265 mW cm$^{-2,\ 750\ ºC}$ | YSZ | [276] |
| $Sr_2Fe_{1.6}Mo_{0.5}O_{6-\delta}$-SDC | SFM-SDC | - | - | -1.27 A cm$^{-2,\ 850\ ºC}$ (1.6 V) | LSGM | [278] |
| $Sr_2FeMoO_{6-\delta}$-LSGM | SFM-LSGM | - | - | -1.24 A cm$^{-2}$ (1.5 V) | LSGM | [279] |

| | | | | | | |
|---|---|---|---|---|---|---|
| $PrBaFe_{1.8}Co_{0.2}O_{5+\delta}$ | PBFC | 0.04 | - | -0.65 A $cm^{-2,\ 850\ ºC}$ (1.3 V) $CO_2$/50%$H_2O$ | LSGM | [42] |
| $SrEu_2Fe_2O_7$ | $SEFO_7$ | $0.07^{850\ ºC}$ | $0.48^{850\ ºC}$ | -1.27 A $cm^{-2,\ 850\ ºC}$ (1.5 V) | LSGM | [280] |
| $MnCo_2O_4$-SDC | MCO-SDC | - | - | -0.75 A $cm^{-2,\ 800\ ºC}$ (1.5 V) | YSZ | [281] |

## 8. Outlook and future perspectives

The main research advances in the development of new symmetrical electrodes in the last decade have been reviewed in this contribution. Based on the reported data, the original approach of using redox stable electrodes, *i.e.* chromites, ferrites and titanates, have demonstrated to be the most studied ones due to the inherent stability and reversibility of such materials. Among the different substitutions, high valence transition metals, such as $Mo^{6+}$ and $W^{6+}$, lead to improved properties of these electrodes in terms of high mixed ionic-electronic conductivity, redox stability and electrocatalytic activity. Nevertheless, the main challenge of achieving high electrocatalytic performance under both oxidizing and reducing atmospheres still remains unaddressed. One of the most studied strategies to enhance the electrochemical performance of symmetrical electrodes in fuel conditions is the incorporation of active metals such as Ni, Ru and Pd into the crystal structure, in order to achieve metal exsolved nanoparticles with improved electrocatalytic properties. The exsolved particles generally show enhanced stability over time, avoiding the typical percolation process observed when noble metals are directly deposited by infiltration on the electrode surface. However, no deep research has been carried out on checking the reversibility and cycling stability of these electrodes, becoming necessary to know whether stable performances are obtained when alternatively working in fuel cell and electrolysis modes.

Another strategy that has gained significant attention in the last years is the use of quasi-symmetrical electrodes, where a drastic phase transformation occurs in fuel atmosphere with the segregation of large amounts of metal particles, thereby enhancing their electrical conductivity and electrocatalytic activity. However, significant structural and microstructural differences between the air and fuel electrodes could negatively affect the mechanical stability of the cell, especially when switching the air-fuel gas flow repeatedly. In particular, alkaline-earth oxides, formed during the transformation, are susceptible to carbonation and hydration under the usual operating conditions of a SOFC. Moreover, metals particles aggregates resulting in significant change of the electrode microstructure and porosity. This issue has not been considered in most of the studies about Q-SSOCs, appointing the need for further research to elucidate the long-term stability and reversibility of these electrodes.

It is also worth noting that most of the symmetrical electrodes have been investigated with oxide ion conductor electrolytes, such as YSZ, GDC and LSGM at the temperature range of 750-950 ºC. Although proton-conducting electrolytes, e.g. doped-$Ba(Ce,Zr)O_3$, are more favorable for operating at reduced temperatures (500-700 ºC) due to the higher proton conductivity. In this context, several symmetrical electrodes are being

investigated in H-SSOCs, achieving higher power outputs than the corresponding O-SSOCs due to lower ohmic resistance of the electrolyte, which represents one of the main drawbacks of conventional electrolyte-supported cell configuration.

Apart from the use of SSOCs for electrical energy and $H_2$ production, the recent implementation of symmetrical electrodes for $CO_2$ electroreduction have gained a great interest in the literature. Among all doping strategies, Ca-doping in quasi-symmetrical electrodes has rendered the most promising results since CaO shows high ability to capture $CO_2$. This, together with the presence of nanoparticle exsolution in the fuel electrode and the incorporation of a proton conducting electrolyte, could be the key to achieve greater performance while lowering the operating temperature. However, the long-stability of the electrodes should be further explored and verified, as it is of the utmost importance to determine both the carbonation and stability under high voltages during long operation times. Moreover, most of the current scientific studies with symmetrical electrodes are still focused on fuel cell mode, while only some of them are implemented on electrolysis cells, despite working in reversible mode is one of the most interesting properties of SSOCs.

Further efforts are required to obtain highly efficient SSOCs with improved performance and durability, becoming this issue an area of concern in future research. Demonstrating solid and consistent studies about SSOCs running without degradation under both fuel and electrolysis modes during long times could turn the situation around, replacing the actual Ni-cermet anode supported cells. The authors would like to note that many of the reported studies have overlooked the great influence of the electrode microstructure on the performance, which definitely can be detrimental for the ultimate SSOC commercialization. In fact, low temperature fabrication methods based on infiltration and spray-pyrolysis deposition have already demonstrated excellent results to obtain nanostructured electrodes with improved efficiency. It is therefore expected and desired that more research will relate to nanostructured electrodes in the future for their application in SSOCs.

Similarly, special effort should be put on innovating the cell designs to be competitive with the traditional Ni-anode supported cells with thin film electrolyte, because SSOCs are supported in a thick electrolyte with high ohmic resistance, and consequently poorer cell performance. Alternatively, a thin film electrolyte sandwiched between two porous layer scaffolds can be prepared and then the active symmetrical electrode could be infiltrated. Another possible strategy, which is still not explored in symmetrical SSOCs, is the use of active interlayers with good electrochemical properties in air and fuel environments. In this case, electrodes with high electronic conductivity but poor electrocatalytic activity such as $(La,Ca)CrO_3$ could be used as current collector layers. Despite finding a good balance between performance and cost of SSOCs still remains challenging due to the complexity of the redox systems, current research on symmetrical electrodes for solid oxide cells is highly promising and it is getting closer to becoming a real alternative to the traditional SOC technology.

**Acknowledgments**

This work was supported by Ministerio de Ciencia, Innovación y Universidades through the RTI2018-093735-B-I00 and UMA18-FEDERJA-033 research projects (Spain). J. Zamudio-García thanks the Ministerio de Ciencia, Innovación y Universidades for the FPU (FPU17/02621) grant.

# REFERENCES

[1] B.C.H. Steele, A. Heinzel, Materials for fuel-cell technologies, Nature. 414 (2001) 345–352. https://doi.org/10.1038/35104620.

[2] A. Kirubakaran, S. Jain, R.K. Nema, A review on fuel cell technologies and power electronic interface, Renew. Sustain. Energy Rev. 13 (2009) 2430–2440. https://doi.org/10.1016/j.rser.2009.04.004.

[3] Y. Haseli, Maximum conversion efficiency of hydrogen fuel cells, Int. J. Hydrogen Energy. 43 (2018) 9015–9021. https://doi.org/10.1016/j.ijhydene.2018.03.076.

[4] U.M. Damo, M.L. Ferrari, A. Turan, A.F. Massardo, Solid oxide fuel cell hybrid system: A detailed review of an environmentally clean and efficient source of energy, Energy. 168 (2019) 235–246. https://doi.org/10.1016/j.energy.2018.11.091.

[5] T.M. Gür, Review of electrical energy storage technologies, materials and systems: Challenges and prospects for large-scale grid storage, Energy Environ. Sci. 11 (2018) 2696–2767. https://doi.org/10.1039/c8ee01419a.

[6] N. Mahato, A. Banerjee, A. Gupta, S. Omar, K. Balani, Progress in material selection for solid oxide fuel cell technology: A review, Prog. Mater. Sci. 72 (2015) 141–337. https://doi.org/10.1016/j.pmatsci.2015.01.001.

[7] Y. Zheng, J. Wang, B. Yu, W. Zhang, J. Chen, J. Qiao, J. Zhang, A review of high temperature co-electrolysis of $H_2O$ and $CO_2$ to produce sustainable fuels using solid oxide electrolysis cells (SOECs): Advanced materials and technology, Chem. Soc. Rev. 46 (2017) 1427–1463. https://doi.org/10.1039/c6cs00403b.

[8] Y. Jiang, F. Chen, C. Xia, A review on cathode processes and materials for electro-reduction of carbon dioxide in solid oxide electrolysis cells, J. Power Sources. 493 (2021) 229713. https://doi.org/10.1016/j.jpowsour.2021.229713.

[9] S. Dwivedi, Solid oxide fuel cell: Materials for anode, cathode and electrolyte, Int. J. Hydrogen Energy. 45 (2020) 23988–24013. https://doi.org/10.1016/j.ijhydene.2019.11.234.

[10] Z. Zakaria, Z. Awang Mat, S.H. Abu Hassan, Y. Boon Kar, A review of solid oxide fuel cell component fabrication methods toward lowering temperature, Int. J. Energy Res. 44 (2020) 594–611. https://doi.org/10.1002/er.4907.

[11] M. Rafique, H. Nawaz, M. Shahid Rafique, M. Bilal Tahir, G. Nabi, N.R. Khalid, Material and method selection for efficient solid oxide fuel cell anode: Recent advancements and reviews, Int. J. Energy Res. 43 (2019) 2423–2446. https://doi.org/10.1002/er.4210.

[12] J.C. Ruiz-Morales, J. Canales-Vázquez, J. Peña-Martínez, D.M. López, P. Núñez, On the simultaneous use of

$La_{0.75}Sr_{0.25}Cr_{0.5}Mn_{0.5}O_{3-\delta}$ as both anode and cathode material with improved microstructure in solid oxide fuel cells, Electrochim. Acta. 52 (2006) 278–284. https://doi.org/10.1016/j.electacta.2006.05.006.

[13] P. Kaur, K. Singh, Review of perovskite-structure related cathode materials for solid oxide fuel cells, Ceram. Int. 46 (2020) 5521–5535. https://doi.org/10.1016/j.ceramint.2019.11.066.

[14] S.P. Jiang, Development of lanthanum strontium manganite perovskite cathode materials of solid oxide fuel cells: A review, J. Mater. Sci. 43 (2008) 6799–6833. https://doi.org/10.1007/s10853-008-2966-6.

[15] N.A. Baharuddin, A. Muchtar, M.R. Somalu, Short review on cobalt-free cathodes for solid oxide fuel cells, Int. J. Hydrogen Energy. 42 (2017) 9149–9155. https://doi.org/10.1016/j.ijhydene.2016.04.097.

[16] S.P. Jiang, Development of lanthanum strontium cobalt ferrite perovskite electrodes of solid oxide fuel cells – A review, Int. J. Hydrogen Energy. 44 (2019) 7448–7493. https://doi.org/10.1016/j.ijhydene.2019.01.212.

[17] Z. Shao, S.M. Halle, A high-performance cathode for the next generation of solid-oxide fuel cells, Nature. 431 (2004) 170–173. https://doi.org/10.1038/nature02863.

[18] L. Dos Santos-Gómez, J.M. Porras-Vázquez, E.R. Losilla, D. Marrero-López, Improving the efficiency of layered perovskite cathodes by microstructural optimization, J. Mater. Chem. A. 5 (2017) 7896–7904. https://doi.org/10.1039/c6ta10946b.

[19] M. Morales, J.J. Roa, J. Tartaj, M. Segarra, A review of doped lanthanum gallates as electrolytes for intermediate temperature solid oxides fuel cells: From materials processing to electrical and thermo-mechanical properties, J. Eur. Ceram. Soc. 36 (2016) 1–16. https://doi.org/10.1016/j.jeurceramsoc.2015.09.025.

[20] A. V. Kasyanova, L.R. Tarutina, A.O. Rudenko, J.G. Lyagaeva, D.A. Medvedev, Ba(Ce,Zr)$O_3$-based electrodes for protonic ceramic electrochemical cells: towards highly compatible functionality and triple-conducting behaviour, Russ. Chem. Rev. 89 (2020) 667–692. https://doi.org/10.1070/rcr4928.

[21] G.K. Vdovin, A.O. Rudenko, B.D. Antonov, V.B. Malkov, A.K. Demin, D.A. Medvedev, Manipulating the grain boundary properties of $BaCeO_3$-based ceramic materials through sintering additives introduction, Chim. Techno Acta. 2019. 6 (2019) 38–45. https://doi.org/10.15826/chimtech.2019.6.2.01.

[22] C. Sun, R. Hui, J. Roller, Cathode materials for solid oxide fuel cells: A review, J. Solid State Electrochem. 14 (2010) 1125–1144. https://doi.org/10.1007/s10008-009-0932-0.

[23] J.C. Ruiz-Morales, D. Marrero-López, J. Canales-Vázquez, J.T.S. Irvine, Symmetric and reversible solid oxide fuel cells, RSC Adv. 1 (2011) 1403–1414. https://doi.org/10.1039/c1ra00284h.

[24] Q. Liu, X. Dong, G. Xiao, F. Zhao, F. Chen, A novel electrode material for symmetrical SOFCs, Adv. Mater. 22 (2010) 5478–5482. https://doi.org/10.1002/adma.201001044.

[25] C. Su, W. Wang, M. Liu, M.O. Tadé, Z. Shao, Progress and Prospects in Symmetrical Solid Oxide Fuel Cells with Two Identical Electrodes, Adv. Energy Mater. 5 (2015) 1–19. https://doi.org/10.1002/aenm.201500188.

[26] C. Zhao, Y. Li, W. Zhang, Y. Zheng, X. Lou, B. Yu, J. Chen, Y. Chen, M. Liu, J. Wang, Heterointerface engineering for enhancing the electrochemical performance of solid oxide cells, Energy Environ. Sci. 13 (2020) 53–85. https://doi.org/10.1039/c9ee02230a.

[27] P. Qiu, X. Yang, W. Wang, T. Wei, Y. Lu, J. Lin, Z. Yuan, L. Jia, J. Li, F. Chen, Redox-Reversible Electrode Material for Direct Hydrocarbon Solid Oxide Fuel Cells, ACS Appl. Mater. Interfaces. 12 (2020) 13988–13995. https://doi.org/10.1021/acsami.0c00922.

[28] S.Y. Gómez, D. Hotza, Current developments in reversible solid oxide fuel cells, Renew. Sustain. Energy Rev. 61 (2016) 155–174. https://doi.org/10.1016/j.rser.2016.03.005.

[29] F. Wang, H. Kishimoto, T. Ishiyama, K. Develos-Bagarinao, K. Yamaji, T. Horita, H. Yokokawa, A review of sulfur poisoning of solid oxide fuel cell cathode materials for solid oxide fuel cells, J. Power Sources. 478 (2020) 228763. https://doi.org/10.1016/j.jpowsour.2020.228763.

[30] P. Boldrin, E. Ruiz-Trejo, J. Mermelstein, J. Josémiguel Bermúdezbermúdez Menéndezmenéndez, T. Tomás, R. Reina, N.P. Brandon, Strategies for Carbon and Sulfur Tolerant Solid Oxide Fuel Cell Materials, Incorporating Lessons from Heterogeneous Catalysis, (2016). https://doi.org/10.1021/acs.chemrev.6b00284.

[31] C. Graves, S.D. Ebbesen, S.H. Jensen, S.B. Simonsen, M.B. Mogensen, Eliminating degradation in solid oxide electrochemical cells by reversible operation, Nat. Mater. 14 (2015) 239–244. https://doi.org/10.1038/nmat4165.

[32] J.H. Myung, D. Neagu, D.N. Miller, J.T.S. Irvine, Switching on electrocatalytic activity in solid oxide cells, Nature. 537 (2016) 528–531. https://doi.org/10.1038/nature19090.

[33] D.M. Bastidas, S. Tao, J.T.S. Irvine, A symmetrical solid oxide fuel cell demonstrating redox stable perovskite electrodes, J. Mater. Chem. 16 (2006) 1603–1605. https://doi.org/10.1039/b600532b.

[34] A. Nikonov, K. Kuterbekov, Kz. Bekmyrza, N. Pavzderin, A brief review of conductivity and thermal expansion of perovskite-related oxides for SOFC cathode, Eurasian J. Phys. Funct. Mater. 2018 (n.d.) 274–292. https://doi.org/10.29317/ejpfm.2018020309.

[35] R. Pelosato, G. Cordaro, D. Stucchi, C. Cristiani, G. Dotelli, Cobalt based layered perovskites as cathode material for intermediate temperature Solid Oxide Fuel Cells: A brief review, J. Power Sources. 298 (2015) 46–67. https://doi.org/10.1016/j.jpowsour.2015.08.034.

[36] S. Afroze, A.H. Karim, Q. Cheok, S. Eriksson, A.K. Azad, Latest development of double perovskite electrode materials for solid oxide fuel cells: a review, Front. Energy. 13 (2019) 770–797. https://doi.org/10.1007/s11708-019-0651-x.

[37] L. Shu, J. Sunarso, S.S. Hashim, J. Mao, W. Zhou, F. Liang, Advanced perovskite anodes for solid oxide fuel cells: A review, Int. J. Hydrogen Energy. 44 (2019) 31275–31304. https://doi.org/10.1016/j.ijhydene.2019.09.220.

[38] S.P.S. Shaikh, A. Muchtar, M.R. Somalu, A review on the selection of anode materials for solid-oxide fuel cells, Renew. Sustain. Energy Rev. 51 (2015) 1–8. https://doi.org/10.1016/j.rser.2015.05.069.

[39] J. Zhang, M.-R. Gao, J.-L. Luo, In Situ Exsolved Metal Nanoparticles: A Smart Approach for Optimization of Catalysts, Chem. Mater. 32 (2020) 5424–5441. https://doi.org/10.1021/acs.chemmater.0c00721.

[40] D. Han, J. Liu, Y.B. He, H.F. Wang, X.Z. Zhang, S.R. Wang, Fabrication of a quasi-symmetrical solid oxide fuel cell using a modified tape casting/screen-printing/infiltrating combined technique, Int. J. Hydrogen Energy. 43 (2018) 960–967. https://doi.org/10.1016/j.ijhydene.2017.11.082.

[41] N. Duan, J. Yang, M. Gao, B. Zhang, J.L. Luo, Y. Du, M. Xu, L. Jia, B. Chi, J. Li, Multi-functionalities enabled fivefold applications of $LaCo_{0.6}Ni_{0.4}O_{3-\delta}$ in intermediate temperature symmetrical solid oxide fuel/electrolysis cells, Nano Energy. 77 (2020) 105207. https://doi.org/10.1016/j.nanoen.2020.105207.

[42] C. Lu, B. Niu, W. Yi, Y. Ji, B. Xu, Efficient symmetrical electrodes of $PrBaFe_{2-x}Co_xO_{5+\delta}$ (x=0, 0.2,0.4) for solid oxide fuel cells and solid oxide electrolysis cells, Electrochim. Acta. 358 (2020) 136916. https://doi.org/10.1016/j.electacta.2020.136916.

[43] J. Kim, S. Sengodan, S. Kim, O. Kwon, Y. Bu, G. Kim, Proton conducting oxides: A review of materials and applications for renewable energy conversion and storage, Renew. Sustain. Energy Rev. 109 (2019) 606–618. https://doi.org/10.1016/j.rser.2019.04.042.

[44] C. Duan, J. Huang, N. Sullivan, R. O'Hayre, Proton-conducting oxides for energy conversion and storage, Appl. Phys. Rev. 7 (2020). https://doi.org/10.1063/1.5135319.

[45] L. Lei, J. Zhang, Z. Yuan, J. Liu, M. Ni, F. Chen, Progress Report on Proton Conducting Solid Oxide Electrolysis Cells, Adv. Funct. Mater. 29 (2019) 1903805. https://doi.org/10.1002/adfm.201903805.

[46] G.C. Mather, D. Muñoz-Gil, J. Zamudio-García, J.M. Porras-Vázquez, D. Marrero-López, D. Pérez-Coll, Perspectives on Cathodes for Protonic Ceramic Fuel Cells, Appl. Sci. 11 (2021) 5363. https://doi.org/10.3390/app11125363.

[47] R.G. Grim, Z. Huang, M.T. Guarnieri, J.R. Ferrell, L. Tao, J.A. Schaidle, Transforming the carbon economy: Challenges and opportunities in the convergence of low-cost electricity and reductive $CO_2$ utilization, Energy Environ. Sci. 13 (2020) 472–494. https://doi.org/10.1039/c9ee02410g.

[48] Y. Song, X. Zhang, K. Xie, G. Wang, X. Bao, High-Temperature $CO_2$ Electrolysis in Solid Oxide Electrolysis Cells: Developments, Challenges, and Prospects, Adv. Mater. 31 (2019) 1–18. https://doi.org/10.1002/adma.201902033.

[49] R. Küngas, Review—Electrochemical $CO_2$ Reduction for CO Production: Comparison of Low- and High-Temperature Electrolysis Technologies, J. Electrochem. Soc. 167 (2020) 044508. https://doi.org/10.1149/1945-7111/ab7099.

[50] M.S. Khan, X. Xu, R. Knibbe, Z. Zhu, Air electrodes and related degradation mechanisms in solid oxide electrolysis and reversible solid oxide cells, Renew. Sustain. Energy Rev. 143 (2021) 110918. https://doi.org/10.1016/j.rser.2021.110918.

[51] P.A. Connor, X. Yue, C.D. Savaniu, R. Price, G. Triantafyllou, M. Cassidy, G. Kerherve, D.J. Payne, R.C. Maher, L.F. Cohen, R.I. Tomov, B.A. Glowacki, R.V. Kumar, J.T.S. Irvine, Tailoring SOFC Electrode Microstructures for Improved Performance, Adv. Energy Mater. 8 (2018) 1800120. https://doi.org/10.1002/aenm.201800120.

[52] Z. Shao, W. Zhou, Z. Zhu, Advanced synthesis of materials for intermediate-temperature solid oxide fuel cells, Prog. Mater. Sci. 57 (2012) 804–874. https://doi.org/10.1016/j.pmatsci.2011.08.002.

[53] N. Hedayat, Y. Du, H. Ilkhani, Review on fabrication techniques for porous electrodes of solid oxide fuel cells by sacrificial template methods, Renew. Sustain. Energy Rev. 77 (2017) 1221–1239. https://doi.org/10.1016/j.rser.2017.03.095.

[54] R.K. Nishihora, P.L. Rachadel, M.G.N. Quadri, D. Hotza, Manufacturing porous ceramic materials by tape casting—A review, J. Eur. Ceram. Soc. 38 (2018) 988–1001. https://doi.org/10.1016/j.jeurceramsoc.2017.11.047.

[55] S. Mi, Z. Liu, C. Luo, L. Cai, Z. Zhang, L. Li, A review on preparing new energy ultrafine powder materials by freeze-drying, Dry. Technol. 38 (2020) 1544–1564. https://doi.org/10.1080/07373937.2019.1651733.

[56] L. dos Santos-Gómez, J. Zamudio-García, J.M. Porras-Vázquez, E.R. Losilla, D. Marrero-López, Recent progress in nanostructured electrodes for solid oxide fuel cells deposited by spray pyrolysis, J. Power Sources. 507 (2021) 230277. https://doi.org/10.1016/j.jpowsour.2021.230277.

[57] A.J. Abd Aziz, N.A. Baharuddin, M.R. Somalu, A. Muchtar, Review of composite cathodes for intermediate-temperature solid oxide fuel cell applications, Ceram. Int. 46 (2020) 23314–23325. https://doi.org/10.1016/j.ceramint.2020.06.176.

[58] D. Ding, X. Li, S.Y. Lai, K. Gerdes, M. Liu, Enhancing SOFC cathode performance by surface modification through infiltration, Energy Environ. Sci. 7 (2014) 552–575. https://doi.org/10.1039/c3ee42926a.

[59] J.W. Fergus, Metallic interconnects for solid oxide fuel cells, Mater. Sci. Eng. A. 397 (2005) 271–283. https://doi.org/10.1016/j.msea.2005.02.047.

[60] R. Doshi, C.B. Alcock, N. Gunasekaran, J.J. Carberry, Carbon monoxide and methane oxidation properties of oxide solid solution catalysts, J. Catal. 140 (1993) 557–563. https://doi.org/10.1006/jcat.1993.1105.

[61] J. Sfeir, P.A. Buffat, P. Mockli, N. Xanthopoulos, R. Vasquez, H.J. Mathieu, J. Van herle, K.R. Thampi, Lanthanum chromite based catalysts for oxidation of methane directly on SOFC anodes, J. Catal. 202 (2001) 229–244. https://doi.org/10.1006/jcat.2001.3286.

[62] S. Tao, J.T.S. Irvine, A redox-stable efficient anode for solid-oxide fuel cells, Nat. Mater. 2 (2003) 320–323. https://doi.org/10.1038/nmat871.

[63] S.W. Tao, J.T.S. Irvine, J.A. Kilner, An Efficient Solid Oxide Fuel Cell Based upon Single-Phase Perovskites, Adv. Mater. 17 (2005) 1734–1737. https://doi.org/10.1002/adma.200402007.

[64] M. Pavone, A.M. Ritzmann, E.A. Carter, Quantum-mechanics-based design principles for solid oxide fuel cell cathode materials, Energy Environ. Sci. 4 (2011) 4933–4937. https://doi.org/10.1039/c1ee02377b.

[65] L. Zhang, S. Ping Jiang, C. Siang Cheng, Y. Zhang, Synthesis and Performance of $(La_{0.75}Sr_{0.25})_{1-x}(Cr_{0.5}Mn_{0.5}O_3)$ Cathode Powders of Solid Oxide Fuel Cells by Gel-Casting Technique, J. Electrochem. Soc. 154 (2007) B577. https://doi.org/10.1149/1.2724759.

[66] J.C. Ruiz-Morales, J. Canales-Vázquez, B. Ballesteros-Pérez, J. Peña-Martínez, D. Marrero-López, J.T.S. Irvine, P. Núñez, LSCM-(YSZ-CGO) composites as improved symmetrical electrodes for solid oxide fuel cells, J. Eur. Ceram. Soc. 27 (2007) 4223–4227. https://doi.org/10.1016/j.jeurceramsoc.2007.02.117.

[67] S. Ping Jiang, L. Zhang ab, Y. Zhang, Lanthanum strontium manganese chromite cathode and anode synthesized by gel-casting for solid oxide fuel cells, J. Mater. Chem. 17 (2007) 2627–2635. https://doi.org/10.1039/b701339f.

[68] C.M. Chanquía, A. Montenegro-Hernández, H.E. Troiani, A. Caneiro, A bottom-up building process of nanostructured $La_{0.75}Sr_{0.25}Cr_{0.5}Mn_{0.5}O_{3-\delta}$ electrodes for symmetrical-solid oxide fuel cell: Synthesis,

characterization and electrocatalytic testing, J. Power Sources. 245 (2014) 377–388. https://doi.org/10.1016/j.jpowsour.2013.06.124.

[69] X. Zhu, Z. Lü, B. Wei, X. Huang, Y. Zhang, W. Su, A symmetrical solid oxide fuel cell prepared by dry-pressing and impregnating methods, J. Power Sources. 196 (2011) 729–733. https://doi.org/10.1016/j.jpowsour.2010.07.055.

[70] L. Zhang, X. Chen, S.P. Jiang, H.Q. He, Y. Xiang, Characterization of doped $La_{0.7}A_{0.3}Cr_{0.5}Mn_{0.5}O_{3-\delta}$ (A = Ca, Sr, Ba) electrodes for solid oxide fuel cells, Solid State Ionics. 180 (2009) 1076–1082. https://doi.org/10.1016/j.ssi.2009.05.010.

[71] J. Peña-Martínez, D. Marrero-López, D. Pérez-Coll, J.C. Ruiz-Morales, P. Núñez, Performance of XSCoF (X= Ba, La and Sm) and LSCrX′ (X′= Mn, Fe and Al) perovskite-structure materials on LSGM electrolyte for IT-SOFC, Electrochim. Acta. 52 (2007) 2950–2958. https://doi.org/10.1016/j.electacta.2006.09.004.

[72] M.K. Rath, K.T. Lee, Investigation of aliovalent transition metal doped $La_{0.7}Ca_{0.3}Cr_{0.8}X_{0.2}O_{3-\delta}$ (X=Ti, Mn, Fe, Co, and Ni) as electrode materials for symmetric solid oxide fuel cells, Ceram. Int. 41 (2015) 10878–10890. https://doi.org/10.1016/j.ceramint.2015.05.029.

[73] M. Chen, S. Paulson, V. Thangadurai, V. Birss, Sr-rich chromium ferrites as symmetrical solid oxide fuel cell electrodes, J. Power Sources. 236 (2013) 68–79. https://doi.org/10.1016/j.jpowsour.2013.02.024.

[74] S. Gupta, H. Sabarou, Y. Zhong, P. Singh, Phase evolution and electrochemical performance of iron doped lanthanum strontium chromite in oxidizing and reducing atmosphere, Int. J. Hydrogen Energy. 42 (2017) 6262–6271. https://doi.org/10.1016/j.ijhydene.2016.11.141.

[75] Z. Shen, J.A. Kilner, S.J. Skinner, Electrical conductivity and oxygen diffusion behaviour of the $(La_{0.8}Sr_{0.2})_{0.95}Cr_xFe_{1-x}O_{3-\delta}$ (x = 0.3, 0.5 and 0.7) A-site deficient perovskites, Phys. Chem. Chem. Phys. 20 (2018) 18279–18290. https://doi.org/10.1039/c8cp02797h.

[76] Z. Sha, E. Cali, G. Kerherve, S.J. Skinner, Oxygen diffusion behaviour of A-site deficient $(La_{0.8}Sr_{0.2})_{0.95}Cr_{0.5}Fe_{0.5}O_{3-\delta}$ perovskites in humid conditions, J. Mater. Chem. A. 8 (2020) 21273–21288. https://doi.org/10.1039/d0ta08899d.

[77] S.P. Jiang, L. Liu, K.P. Ong, P. Wu, J. Li, J. Pu, Electrical conductivity and performance of doped $LaCrO_3$ perovskite oxides for solid oxide fuel cells, J. Power Sources. 176 (2008) 82–89. https://doi.org/10.1016/j.jpowsour.2007.10.053.

[78] J.C. Ruiz-Morales, H. Lincke, D. Marrero-López, J. Canales-Vázquez, Lanthanum chromite materials as potential symmetrical electrodes for Solid Oxide Fuel Cells, Boletín La Soc. Española Cerámica y Vidr. 46 (2007) 218–223.

[79] Y. Zhang, Q. Zhou, T. He, $La_{0.7}Ca_{0.3}CrO_3$-$Ce_{0.8}Gd_{0.2}O_{1.9}$ composites as symmetrical electrodes for solid-oxide fuel cells, J. Power Sources. 196 (2011) 76–83. https://doi.org/10.1016/j.jpowsour.2010.07.035.

[80] Y. Zhang, Y. Shen, X. Du, J. Li, X. Cao, T. He, Nanostructured GDC-impregnated $La_{0.7}Ca_{0.3}CrO_{3-\delta}$symmetrical electrodes for solid oxide fuel cells operating on hydrogen and city gas, Int. J. Hydrogen Energy. 36 (2011) 3673–3680. https://doi.org/10.1016/j.ijhydene.2010.12.104.

[81] B. Lin, S. Wang, X. Liu, G. Meng, Simple solid oxide fuel cells, J. Alloys Compd. 490 (2010) 214–222.

https://doi.org/10.1016/j.jallcom.2009.09.111.

[82] Y. Wan, Y. Xing, Z. Xu, S. Xue, S. Zhang, C. Xia, A-site bismuth doping, a new strategy to improve the electrocatalytic performances of lanthanum chromate anodes for solid oxide fuel cells, Appl. Catal. B Environ. 269 (2020) 118809. https://doi.org/10.1016/j.apcatb.2020.118809.

[83] J. Beckers, G. Rothenberg, Sustainable selective oxidations using ceria-based materials, Green Chem. 12 (2010) 939–94. https://doi.org/10.1039/c000191k.

[84] M. Stoian, V. Rogé, L. Lazar, T. Maurer, J.C. Védrine, I.C. Marcu, I. Fechete, Total oxidation of methane on oxide and mixed oxide ceria-containing catalysts, Catalysts. 11 (2021) 1–42. https://doi.org/10.3390/catal11040427.

[85] E. Lay, M. Benamira, C. Pirovano, G. Gauthier, L. Dessemond, Effect of Ce-Doping on the Electrical and Electrocatalytical Behavior of La/Sr Chromo-Manganite Perovskite as New SOFC Anode, Fuel Cells. 12 (2012) 265–274. https://doi.org/10.1002/fuce.201100070.

[86] Y. Song, W. Tan, D. Xu, Y. Bu, Q. Zhong, $La_{0.75}Sr_{0.25-x}Ce_xCr_{0.5}Mn_{0.5}O_{3-\delta}$ electrode material for symmetric solid oxide fuel cells with $H_2S$-containing fuel, J. Alloys Compd. 576 (2013) 341–344. https://doi.org/10.1016/j.jallcom.2013.05.219.

[87] Y. Song, Q. Zhong, W. Tan, Synthesis and electrochemical behaviour of ceria-substitution LSCM as a possible symmetric solid oxide fuel cell electrode material exposed to $H_2$ fuel containing $H_2S$, Int. J. Hydrogen Energy. 39 (2014) 13694–13700. https://doi.org/10.1016/j.ijhydene.2014.03.179.

[88] X. Luo, Y. Yang, Y. Yang, D. Tian, X. Lu, Y. Chen, Q. Huang, B. Lin, Reduced-temperature redox-stable LSM as a novel symmetrical electrode material for SOFCs, Electrochim. Acta. 260 (2018) 121–128. https://doi.org/10.1016/j.electacta.2017.11.071.

[89] Y. Zheng, C. Zhang, R. Ran, R. Cai, Z. Shao, D. Farrusseng, A new symmetric solid-oxide fuel cell with $La_{0.8}Sr_{0.2}Sc_{0.2}Mn_{0.8}O_{3-\delta}$ perovskite oxide as both the anode and cathode, Acta Mater. 57 (2009) 1165–1175. https://doi.org/10.1016/J.ACTAMAT.2008.10.047.

[90] A. El-Himri, D. Marrero-López, J.C. Ruiz-Morales, J. Peña-Martínez, P. Núñez, Structural and electrochemical characterisation of $Pr_{0.7}Ca_{0.3}Cr_{1-y}Mn_yO_{3-\delta}$ as symmetrical solid oxide fuel cell electrodes, J. Power Sources. 188 (2009) 230–237. https://doi.org/10.1016/j.jpowsour.2008.11.050.

[91] D.M. Amaya-Dueñas, G. Chen, A. Weidenkaff, N. Sata, F. Han, I. Biswas, R. Costa, K.A. Friedrich, A-site deficient chromite within situ Ni exsolution as a fuel electrode for solid oxide cells (SOCs), J. Mater. Chem. A. 9 (2021) 5685–5701. https://doi.org/10.1039/d0ta07090d.

[92] Y.F. Bu, Q. Zhong, D.D. Xu, X.L. Zhao, W.Y. Tan, Performance of $Y_{0.9}Sr_{0.1}Cr_{0.9}Fe_{0.1}O_{3-\delta}$ as a sulfur-tolerant anode material for intermediate temperate solid oxide fuel cells, J. Power Sources. 250 (2014) 143–151. https://doi.org/10.1016/j.jpowsour.2013.11.005.

[93] A.M. Hussain, K.-J. Pan, Y.-L. Huang, I.A. Robinson, C. Gore, E.D. Wachsman, Highly Performing Chromate-Based Ceramic Anodes ($Y_{0.7}Ca_{0.3}Cr_{1-x}Cu_xO_{3-\delta}$) for Low-Temperature Solid Oxide Fuel Cells, ACS Appl. Mater. Interfaces. 10 (2018) 36075–36081. https://doi.org/10.1021/acsami.8b07987.

[94] S. Zhang, Y. Wan, Z. Xu, S. Xue, L. Zhang, B. Zhang, C. Xia, Bismuth doped $La_{0.75}Sr_{0.25}Cr_{0.5}Mn_{0.5}O_{3-\delta}$ perovskite

as a novel redox-stable efficient anode for solid oxide fuel cells, J. Mater. Chem. A. 8 (2020) 11553–11563. https://doi.org/10.1039/d0ta03328f.

[95] L. Dos Santos-Gómez, J.M. Porras-Vázquez, E.R. Losilla, D. Marrero-López, Ti-doped $SrFeO_3$ nanostructured electrodes for symmetric solid oxide fuel cells, RSC Adv. 5 (2015) 107889–107895. https://doi.org/10.1039/c5ra23771h.

[96] A. Jun, J. Kim, J. Shin, G. Kim, Perovskite as a Cathode Material: A Review of its Role in Solid-Oxide Fuel Cell Technology, ChemElectroChem. 3 (2016) 511–530. https://doi.org/10.1002/CELC.201500382.

[97] S.K. Burnwal, S. Bharadwaj, P. Kistaiah, Review on MIEC Cathode Materials for Solid Oxide Fuel Cells, Http://Dx.Doi.Org/10.1142/S2251237316300011. 04 (2016) 1630001. https://doi.org/10.1142/S2251237316300011.

[98] Y. Niu, W. Zhou, J. Sunarso, L. Ge, Z. Zhu, Z. Shao, High performance cobalt-free perovskite cathode for intermediate temperature solid oxide fuel cells, J. Mater. Chem. 20 (2010) 9619–9622. https://doi.org/10.1039/c0jm02816a.

[99] J.P. Hodges, S. Short, J.D. Jorgensen, X. Xiong, B. Dabrowski, S.M. Mini, C.W. Kimball, Evolution of oxygen-vacancy ordered crystal structures in the perovskite series $Sr_nFe_nO_{3n-1}$ (n = 2, 4, 8, and ∞), and the relationship to electronic and magnetic properties, J. Solid State Chem. 151 (2000) 190–209. https://doi.org/10.1006/jssc.1999.8640.

[100] V. V. Vashuk, L. V. Kokhanovskii, I.I. Yushkevich, Electrical conductivity and oxygen stoichiometry of $SrFeO_{3-\delta}$, Inorg. Mater. 36 (2000) 79–83. https://doi.org/10.1007/BF02758386.

[101] V. V. Bannikov, I.R. Shein, V.L. Kozhevnikov, A.L. Ivanovskii, Electronic structure and magnetic properties of double perovskites $Sr_2FeMO_6$ (M= Sc, Ti, ..., Ni, Cu) according to the data of FLAPW-GGA band structure calculations, J. Struct. Chem. 49 (2008) 781–787. https://doi.org/10.1007/s10947-008-0139-8.

[102] A.J. Fernández-Ropero, J.M. Porras-Vázquez, A. Cabeza, P.R. Slater, D. Marrero-López, E.R. Losilla, High valence transition metal doped strontium ferrites for electrode materials in symmetrical SOFCs, J. Power Sources. 249 (2014) 405–413. https://doi.org/10.1016/j.jpowsour.2013.10.118.

[103] G. Hong, T.W. Kim, M.J. Kwak, J. Song, Y. Choi, S.K. Woo, M.H. Han, C.H. Cho, S.D. Kim, Composite electrodes of Ti-doped $SrFeO_{3-\delta}$ and LSGMZ electrolytes as both the anode and cathode in symmetric solid oxide fuel cells, J. Alloys Compd. 846 (2020) 156154. https://doi.org/10.1016/j.jallcom.2020.156154.

[104] V. Zapata-Ramírez, G.C. Mather, M.T. Azcondo, U. Amador, D. Pérez-Coll, Electrical and electrochemical properties of the $Sr(Fe,Co,Mo)O_{3-\Delta}$ system as air electrode for reversible solid oxide cells, J. Power Sources. 437 (2019) 226895. https://doi.org/10.1016/j.jpowsour.2019.226895.

[105] A.D. Bamburov, B. V. Politov, Nd doping as a promising method to improve transport properties of $SrFe(Mo)O_{3-\delta}$ materials for symmetrical fuel cells and hydrogen production membranes, J. Solid State Chem. 296 (2021) 122012. https://doi.org/10.1016/j.jssc.2021.122012.

[106] O. V. Merkulov, A.A. Markov, M. V. Patrakeev, I.A. Leonidov, E. V. Shalaeva, A.P. Tyutyunnik, V.L. Kozhevnikov, Structural features and high-temperature transport in $SrFe_{0.7}Mo_{0.3}O_{3-\delta}$, J. Solid State Chem. 258

(2018) 447–452. https://doi.org/10.1016/j.jssc.2017.11.008.

[107] O. V. Merkulov, A.A. Markov, E.N. Naumovich, E. V. Shalaeva, I.A. Leonidov, M. V. Patrakeev, Non-uniform electron conduction in weakly ordered $SrFe_{1-x}Mo_xO_{3-\delta}$, Dalt. Trans. 48 (2019) 4530–4537. https://doi.org/10.1039/c9dt00461k.

[108] T. Su, Y. Li, Y. Yang, Z. Xu, N. Shi, Y. Wan, Y. Xie, D. Huan, S. Xue, C. Xia, Effect of tungsten doping on strontium ferrite electrode for symmetrical solid oxide electrochemical cell, Int. J. Hydrogen Energy. 45 (2020) 23401–23410. https://doi.org/10.1016/j.ijhydene.2020.06.111.

[109] Y. Cao, Z. Zhu, Y. Zhao, W. Zhao, Z. Wei, T. Liu, Development of tungsten stabilized $SrFe_{0.8}W_{0.2}O_{3-\delta}$ material as novel symmetrical electrode for solid oxide fuel cells, J. Power Sources. 455 (2020) 227951. https://doi.org/10.1016/j.jpowsour.2020.227951.

[110] L. Dos Santos-Gómez, J.M. Compana, S. Bruque, E.R. Losilla, D. Marrero-López, Symmetric electrodes for solid oxide fuel cells based on Zr-doped $SrFeO_{3-\delta}$, J. Power Sources. 279 (2015) 419–427. https://doi.org/10.1016/j.jpowsour.2015.01.043.

[111] K. Zheng, K. Świerczek, J.M. Polfus, M.F. Sunding, M. Pishahang, T. Norby, Carbon Deposition and Sulfur Poisoning in $SrFe_{0.75}Mo_{0.25}O_{3-\delta}$ and $SrFe_{0.5}Mn_{0.25}Mo_{0.25}O_{3-\delta}$ Electrode Materials for Symmetrical SOFCs, J. Electrochem. Soc. 162 (2015) F1078–F1087. https://doi.org/10.1149/2.0981509jes.

[112] W. He, J. Fan, H. Zhang, M. Chen, Z. Sun, M. Ni, Zr doped $BaFeO_{3-\delta}$ as a robust electrode for symmetrical solid oxide fuel cells, Int. J. Hydrogen Energy. 44 (2019) 32164–32169. https://doi.org/10.1016/j.ijhydene.2019.10.091.

[113] J.M. Porras-Vazquez, T. Pike, C.A. Hancock, J.F. Marco, F.J. Berry, P.R. Slater, Investigation into the effect of Si doping on the performance of $SrFeO_{3-\delta}$ SOFC electrode materials, J. Mater. Chem. A. 1 (2013) 11834–11841. https://doi.org/10.1039/c3ta12113e.

[114] A. Chroneos, R. V. Vovk, I.L. Goulatis, L.I. Goulatis, Oxygen transport in perovskite and related oxides: A brief review, J. Alloys Compd. 494 (2010) 190–195. https://doi.org/10.1016/j.jallcom.2010.01.071.

[115] S. (Rob) Hui, J. Roller, S. Yick, X. Zhang, C. Decès-Petit, Y. Xie, R. Maric, D. Ghosh, A brief review of the ionic conductivity enhancement for selected oxide electrolytes, J. Power Sources. 172 (2007) 493–502. https://doi.org/10.1016/j.jpowsour.2007.07.071.

[116] D. Tian, B. Lin, Y. Yang, Y. Chen, X. Lu, Z. Wang, W. Liu, E. Traversa, Enhanced performance of symmetrical solid oxide fuel cells using a doped ceria buffer layer, Electrochim. Acta. 208 (2016) 318–324. https://doi.org/10.1016/j.electacta.2016.04.189.

[117] W. Fan, Z. Sun, J. Wang, J. Zhou, K. Wu, Y. Cheng, A new family of Ce-doped $SmFeO_3$ perovskite for application in symmetrical solid oxide fuel cells, J. Power Sources. 312 (2016) 223–233. https://doi.org/10.1016/j.jpowsour.2016.02.069.

[118] K.-J. Lee, M.-J. Lee, S. Park, H.-J. Hwang, K.-J. Lee, M.-J. Lee, S. Park, H.-J. Hwang, Symmetrical Solid Oxide Electrolyzer Cells (SOECs) with $La_{0.6}Sr_{0.4}Co_{0.2}Fe_{0.8}O_3$ (LSCF)-Gadolinium Doped Ceria (GDC) Composite Electrodes, J. Korean Ceram. Soc. 53 (2016) 489–493. https://doi.org/10.4191/KCERS.2016.53.5.489.

[119] S. Park, H. Han, J. Choi, S. Lee, M. Park, W.B. Kim, Ruddlesden–Popper Oxide $(La_{0.6}Sr_{0.4})_2$ (Co,Fe)$O_4$ with

Exsolved CoFe Nanoparticles for a Solid Oxide Fuel Cell Anode Catalyst, Energy Technol. (2021) 2100116. https://doi.org/10.1002/ente.202100116.

[120] A. Kulkarni, F.T. Ciacchi, S. Giddey, C. Munnings, S.P.S. Badwal, J.A. Kimpton, D. Fini, Mixed ionic electronic conducting perovskite anode for direct carbon fuel cells, Int. J. Hydrogen Energy. 37 (2012) 19092–19102. https://doi.org/10.1016/j.ijhydene.2012.09.141.

[121] B. Niu, F. Jin, T. Feng, L. Zhang, Y. Zhang, T. He, A-site deficient $(La_{0.6}Sr_{0.4})_{1-x}Co_{0.2}Fe_{0.6}Nb_{0.2}O_{3-\delta}$ symmetrical electrode materials for solid oxide fuel cells, Elsevier Ltd, 2018. https://doi.org/10.1016/j.electacta.2018.03.085.

[122] X. Kong, X. Zhou, Y. Tian, X. Wu, J. Zhang, W. Zuo, Niobium doped lanthanum calcium ferrite perovskite as a novel electrode material for symmetrical solid oxide fuel cells, J. Power Sources. 326 (2016) 35–42. https://doi.org/10.1016/j.jpowsour.2016.06.111.

[123] X. Liu, E. Zhao, Z. Wang, K. Gao, Y. Xiong, Nanofiber-structured $Pr_{0.4}Sr_{0.6}Co_{0.2}Fe_{0.7}Nb_{0.1}O_{3-\delta}$-$Gd_{0.2}Ce_{0.8}O_{1.9}$ symmetrical composite electrode for solid oxide fuel cells, Ceram. Int. 43 (2017) 10960–10966. https://doi.org/10.1016/j.ceramint.2017.05.135.

[124] L. Bian, C. Liu, S. Li, J. Peng, X. Li, L. Guan, Y. Liu, J.H. Peng, S. An, X. Song, Highly stable $La_{0.5}Sr_{0.5}Fe_{0.9}Mo_{0.1}O_{3-\delta}$ electrode for reversible symmetric solid oxide cells, Int. J. Hydrogen Energy. 45 (2020) 19813–19822. https://doi.org/10.1016/j.ijhydene.2020.05.117.

[125] H. Cai, L. Zhang, J. Xu, J. Huang, X.L. Wei, L. Wang, Z. Song, W. Long, Cobalt–free $La_{0.5}Sr_{0.5}Fe_{0.9}Mo_{0.1}O_{3-\delta}$ electrode for symmetrical SOFC running on H2 and CO fuels, Electrochim. Acta. 320 (2019) 134642. https://doi.org/10.1016/j.electacta.2019.134642.

[126] C. Lu, B. Niu, S. Yu, W. Yi, S. Luo, B. Xu, Y. Ji, Efficient and stable symmetrical electrode $La_{0.6}Sr_{0.4}Co_{0.2}Fe_{0.7}Mo_{0.1}O_{3-\delta}$ for direct hydrocarbon solid oxide fuel cells, Electrochim. Acta. 323 (2019) 134857. https://doi.org/10.1016/j.electacta.2019.134857.

[127] S. Wang, B. Wei, Z. Lü, Electrochemical performance and distribution of relaxation times analysis of tungsten stabilized $La_{0.5}Sr_{0.5}Fe_{0.9}W_{0.1}O_{3-\delta}$ electrode for symmetric solid oxide fuel cells, Int. J. Hydrogen Energy. 46 (2021) 30101–30111. https://doi.org/10.1016/j.ijhydene.2021.06.140.

[128] Z. Yang, Y. Chen, C. Jin, G. Xiao, M. Han, F. Chen, $La_{0.7}Sr_{0.3}Fe_{0.7}Ga_{0.3}O_{3-\delta}$ as electrode material for a symmetrical solid oxide fuel cell, RSC Adv. 5 (2015) 2702–2705. https://doi.org/10.1039/c4ra11358f.

[129] X. Liu, D. Han, Y. Zhou, X. Meng, H. Wu, J. Li, F. Zeng, Z. Zhan, Sc-substituted $La_{0.6}Sr_{0.4}FeO_{3-\delta}$ mixed conducting oxides as promising electrodes for symmetrical solid oxide fuel cells, J. Power Sources. 246 (2014) 457–463. https://doi.org/10.1016/j.jpowsour.2013.07.111.

[130] X. Yang, R. Li, Y. Yang, G. Wen, D. Tian, X. Lu, Y. Ding, Y. Chen, B. Lin, Improving stability and electrochemical performance of $Ba_{0.5}Sr_{0.5}Co_{0.2}Fe_{0.8}O_{3-\delta}$ electrode for symmetrical solid oxide fuel cells by Mo doping, J. Alloys Compd. 831 (2020) 154711. https://doi.org/10.1016/j.jallcom.2020.154711.

[131] L. Ma, Y. Wang, W. Li, B. Guan, H. Qi, H. Tian, L. Zhou, H.A. De Santiago, X. Liu, Redox-stable symmetrical solid oxide fuel cells with exceptionally high performance enabled by electrode/electrolyte diffuse interface, J. Power Sources. 488 (2021) 229458. https://doi.org/10.1016/j.jpowsour.2021.229458.

[132] J.J. Alvarado Flores, M.L. Ávalos Rodríguez, G. Andrade Espinosa, J.V. Alcaraz Vera, Advances in the development of titanates for anodes in SOFC, Int. J. Hydrogen Energy. 44 (2019) 12529–12542. https://doi.org/10.1016/j.ijhydene.2018.05.171.

[133] Y. Li, J. Zhou, D. Dong, Y. Wang, J.Z. Jiang, H. Xiang, K. Xie, Composite fuel electrode $La_{0.2}Sr_{0.8}TiO_{3-\delta}$-$Ce_{0.8}Sm_{0.2}O_{2-\delta}$ for electrolysis of $CO_2$ in an oxygen-ion conducting solid oxide electrolyser, Phys. Chem. Chem. Phys. 14 (2012) 15547–15553. https://doi.org/10.1039/c2cp42232h.

[134] J. Canales-Vázquez, J.C. Ruiz-Morales, D. Marrero-López, J. Peña-Martínez, P. Núñez, P. Gómez-Romero, Fe-substituted (La,Sr)$TiO_3$ as potential electrodes for symmetrical fuel cells (SFCs), J. Power Sources. 171 (2007) 552–557. https://doi.org/10.1016/j.jpowsour.2007.05.094.

[135] J. Xu, X. Zhou, X. Dong, L. Pan, K. Sun, Catalytic activity improvement for efficient hydrogen oxidation of infiltrated $La_{0.3}Sr_{0.7}Ti_{0.3}Fe_{0.7}O_{3-\delta}$ anode for solid oxide fuel cell, Ceram. Int. 43 (2017) 10750–10756. https://doi.org/10.1016/j.ceramint.2017.05.081.

[136] J. Xu, X. Zhou, X. Dong, L. Pan, K. Sun, Catalytic activity of infiltrated $La_{0.3}Sr_{0.7}Ti_{0.3}Fe_{0.7}O_{3-\Delta}$–$CeO_2$ as a composite SOFC anode material for $H_2$ and CO oxidation, Int. J. Hydrogen Energy. 42 (2017) 15632–15640. https://doi.org/10.1016/j.ijhydene.2017.05.016.

[137] J. Xu, X. Zhou, J. Cheng, L. Pan, M. Wu, X. Dong, K. Sun, Electrochemical performance of highly active ceramic symmetrical electrode $La_{0.3}Sr_{0.7}Ti_{0.3}Fe_{0.7}O_{3-\delta}$-$CeO_2$ for reversible solid oxide cells, Electrochim. Acta. 257 (2017) 64–72. https://doi.org/10.1016/j.electacta.2017.10.061.

[138] F. Napolitano, D.G. Lamas, A. Soldati, A. Serquis, Synthesis and structural characterization of Co-doped lanthanum strontium titanates, Int. J. Hydrogen Energy. 37 (2012) 18302–18309. https://doi.org/10.1016/j.ijhydene.2012.09.052.

[139] F. Napolitano, A.L. Soldati, J. Geck, D.G. Lamas, A. Serquis, Electronic and structural properties of $La_{0.4}Sr_{0.6}Ti_{1-y}Co_yO_{3\pm\delta}$ electrode materials for symmetric SOFC studied by hard X-ray absorption spectroscopy, Int. J. Hydrogen Energy. 38 (2013) 8965–8973. https://doi.org/10.1016/j.ijhydene.2013.05.005.

[140] F. Napolitano, A. Soldati, J. Geck, L. Suescun, L. Acuna, A. Fernandez Zuvich, D.G. Lamas, A. Serquis, Characterization of (La,Sr)(Ti,Co)$O_3$ Oxides for Symmetrical Solid Oxide Fuel Cell Electrodes, ECS Trans. 58 (2013) 185–193. https://doi.org/10.1149/05803.0185ecst.

[141] R. Martínez-Coronado, A. Aguadero, D. Pérez-Coll, L. Troncoso, J.A. Alonso, M.T. Fernández-Díaz, Characterization of $La_{0.5}Sr_{0.5}Co_{0.5}Ti_{0.5}O_{3-\delta}$ as symmetrical electrode material for intermediate-temperature solid-oxide fuel cells, Int. J. Hydrogen Energy. 37 (2012) 18310–18318. https://doi.org/10.1016/j.ijhydene.2012.09.033.

[142] J. Li, T. Lv, N. Hou, P. Li, X. Yao, L. Fan, T. Gan, Y. Zhao, Y. Li, Molybdenum substitution at the B-site of lanthanum strontium titanate anodes for solid oxide fuel cells, Int. J. Hydrogen Energy. 42 (2017) 22294–22301. https://doi.org/10.1016/j.ijhydene.2017.03.189.

[143] A. Ovalle, J.C. Ruiz-Morales, J. Canales-Vázquez, D. Marrero-López, J.T.S. Irvine, Mn-substituted titanates as efficient anodes for direct methane SOFCs, Solid State Ionics. 177 (2006) 1997–2003. https://doi.org/10.1016/J.SSI.2006.06.014.

[144] W. Dong, A. Yaqub, N.K. Janjua, R. Raza, M. Afzal, B. Zhu, All in One Multifunctional Perovskite Material for Next Generation SOFC, Electrochim. Acta. 193 (2016) 225–230. https://doi.org/10.1016/j.electacta.2016.02.061.

[145] J. Zhang, K. Xie, Y. Zhang, L. Yang, G. Wu, Q. Qin, Y. Li, Y. Wu, Composite titanate cathode decorated with heterogeneous electrocatalytic sites towards efficient carbon dioxide electrolysis, RSC Adv. 4 (2014) 22697–22709. https://doi.org/10.1039/c4ra02984d.

[146] L. Bai, H. Li, Z. Yan, X. Hao, M. Ke, K. Xie, B. Li, New Insight into the Doped Strontium Titanate Cathode with In Situ Exsolved Nickel Nanoparticles for Electrolysis of Carbon Dioxide, Adv. Mater. Interfaces. 8 (2021) 2001598. https://doi.org/10.1002/admi.202001598.

[147] X. Yang, W. Sun, M. Ma, C. Xu, R. Ren, J. Qiao, Z. Wang, Z. Li, S. Zhen, K. Sun, Achieving Highly Efficient Carbon Dioxide Electrolysis by *In Situ* Construction of the Heterostructure, ACS Appl. Mater. Interfaces. 13 (2021) 20060–20069. https://doi.org/10.1021/acsami.1c02146.

[148] V. Kyriakou, D. Neagu, G. Zafeiropoulos, R.K. Sharma, C. Tang, K. Kousi, I.S. Metcalfe, M.C.M. Van De Sanden, M.N. Tsampas, Symmetrical Exsolution of Rh Nanoparticles in Solid Oxide Cells for Efficient Syngas Production from Greenhouse Gases, ACS Catal. 10 (2020) 1278–1288. https://doi.org/10.1021/acscatal.9b04424.

[149] L. dos Santos-Gómez, J.M. Porras-Vázquez, E.R. Losilla, D. Marrero-López, P.R. Slater, Investigation of $PO_4^{3-}$ oxyanion-doping on the properties of $CaFe_{0.4}Ti_{0.6}O_{3-\delta}$ for potential application as symmetrical electrodes for SOFCs, J. Alloys Compd. 835 (2020). https://doi.org/10.1016/j.jallcom.2020.155437.

[150] N. Dai, Z. Wang, T. Jiang, J. Feng, W. Sun, J. Qiao, D. Rooney, K. Sun, A new family of barium-doped $Sr_2Fe_{1.5}Mo_{0.5}O_{6-\delta}$ perovskites for application in intermediate temperature solid oxide fuel cells, J. Power Sources. 268 (2014) 176–182. https://doi.org/10.1016/J.JPOWSOUR.2014.05.146.

[151] M. Hou, W. Sun, P. Li, J. Feng, G. Yang, J. Qiao, Z. Wang, D. Rooney, J. Feng, K. Sun, Investigation into the effect of molybdenum-site substitution on the performance of $Sr_2Fe_{1.5}Mo_{0.5}O_{6-\delta}$ for intermediate temperature solid oxide fuel cells, J. Power Sources. 272 (2014) 759–765. https://doi.org/10.1016/J.JPOWSOUR.2014.09.043.

[152] Y. Yang, Y. Wang, Z. Yang, Z. Lei, C. Jin, Y. Liu, Y. Wang, S. Peng, Co-substituted $Sr_2Fe_{1.5}Mo_{0.5}O_{6-\delta}$ as anode materials for solid oxide fuel cells: Achieving high performance via nanoparticle exsolution, J. Power Sources. 438 (2019) 226989. https://doi.org/10.1016/J.JPOWSOUR.2019.226989.

[153] M. Gou, R. Ren, W. Sun, C. Xu, X. Meng, Z. Wang, J. Qiao, K. Sun, Nb-doped $Sr_2Fe_{1.5}Mo_{0.5}O_{6-\delta}$ electrode with enhanced stability and electrochemical performance for symmetrical solid oxide fuel cells, Ceram. Int. 45 (2019) 15696–15704. https://doi.org/10.1016/j.ceramint.2019.03.130.

[154] D.A. Osinkin, A.A. Kolchugin, N.M. Bogdanovich, S.M. Beresnev, Performance and redox stability of a double–layer $Sr_2Fe_{1.5}Mo_{0.5}O_{6-\delta}$ – based electrode for solid state electrochemical application, Electrochim. Acta. 361 (2020) 137058. https://doi.org/10.1016/j.electacta.2020.137058.

[155] D.A. Osinkin, S.M. Beresnev, N.I. Lobachevskaya, Symmetrical solid oxide fuel cell with strontium ferrite-molybdenum electrodes, Russ. J. Electrochem. 53 (2017) 665–669. https://doi.org/10.1134/S1023193517060131.

[156] D.A. Osinkin, Kinetics of CO oxidation and redox cycling of $Sr_2Fe_{1.5}Mo_{0.5}O_{6-\Delta}$ electrode for symmetrical solid state electrochemical devices, J. Power Sources. 418 (2019) 17–23.

https://doi.org/10.1016/j.jpowsour.2019.02.026.

[157] J. Liu, Y. Lei, Y. Li, J. Gao, D. Han, W. Zhan, F. Huang, S. Wang, Infiltrated $Sr_2Fe_{1.5}Mo_{0.5}O_6/La_{0.9}Sr_{0.1}Ga_{0.8}Mg_{0.2}O_3$ electrodes towards high performance symmetrical solid oxide fuel cells fabricated by an ultra-fast and time-saving procedure, Electrochem. Commun. 78 (2017) 6–10. https://doi.org/10.1016/j.elecom.2017.02.019.

[158] J. Gao, X. Meng, T. Luo, H. Wu, Z. Zhan, Symmetrical solid oxide fuel cells fabricated by phase inversion tape casting with impregnated $SrFe_{0.75}Mo_{0.25}O_{3-\Delta}$ (SFMO) electrodes, Int. J. Hydrogen Energy. 42 (2017) 18499–18503. https://doi.org/10.1016/j.ijhydene.2017.03.205.

[159] L. Bernadet, C. Moncasi, M. Torrell, A. Tarancón, High-performing electrolyte-supported symmetrical solid oxide electrolysis cells operating under steam electrolysis and co-electrolysis modes, Int. J. Hydrogen Energy. 45 (2020) 14208–14217. https://doi.org/10.1016/j.ijhydene.2020.03.144.

[160] Y. Song, Q. Zhong, W. Tan, C. Pan, Effect of cobalt-substitution $Sr_2Fe_{1.5-x}Co_xMo_{0.5}O_{6-\delta}$ for intermediate temperature symmetrical solid oxide fuel cells fed with $H_2$-$H_2S$, Electrochim. Acta. 139 (2014) 13–20. https://doi.org/10.1016/j.electacta.2014.07.022.

[161] Y. Yang, S. Li, Z. Yang, Y. Chen, P. Zhang, Y. Wang, F. Chen, S. Peng, One Step Synthesis of $Sr_2Fe_{1.3}Co_{0.2}Mo_{0.5}O_{6-\delta}$ -$Gd_{0.1}Ce_{0.9}O_{2-\delta}$ for Symmetrical Solid Oxide Fuel Cells, J. Electrochem. Soc. 167 (2020) 084503. https://doi.org/10.1149/1945-7111/ab8927.

[162] Y. Song, Q. Zhong, D. Wang, Y. Xu, W. Tan, Interaction between electrode materials $Sr_2FeCo_{0.5}Mo_{0.5}O_{6-\Delta}$ and hydrogen sulfide in symmetrical solid oxide fuel cells, Int. J. Hydrogen Energy. 42 (2017) 22266–22272. https://doi.org/10.1016/j.ijhydene.2017.04.216.

[163] T. Wei, Q. Zhang, Y.H. Huang, J.B. Goodenough, Cobalt-based double-perovskite symmetrical electrodes with low thermal expansion for solid oxide fuel cells, J. Mater. Chem. 22 (2012) 225–231. https://doi.org/10.1039/c1jm14756k.

[164] L. Dos Santos-Gómez, L. León-Reina, J.M. Porras-Vázquez, E.R. Losilla, D. Marrero-López, Chemical stability and compatibility of double perovskite anode materials for SOFCs, Solid State Ionics. 239 (2013) 1–7. https://doi.org/10.1016/J.SSI.2013.03.005.

[165] R. Fu, P. Jiang, H. Xu, B. Niu, F. Jiang, L. Yang, T. Feng, T. He, Performance of Pd-impregnated $Sr_{1.9}FeNb_{0.9}Mo_{0.1}O_{6-\delta}$ double perovskites as symmetrical electrodes for direct hydrocarbon solid oxide fuel cells, Int. J. Hydrogen Energy. 44 (2019) 31394–31405. https://doi.org/10.1016/j.ijhydene.2019.09.221.

[166] Z. Xu, X. Hu, Y. Wan, S. Xue, S. Zhang, L. Zhang, B. Zhang, C. Xia, Electrochemical performance and anode reaction process for Ca doped $Sr_2Fe_{1.5}Mo_{0.5}O_{6-\delta}$ as electrodes for symmetrical solid oxide fuel cells, Electrochim. Acta. 341 (2020). https://doi.org/10.1016/j.electacta.2020.136067.

[167] X. Peng, Y. Tian, Y. Liu, W. Wang, Jing chen, J. Li, B. Chi, J. Pu, J. Li, A double perovskite decorated carbon-tolerant redox electrode for symmetrical SOFC, Int. J. Hydrogen Energy. 45 (2020) 14461–14469. https://doi.org/10.1016/j.ijhydene.2020.03.151.

[168] P. Ding, W. Li, H. Zhao, C. Wu, L. Zhao, B. Dong, S. Wang, Review on Ruddlesden-Popper perovskites as cathode

for solid oxide fuel cells, JPhys Mater. 4 (2021) 22002. https://doi.org/10.1088/2515-7639/abe392.

[169] A.P. Tarutin, J.G. Lyagaeva, D.A. Medvedev, L. Bi, A.A. Yaremchenko, Recent advances in layered $Ln_2NiO_{4+\delta}$ nickelates: Fundamentals and prospects of their applications in protonic ceramic fuel and electrolysis cells, J. Mater. Chem. A. 9 (2021) 154–195. https://doi.org/10.1039/d0ta08132a.

[170] X. Xu, Y. Pan, Y. Zhong, R. Ran, Z. Shao, Ruddlesden–Popper perovskites in electrocatalysis, Mater. Horizons. 7 (2020) 2519–2565. https://doi.org/10.1039/D0MH00477D.

[171] J. Zhou, G. Chen, K. Wu, Y. Cheng, The performance of $La_{0.6}Sr_{1.4}MnO_4$ layered perovskite electrode material for intermediate temperature symmetrical solid oxide fuel cells, J. Power Sources. 270 (2014) 418–425. https://doi.org/10.1016/j.jpowsour.2014.06.163.

[172] M. V. Sandoval, C. Pirovano, E. Capoen, R. Jooris, F. Porcher, P. Roussel, G.H. Gauthier, In-depth study of the Ruddlesden-Popper $La_xSr_{2-x}MnO_{4\pm\Delta}$ family as possible electrode materials for symmetrical SOFC, Int. J. Hydrogen Energy. 42 (2017) 21930–21943. https://doi.org/10.1016/j.ijhydene.2017.07.062.

[173] M. V. Sandoval, C. Cardenas, E. Capoen, P. Roussel, C. Pirovano, G.H. Gauthier, Performance of $La_{0.5}Sr_{1.5}MnO_{4\pm\delta}$ Ruddlesden-Popper manganite as electrode material for symmetrical solid oxide fuel cells. Part B. the hydrogen oxidation reaction, Electrochim. Acta. 353 (2020) 1–10. https://doi.org/10.1016/j.electacta.2020.136494.

[174] M. V. Sandoval, C. Cárdenas, E. Capoen, C. Pirovano, P. Roussel, G.H. Gauthier, Performance of $La_{0.5}Sr_{1.5}$ $MnO_{4\pm\delta}$ Ruddlesden-Popper manganite as electrode material for symmetrical solid oxide fuel cells. Part A. The oxygen reduction reaction, Electrochim. Acta. 304 (2019) 415–427. https://doi.org/10.1016/j.electacta.2019.03.037.

[175] J. Shen, G. Yang, Z. Zhang, W. Zhou, W. Wang, Z. Shao, Tuning layer-structured $La_{0.6}Sr_{1.4}MnO_{4+\delta}$ into a promising electrode for intermediate-temperature symmetrical solid oxide fuel cells through surface modification, J. Mater. Chem. A. 4 (2016) 10641–10649. https://doi.org/10.1039/c6ta02986h.

[176] J. Shen, G. Yang, Z. Zhang, M.O. Tadé, W. Zhou, Z. Shao, Improved performance of a symmetrical solid oxide fuel cell by swapping the roles of doped ceria and $La_{0.6}Sr_{1.4}MnO_{4+\delta}$ in the electrode, J. Power Sources. 342 (2017) 644–651. https://doi.org/10.1016/j.jpowsour.2016.12.109.

[177] J. Zhou, Y. Chen, G. Chen, K. Wu, Y. Cheng, Evaluation of $La_xSr_{2-x}FeO_4$ layered perovskite as potential electrode materials for symmetrical solid oxide fuel cells, J. Alloys Compd. 647 (2015) 778–783. https://doi.org/10.1016/j.jallcom.2015.05.261.

[178] Y. Ling, T. Li, Y. Yang, Y. Tian, X. Wang, K. Chen, Oxygen vacancies-rich iron-based perovskite-like electrodes for symmetrical solid oxide fuel cells, Ceram. Int. 47 (2021) 12916–12925. https://doi.org/10.1016/j.ceramint.2021.01.154.

[179] S. Durán, N. Rangel, C. Silva, M.A. Macias, E. Capoen, C. Pirovano, A. Niemczyk, L. Suescun, P. Roussel, G.H. Gauthier, Study of $La_4BaCu_{5-x}Mn_xO_{13+\delta}$ materials as potential electrode for symmetrical-SOFC, Solid State Ionics. 341 (2019) 115031. https://doi.org/10.1016/j.ssi.2019.115031.

[180] J.H. Kim, A. Manthiram, Layered $LnBaCo_2O_{5+\delta}$ perovskite cathodes for solid oxide fuel cells: An overview and perspective, J. Mater. Chem. A. 3 (2015) 24195–24210. https://doi.org/10.1039/c5ta06212h.

[181] S. Sengodan, S. Choi, A. Jun, T.H. Shin, Y.W. Ju, H.Y. Jeong, J. Shin, J.T.S. Irvine, G. Kim, Layered oxygen-

deficient double perovskite as an efficient and stable anode for direct hydrocarbon solid oxide fuel cells, Nat. Mater. 14 (2015) 205–209. https://doi.org/10.1038/nmat4166.

[182] H. Ding, X. Xue, $BaZr_{0.1}Ce_{0.7}Y_{0.1}Yb_{0.1}O_{3-\delta}$ electrolyte-based solid oxide fuel cells with cobalt-free $PrBaFe_2O_{5+\delta}$ layered perovskite cathode, J. Power Sources. 195 (2010) 7038–7041. https://doi.org/10.1016/j.jpowsour.2010.05.010.

[183] Y. Kwon, S. Kang, J. Bae, Development of a $PrBaMn_2O_{5+\delta}$-$La_{0.8}Sr_{0.2}Ga_{0.85}Mg_{0.15}O_{3-\delta}$ composite electrode by scaffold infiltration for reversible solid oxide fuel cell applications, Int. J. Hydrogen Energy. 45 (2019) 1748–1758. https://doi.org/10.1016/j.ijhydene.2019.11.054.

[184] Y. Gu, Y. Zhang, Y. Zheng, H. Chen, L. Ge, L. Guo, $PrBaMn_2O_{5+\Delta}$ with praseodymium oxide nano-catalyst as electrode for symmetrical solid oxide fuel cells, Appl. Catal. B Environ. 257 (2019) 117868. https://doi.org/10.1016/j.apcatb.2019.117868.

[185] S. Choi, S. Sengodan, S. Park, Y.W. Ju, J. Kim, J. Hyodo, H.Y. Jeong, T. Ishihara, J. Shin, G. Kim, A robust symmetrical electrode with layered perovskite structure for direct hydrocarbon solid oxide fuel cells: $PrBa_{0.8}Ca_{0.2}Mn_2O_{5+\delta}$, J. Mater. Chem. A. 4 (2016) 1747–1753. https://doi.org/10.1039/c5ta08878j.

[186] Y. Chen, Z. Cheng, Y. Yang, Q. Gu, D. Tian, X. Lu, W. Yu, B. Lin, Novel quasi-symmetric solid oxide fuel cells with enhanced electrochemical performance, J. Power Sources. 310 (2016) 109–117. https://doi.org/10.1016/j.jpowsour.2016.02.013.

[187] H. Ding, S. Fang, Y. Yang, Y. Yang, W. Wu, Z. Tao, High-performing and stable electricity generation by ceramic fuel cells operating in dry methane over 1000 hours, J. Power Sources. 401 (2018) 322–328. https://doi.org/10.1016/J.JPOWSOUR.2018.08.084.

[188] B. Zhang, Y. Wan, Z. Hua, K. Tang, C. Xia, Tungsten-Doped $PrBaFe_2O_{5+\delta}$ Double Perovskite as a High-Performance Electrode Material for Symmetrical Solid Oxide Fuel Cells, ACS Appl. Energy Mater. 4 (2021) 8401–8409. https://doi.org/10.1021/ACSAEM.1C01618.

[189] W. He, X. Wu, F. Dong, M. Ni, A novel layered perovskite electrode for symmetrical solid oxide fuel cells: $PrBa(Fe_{0.8}Sc_{0.2})_2O_{5+\Delta}$, J. Power Sources. 363 (2017) 16–19. https://doi.org/10.1016/j.jpowsour.2017.07.059.

[190] J. Zhou, L. Xu, C. Ding, C. Wei, Z. Tao, Layered perovskite $(PrBa)_{0.95}(Fe_{0.9}Mo_{0.1})_2O_{5+\delta}$ as electrode materials for high-performing symmetrical solid oxide electrolysis cells, Mater. Lett. 257 (2019) 126758. https://doi.org/10.1016/j.matlet.2019.126758.

[191] Y. Zhang, B. Niu, X. Hao, Y. Wang, J. Liu, P. Jiang, T. He, Layered oxygen-deficient double perovskite $GdBaFe_2O_{5+\delta}$ as electrode material for symmetrical solid-oxide fuel cells, Electrochim. Acta. 370 (2021) 137807. https://doi.org/10.1016/j.electacta.2021.137807.

[192] Y. Zhang, B. Zhang, H. Zhao, K. Świerczek, Z. Du, Y. Li, L. Xu, H. Li, Electrochemical performance and structural durability of Mg-doped $SmBaMn_2O_{5+\delta}$ layered perovskite electrode for symmetrical solid oxide fuel cell, Catal. Today. (2020). https://doi.org/10.1016/j.cattod.2020.05.057.

[193] X. Sun, H. Chen, Y. Yin, M.T. Curnan, J.W. Han, Y. Chen, Z. Ma, Progress of Exsolved Metal Nanoparticles on Oxides as High Performance (Electro)Catalysts for the Conversion of Small Molecules, Small. 17 (2021) 2005383.

https://doi.org/10.1002/smll.202005383.

[194] T. Cao, O. Kwon, R.J. Gorte, J.M. Vohs, Metal Exsolution to Enhance the Catalytic Activity of Electrodes in Solid Oxide Fuel Cells, Nanomaterials. 10 (2020) 2445. https://doi.org/10.3390/nano10122445.

[195] C. Tang, K. Kousi, D. Neagu, I.S. Metcalfe, Trends and Prospects of Bimetallic Exsolution, Chem. – A Eur. J. 27 (2021) chem.202004950. https://doi.org/10.1002/chem.202004950.

[196] O. Kwon, S. Joo, S. Choi, S. Sengodan, G. Kim, Review on exsolution and its driving forces in perovskites, J. Phys. Energy. 2 (2020) 032001. https://doi.org/10.1088/2515-7655/ab8c1f.

[197] L. Thommy, O. Joubert, J. Hamon, M.T. Caldes, Impregnation versus exsolution: Using metal catalysts to improve electrocatalytic properties of LSCM-based anodes operating at 600 °C, Int. J. Hydrogen Energy. 41 (2016) 14207–14216. https://doi.org/10.1016/j.ijhydene.2016.06.088.

[198] S. Futamura, A. Muramoto, Y. Tachikawa, J. Matsuda, S.M. Lyth, Y. Shiratori, S. Taniguchi, K. Sasaki, SOFC anodes impregnated with noble metal catalyst nanoparticles for high fuel utilization, Int. J. Hydrogen Energy. 44 (2019) 8502–8518. https://doi.org/10.1016/j.ijhydene.2019.01.223.

[199] H. Su, Y.H. Hu, Progress in low-temperature solid oxide fuel cells with hydrocarbon fuels, Chem. Eng. J. 402 (2020) 126235. https://doi.org/10.1016/j.cej.2020.126235.

[200] N. Shi, Y. Xie, Y. Yang, S. Xue, X. Li, K. Zhu, D. Huan, R. Peng, C. Xia, Y. Lu, Review of anodic reactions in hydrocarbon fueled solid oxide fuel cells and strategies to improve anode performance and stability, Mater. Renew. Sustain. Energy. 9 (2020) 3. https://doi.org/10.1007/s40243-020-0166-8.

[201] T. Jardiel, M.T. Caldes, F. Moser, J. Hamon, G. Gauthier, O. Joubert, New SOFC electrode materials: The Ni-substituted LSCM-based compounds $(La_{0.75}Sr_{0.25})(Cr_{0.5}Mn_{0.5-x}Ni_x)O_{3-\delta}$ and (La0.75Sr0.25)(Cr0.5−xNixMn0.5)O3−δ, Solid State Ionics. 181 (2010) 894–901. https://doi.org/10.1016/j.ssi.2010.05.012.

[202] T. Delahaye, T. Jardiel, O. Joubert, R. Laucournet, G. Gauthier, M.T. Caldes, Electrochemical properties of novel SOFC dual electrode $La_{0.75}Sr_{0.25}Cr_{0.5}Mn_{0.3}Ni_{0.2}O_{3-\delta}$, Solid State Ionics. 184 (2011) 39–41. https://doi.org/10.1016/j.ssi.2010.10.015.

[203] Y. Tian, Y. Liu, L. Jia, A. Naden, J. Chen, B. Chi, J. Pu, J.T.S. Irvine, J. Li, A novel electrode with multifunction and regeneration for highly efficient and stable symmetrical solid oxide cell, J. Power Sources. 475 (2020) 228620. https://doi.org/10.1016/j.jpowsour.2020.228620.

[204] L. Bian, C. Duan, L. Wang, R. O'Hayre, J. Cheng, K.C. Chou, Ce-doped $La_{0.7}Sr_{0.3}Fe_{0.9}Ni_{0.1}O_{3-\delta}$ as symmetrical electrodes for high performance direct hydrocarbon solid oxide fuel cells, J. Mater. Chem. A. 5 (2017) 15253–15259. https://doi.org/10.1039/c7ta03001k.

[205] C. Arrivé, T. Delahaye, O. Joubert, G.H. Gauthier, Study of $(La,Sr)(Ti,Ni)O_{3-\delta}$ materials for symmetrical Solid Oxide Cell electrode - Part C: Electrical and electrochemical behavior, Ceram. Int. 46 (2020) 23442–23456. https://doi.org/10.1016/j.ceramint.2020.06.114.

[206] C. Arrivé, T. Delahaye, O. Joubert, G.H. Gauthier, Study of $(La,Sr)(Ti,Ni)O_{3-\delta}$ materials for symmetrical Solid Oxide Cell electrode - Part B: Conditions of Ni exsolution, Ceram. Int. 46 (2020) 5841–5849. https://doi.org/10.1016/j.ceramint.2019.11.034.

[207] M. Bilal Hanif, J.-T. Gao, K. Shaheen, Y.-P. Wang, M. Yasir, S. Zhang, C.-J. Li, C.-X. Li, Performance evaluation of highly active and novel $La_{0.7}Sr_{0.3}Ti_{0.1}Fe_{0.6}Ni_{0.3}O_{3-\delta}$ material both as cathode and anode for intermediate-temperature symmetrical solid oxide fuel cell, J. Power Sources. 472 (2020) 228498. https://doi.org/10.1016/j.jpowsour.2020.228498.

[208] O. Ben Mya, L. dos Santos-Gómez, J.M. Porras-Vázquez, M. Omari, J.R. Ramos-Barrado, D. Marrero-López, $La_{1-x}Sr_xFe_{0.7}Ni_{0.3}O_{3-\Delta}$ as both cathode and anode materials for Solid Oxide Fuel Cells, Int. J. Hydrogen Energy. 42 (2017) 23160–23169. https://doi.org/10.1016/j.ijhydene.2017.07.150.

[209] M. Bilal Hanif, J.T. Gao, K. Shaheen, Y.P. Wang, M. Yasir, C.J. Li, C.X. Li, Highly active and novel A-site deficient symmetric electrode material (Sr0.3La0.7)1−x (Fe0.7Ti0.3)0.9Ni0.1O3−δ and its effect on electrochemical performance of SOFCs, Int. J. Hydrogen Energy. 46 (2021) 8778–8791. https://doi.org/10.1016/J.IJHYDENE.2020.12.093.

[210] P.S. Barros Julião, A-site cation influences on performance, structure and conductivity of a lanthanide-based perovskite electrode for symmetrical solid oxide fuel cells, J. Power Sources. 450 (2020) 227723. https://doi.org/10.1016/j.jpowsour.2020.227723.

[211] D.A. Osinkin, E.P. Antonova, K.S. Shubin, N.M. Bogdanovich, Influence of nickel exsolution on the electrochemical performance and rate-determining stages of hydrogen oxidation on $Sr_{1.95}Fe_{1.4}Ni_{0.1}Mo_{0.5}O_{6-\delta}$ promising electrode for solid state electrochemical dev, Electrochim. Acta. 369 (2021). https://doi.org/10.1016/j.electacta.2020.137673.

[212] Z. Xu, Y. Li, Y. Wan, S. Zhang, C. Xia, Nickel enriched Ruddlesden-Popper type lanthanum strontium manganite as electrode for symmetrical solid oxide fuel cell, J. Power Sources. 425 (2019) 153–161. https://doi.org/10.1016/j.jpowsour.2019.04.005.

[213] Z. Yang, N. Xu, M. Han, F. Chen, Performance evaluation of $La_{0.4}Sr_{0.6}Co_{0.2}Fe_{0.7}Nb_{0.1}O_{3-\delta}$ as both anode and cathode material in solid oxide fuel cells, Int. J. Hydrogen Energy. 39 (2014) 7402–7406. https://doi.org/10.1016/j.ijhydene.2014.01.009.

[214] J. Song, T. Zhu, X. Chen, W. Ni, Q. Zhong, Cobalt and Titanium substituted $SrFeO_3$ based perovskite as efficient symmetrical electrode for solid oxide fuel cell, J. Mater. 6 (2020) 377–384. https://doi.org/10.1016/j.jmat.2020.02.009.

[215] C. Yang, Z. Yang, C. Jin, G. Xiao, F. Chen, M. Han, Sulfur-tolerant redox-reversible anode material for direct hydrocarbon solid oxide fuel cells, Adv. Mater. 24 (2012) 1439–1443. https://doi.org/10.1002/adma.201104852.

[216] P. Zhang, G. Guan, D.S. Khaerudini, X. Hao, M. Han, Y. Kasai, K. Sasagawa, A. Abudula, Properties of A-site nonstoichiometry $(Pr_{0.4})_xSr_{0.6}Co_{0.2}Fe_{0.7}Nb_{0.1}O_{3-\delta}$ ($0.9 \leq x \leq 1.1$) as symmetrical electrode material for solid oxide fuel cells, J. Power Sources. 248 (2014) 163–171. https://doi.org/10.1016/j.jpowsour.2013.09.077.

[217] J. Zhou, T.-H. Shin, C. Ni, G. Chen, K. Wu, Y. Cheng, J.T.S. Irvine, In Situ Growth of Nanoparticles in Layered Perovskite $La_{0.8}Sr_{1.2}Fe_{0.9}Co_{0.1}O_{4-\delta}$ as an Active and Stable Electrode for Symmetrical Solid Oxide Fuel Cells, Chem. Mater. 28 (2016) 2981–2993. https://doi.org/10.1021/acs.chemmater.6b00071.

[218] S. Zhou, Y. Yang, H. Chen, Y. Ling, In situ exsolved Co–Fe nanoparticles on the Ruddlesden-Popper-type

symmetric electrodes for intermediate temperature solid oxide fuel cells, Ceram. Int. 46 (2020) 18331–18338. https://doi.org/10.1016/j.ceramint.2020.05.057.

[219] Y.S. Chung, T. Kim, T.H. Shin, H. Yoon, S. Park, N.M. Sammes, W.B. Kim, J.S. Chung, In situ preparation of a $La_{1.2}Sr_{0.8}Mn_{0.4}Fe_{0.6}O_4$ Ruddlesden-Popper phase with exsolved Fe nanoparticles as an anode for SOFCs, J. Mater. Chem. A. 5 (2017) 6437–6446. https://doi.org/10.1039/c6ta09692a.

[220] B. Niu, C. Lu, W. Yi, S. Luo, X. Li, X. Zhong, X. Zhao, B. Xu, In-situ growth of nanoparticles-decorated double perovskite electrode materials for symmetrical solid oxide cells, Appl. Catal. B Environ. 270 (2020) 118842. https://doi.org/10.1016/j.apcatb.2020.118842.

[221] M.K. Rath, A. Kossenko, M. Zinigrad, A. Kalashnikov, In-operando gas switching to suppress the degradation of symmetrical solid oxide fuel cells, J. Power Sources. 476 (2020) 228630. https://doi.org/10.1016/j.jpowsour.2020.228630.

[222] J. Wang, J. Zhou, J. Yang, Z. Zong, L. Fu, Z. Lian, X. Zhang, X. Wang, C. Chen, W. Ma, K. Wu, Nanoscale architecture of $(La_{0.6}Sr_{1.4})_{0.95}Mn_{0.9}B_{0.1}O_4$ (B= Co, Ni, Cu) Ruddlesden–Popper oxides as efficient and durable catalysts for symmetrical solid oxide fuel cells, Renew. Energy. 157 (2020) 840–850. https://doi.org/10.1016/j.renene.2020.05.014.

[223] W. Kobsiriphat, B.D. Madsen, Y. Wang, M. Shah, L.D. Marks, S.A. Barnett, Nickel- and Ruthenium-Doped Lanthanum Chromite Anodes: Effects of Nanoscale Metal Precipitation on Solid Oxide Fuel Cell Performance, J. Electrochem. Soc. 157 (2010) B279. https://doi.org/10.1149/1.3269993.

[224] R. Glaser, T. Zhu, H. Troiani, A. Caneiro, L. Mogni, S. Barnett, The enhanced electrochemical response of $Sr(Ti_{0.3}Fe_{0.7}Ru_{0.07})O_{3-\delta}$ anodes due to exsolved Ru-Fe nanoparticles, J. Mater. Chem. A. 6 (2018) 5193–5201. https://doi.org/10.1039/c7ta10762e.

[225] B. Li, S. He, J. Li, X. Yue, J.T.S. Irvine, D. Xie, J. Ni, C. Ni, A Ce/Ru codoped $SrFeO_{3-\delta}$ perovskite for a coke-resistant anode of a symmetrical solid oxide fuel cell, ACS Catal. 10 (2020) 14398–14409. https://doi.org/10.1021/acscatal.0c03554.

[226] J. Zhou, N. Wang, J. Cui, J. Wang, J. Yang, Z. Zong, Z. Zhang, Q. Chen, X. Zheng, K. Wu, Structural and electrochemical properties of B-site Ru-doped $(La_{0.8}Sr_{0.2})_{0.9}Sc_{0.2}Mn_{0.8}O_{3-\delta}$ as symmetrical electrodes for reversible solid oxide cells, J. Alloys Compd. 792 (2019) 1132–1140. https://doi.org/10.1016/j.jallcom.2019.04.103.

[227] W. Fan, Z. Sun, J. Zhou, K. Wu, Y. Cheng, Characterization of Sr/Ru co-doped ferrite based perovskite as a symmetrical electrode material for solid oxide fuel cells, J. Power Sources. 348 (2017) 94–106. https://doi.org/10.1016/j.jpowsour.2017.02.090.

[228] W. Fan, Z. Sun, Y. Bai, K. Wu, J. Zhou, Y. Cheng, In situ growth of nanoparticles in A-site deficient ferrite perovskite as an advanced electrode for symmetrical solid oxide fuel cells, J. Power Sources. 456 (2020) 228000. https://doi.org/10.1016/j.jpowsour.2020.228000.

[229] A. Marcucci, F. Zurlo, I.N. Sora, E. Placidi, S. Casciardi, S. Licoccia, E. Di Bartolomeo, A redox stable Pd-doped perovskite for SOFC applications, J. Mater. Chem. A. 7 (2019) 5344–5352. https://doi.org/10.1039/c8ta10645b.

[230] Z. Ma, C. Sun, C. Ma, H. Wu, Z. Zhan, L. Chen, Ni doped $La_{0.6}Sr_{0.4}FeO_{3-\delta}$ symmetrical electrode for solid oxide

fuel cells, Cuihua Xuebao/Chinese J. Catal. 37 (2016) 1347–1353. https://doi.org/10.1016/S1872-2067(15)61116-0.

[231] J. Wang, L. Fu, J. Yang, K. Wu, J. Zhou, K. Wu, Cerium and ruthenium co-doped $La_{0.7}Sr_{0.3}FeO_{3-\delta}$ as a high-efficiency electrode for symmetrical solid oxide fuel cell, J. Rare Earths. (2021). https://doi.org/10.1016/j.jre.2021.01.009.

[232] J. Shen, Y. Chen, G. Yang, W. Zhou, M.O. Tadé, Z. Shao, Impregnated $LaCo_{0.3}Fe_{0.67}Pd_{0.03}O_{3-\delta}$ as a promising electrocatalyst for "symmetrical" intermediate-temperature solid oxide fuel cells, J. Power Sources. 306 (2016) 92–99. https://doi.org/10.1016/j.jpowsour.2015.12.021.

[233] Y. Tao, Y. Zhou, W. Li, J. Shao, L. Bai, X. Liu, Intermediate-temperature solid oxide fuel cells with high performance cobalt-doped $Pr_{0.5}Ba_{0.5}FeO_{3-\delta}$ anodes, J. Alloys Compd. 741 (2018) 1091–1097. https://doi.org/10.1016/j.jallcom.2018.01.167.

[234] L. Zhu, B. Wei, Y. Zhang, Z. Lü, Z. Wang, X. Huang, Z. Cao, W. Jiang, Y. Li, Investigation on a novel composite solid oxide fuel cell anode with $La_{0.6}Sr_{0.4}Co_{0.2}Fe_{0.8}O_{3-\delta}$ derived phases, Electrochim. Acta. 160 (2015) 89–93. https://doi.org/10.1016/j.electacta.2015.02.024.

[235] Y. Zheng, T. Guo, Y. Wu, Y. Yang, S. Zhang, X. Ou, Y. Ling, Ni–$La_2O_3$ cermet hydrogen electrode originating from the in-situ decomposition of the $La_2NiO_{4+\delta}$ oxide for quasi-symmetrical solid oxide fuel cells, Int. J. Hydrogen Energy. 45 (2020) 27764–27771. https://doi.org/10.1016/j.ijhydene.2020.07.151.

[236] P. Zhang, G. Guan, D.S. Khaerudini, X. Hao, C. Xue, M. Han, Y. Kasai, A. Abudula, B-site Mo-doped perovskite $Pr_{0.4}Sr_{0.6}$ $(Co_{0.2}Fe_{0.8})_{1-x}Mo_xO_{3-\sigma}$ (x = 0, 0.05, 0.1 and 0.2) as electrode for symmetrical solid oxide fuel cell, J. Power Sources. 276 (2015) 347–356. https://doi.org/10.1016/j.jpowsour.2014.11.141.

[237] X. Lu, Y. Yang, Y. Ding, Y. Chen, Q. Gu, D. Tian, W. Yu, B. Lin, Mo-doped $Pr_{0.6}Sr_{0.4}Fe_{0.8}Ni_{0.2}O_{3-\delta}$ as potential electrodes for intermediate-temperature symmetrical solid oxide fuel cells, Electrochim. Acta. 227 (2017) 33–40. https://doi.org/10.1016/j.electacta.2016.12.170.

[238] X. Zhao, X. Yang, D. Tian, X. Lu, Y. Ding, Y. Chen, H. Li, Tailoring an interstitial oxygen conducting electrode by in situ fabrication for quasi-symmetrical solid oxide fuel cells, Ionics (Kiel). 27 (2021) 259–268. https://doi.org/10.1007/s11581-020-03790-4.

[239] Y. Yang, Y. Wu, H. Bao, W. Song, H. Ni, D. Tian, B. Lin, P. Feng, Y. Ling, An efficient and prospective self-assembled hybrid electrocatalyst for symmetrical and reversible solid oxide cells, Electrochim. Acta. 362 (2020) 137171. https://doi.org/10.1016/j.electacta.2020.137171.

[240] H. Tao, J. Xie, Y. Wu, S. Wang, Evaluation of $PrNi_{0.4}Fe_{0.6}O_{3-\Delta}$ as a symmetrical SOFC electrode material, Int. J. Hydrogen Energy. 43 (2018) 15423–15432. https://doi.org/10.1016/j.ijhydene.2018.06.047.

[241] J. Lu, Y.M. Yin, J. Li, L. Xu, Z.F. Ma, A cobalt-free electrode material $La_{0.5}Sr_{0.5}Fe_{0.8}Cu_{0.2}O_{3-\delta}$ for symmetrical solid oxide fuel cells, Electrochem. Commun. 61 (2015) 18–22. https://doi.org/10.1016/j.elecom.2015.09.020.

[242] L. dos Santos-Gómez, J. Hurtado, J.M. Porras-Vázquez, E.R. Losilla, D. Marrero-López, Durability and performance of CGO barriers and LSCF cathode deposited by spray-pyrolysis, J. Eur. Ceram. Soc. 38 (2018) 3518–3526. https://doi.org/10.1016/J.JEURCERAMSOC.2018.03.024.

[243] Z. Gao, X. Ding, D. Ding, L. Ding, S. Zhang, G. Yuan, Infiltrated $Pr_2NiO_4$ as promising bi-electrode for symmetrical solid oxide fuel cells, Int. J. Hydrogen Energy. 43 (2018) 8953–8961. https://doi.org/10.1016/j.ijhydene.2018.03.164.

[244] G. Chen, W. Sun, Y. Luo, H. Liu, S. Geng, K. Yu, G. Liu, Investigation of layered $Ni_{0.8}Co_{0.15}Al_{0.05}LiO_2$ in electrode for low-temperature solid oxide fuel cells, Int. J. Hydrogen Energy. 43 (2018) 417–425. https://doi.org/10.1016/j.ijhydene.2017.11.056.

[245] L. Zhang, S. Tao, An intermediate temperature solid oxide fuel cell fabricated by one step co-press-sintering, Int. J. Hydrogen Energy. 36 (2011) 14643–14647. https://doi.org/10.1016/j.ijhydene.2011.08.054.

[246] R. Raza, Q. Liu, J. Nisar, X. Wang, Y. Ma, B. Zhu, ZnO/NiO nanocomposite electrodes for low-temperature solid oxide fuel cells, Electrochem. Commun. 13 (2011) 917–920. https://doi.org/10.1016/j.elecom.2011.05.032.

[247] L. Fan, H. Zhang, M. Chen, C. Wang, H. Wang, M. Singh, B. Zhu, Electrochemical study of lithiated transition metal oxide composite as symmetrical electrode for low temperature ceramic fuel cells, Int. J. Hydrogen Energy. 38 (2013) 11398–11405. https://doi.org/10.1016/j.ijhydene.2013.06.050.

[248] Y. Chen, Z. Cheng, Y. Yang, W. Yu, D. Tian, X. Lu, Y. Ding, B. Lin, Improved performance of symmetrical solid oxide fuel cells with redox-reversible cermet electrodes, Mater. Lett. 188 (2017) 413–416. https://doi.org/10.1016/j.matlet.2016.11.074.

[249] K.D. Kreuer, Proton conductivity: Materials and applications, Chem. Mater. 8 (1996) 610–641. https://doi.org/10.1021/cm950192a.

[250] S. Choi, C.J. Kucharczyk, Y. Liang, X. Zhang, I. Takeuchi, H. Il Ji, S.M. Haile, Exceptional power density and stability at intermediate temperatures in protonic ceramic fuel cells, Nat. Energy. 3 (2018) 202–210. https://doi.org/10.1038/s41560-017-0085-9.

[251] H. Ding, W. Wu, C. Jiang, Y. Ding, W. Bian, B. Hu, P. Singh, C.J. Orme, L. Wang, Y. Zhang, D. Ding, Self-sustainable protonic ceramic electrochemical cells using a triple conducting electrode for hydrogen and power production, Nat. Commun. 11 (2020) 1–11. https://doi.org/10.1038/s41467-020-15677-z.

[252] C. Duan, R.J. Kee, H. Zhu, C. Karakaya, Y. Chen, S. Ricote, A. Jarry, E.J. Crumlin, D. Hook, R. Braun, N.P. Sullivan, R. O'Hayre, Highly durable, coking and sulfur tolerant, fuel-flexible protonic ceramic fuel cells, Nature. 557 (2018) 217–222. https://doi.org/10.1038/s41586-018-0082-6.

[253] J. Li, J. Hou, X. Xi, Y. Lu, M. Li, Y. Fan, L. Wang, L. Wang, X.Z. Fu, J.L. Luo, Cogeneration of ethylene and electricity in symmetrical protonic solid oxide fuel cells based on a $La_{0.6}Sr_{0.4}Fe_{0.8}Nb_{0.1}Cu_{0.1}O_{3-\delta}$ electrode, J. Mater. Chem. A. 8 (2020) 25978–25985. https://doi.org/10.1039/d0ta08974e.

[254] S. Liu, Q. Liu, X.Z. Fu, J.L. Luo, Cogeneration of ethylene and energy in protonic fuel cell with an efficient and stable anode anchored with in-situ exsolved functional metal nanoparticles, Appl. Catal. B Environ. 220 (2018) 283–289. https://doi.org/10.1016/j.apcatb.2017.08.051.

[255] L.R. Tarutina, J.G. Lyagaeva, A.S. Farlenkov, A.I. Vylkov, G.K. Vdovin, A.A. Murashkina, A.K. Demin, D.A. Medvedev, Doped (Nd,Ba)$FeO_3$ oxides as potential electrodes for symmetrically designed protonic ceramic electrochemical cells, J. Solid State Electrochem. 24 (2020) 1453–1462. https://doi.org/10.1007/s10008-020-

04522-4.

[256] L. Fu, J. Zhou, J. Yang, Z. Lian, J. Wang, Y. Cheng, K. Wu, Exsolution of Cu nanoparticles in $(LaSr)_{0.9}Fe_{0.9}Cu_{0.1}O_4$ Ruddlesden-Popper oxide as symmetrical electrode for solid oxide cells, Appl. Surf. Sci. 511 (2020) 145525. https://doi.org/10.1016/j.apsusc.2020.145525.

[257] D. Kim, S.J. Son, M. Kim, H.J. Park, J.H. Joo, $PrBaFe_2O_{5+\delta}$ promising electrode for redox-stable symmetrical proton-conducting solid oxide fuel cells, J. Eur. Ceram. Soc. 41 (2021) 5939–5946. https://doi.org/10.1016/j.jeurceramsoc.2021.05.031.

[258] W. Skubida, K. Zheng, A. Stępień, K. Świerczek, A. Klimkowicz, $SrCe_{0.9}In_{0.1}O_{3-\delta}$-based reversible symmetrical Protonic Ceramic Cell, Mater. Res. Bull. 135 (2021). https://doi.org/10.1016/j.materresbull.2020.111154.

[259] A. Tarutin, J. Lyagaeva, A. Farlenkov, S. Plaksin, G. Vdovin, A. Demin, D. Medvedev, A reversible protonic ceramic cell with symmetrically designed $Pr_2NiO_{4+\delta}$-based electrodes: Fabrication and electrochemical features, Materials (Basel). 12 (2019) 1–21. https://doi.org/10.3390/ma12010118.

[260] Y. Yu, L. Yu, K. Shao, Y. Li, K. Maliutina, W. Yuan, Q. Wu, L. Fan, $BaZr_{0.1}Co_{0.4}Fe_{0.4}Y_{0.1}O_3$-SDC composite as quasi-symmetrical electrode for proton conducting solid oxide fuel cells, Ceram. Int. 46 (2020) 11811–11818. https://doi.org/10.1016/j.ceramint.2020.01.215.

[261] M. Zhong, K. Tran, Y. Min, C. Wang, Z. Wang, C.T. Dinh, P. De Luna, Z. Yu, A.S. Rasouli, P. Brodersen, S. Sun, O. Voznyy, C.S. Tan, M. Askerka, F. Che, M. Liu, A. Seifitokaldani, Y. Pang, S.C. Lo, A. Ip, Z. Ulissi, E.H. Sargent, Accelerated discovery of $CO_2$ electrocatalysts using active machine learning, Nature. 581 (2020) 178–183. https://doi.org/10.1038/s41586-020-2242-8.

[262] L. Zhang, S. Hu, X. Zhu, W. Yang, Electrochemical reduction of $CO_2$ in solid oxide electrolysis cells, J. Energy Chem. 26 (2017) 593–601. https://doi.org/10.1016/j.jechem.2017.04.004.

[263] S. Xu, S. Li, W. Yao, D. Dong, K. Xie, Direct electrolysis of $CO_2$ using an oxygen-ion conducting solid oxide electrolyzer based on $La_{0.75}Sr_{0.25}Cr_{0.5}Mn_{0.5}O_{3-\delta}$ electrode, J. Power Sources. 230 (2013) 115–121. https://doi.org/10.1016/j.jpowsour.2012.12.068.

[264] L. Gan, L. Ye, S. Wang, M. Liu, S. Tao, K. Xie, Demonstration of direct conversion of $CO_2/H_2O$ into syngas in a symmetrical proton-conducting solid oxide electrolyzer, Int. J. Hydrogen Energy. 41 (2016) 1170–1175. https://doi.org/10.1016/j.ijhydene.2015.11.032.

[265] P.K. Addo, B. Molero-Sanchez, M. Chen, S. Paulson, V. Birss, $CO/CO_2$ study of high performance $La_{0.3}Sr_{0.7}Fe_{0.7}Cr_{0.3}O_{3-\delta}$ reversible SOFC electrodes, Fuel Cells. 15 (2015) 689–696. https://doi.org/10.1002/fuce.201400196.

[266] Y. Tian, Y. Liu, A. Naden, L. Jia, M. Xu, W. Cui, B. Chi, J. Pu, J.T.S. Irvine, J. Li, Boosting $CO_2$ electrolysis performance via calcium-oxide-looping combined with in situ exsolved Ni-Fe nanoparticles in a symmetrical solid oxide electrolysis cell, J. Mater. Chem. A. 8 (2020). https://doi.org/10.1039/d0ta05518b.

[267] Y. Tian, H. Zheng, L. Zhang, B. Chi, J. Pu, J. Li, Direct Electrolysis of $CO_2$ in Symmetrical Solid Oxide Electrolysis Cell Based on $La_{0.6}Sr_{0.4}Fe_{0.8}Ni_{0.2}O_{3-\delta}$ Electrode, J. Electrochem. Soc. 165 (2018) F17–F23. https://doi.org/10.1149/2.0351802jes.

[268] Y. Tian, L. Zhang, L. Jia, X. Wang, J. Yang, B. Chi, J. Pu, J. Li, Novel quasi-symmetrical solid oxide electrolysis cells with in-situ exsolved cathode for $CO_2$ electrolysis, J. CO2 Util. 31 (2019) 43–50. https://doi.org/10.1016/j.jcou.2019.02.017.

[269] L. Bian, C. Duan, L. Wang, Y. Hou, L. Zhu, R. O'Hayre, K.-C. Chou, Highly Efficient, Redox-Stable, $La_{0.5}Sr_{0.5}Fe_{0.9}Nb_{0.1}O_{3-\delta}$ Symmetric Electrode for Both Solid-Oxide Fuel Cell and $H_2O/CO_2$ Co-Electrolysis Operation, J. Electrochem. Soc. 165 (2018) F981–F985. https://doi.org/10.1149/2.0961811jes.

[270] Z. Yang, C. Ma, N. Wang, X. Jin, C. Jin, S. Peng, Electrochemical reduction of $CO_2$ in a symmetrical solid oxide electrolysis cell with $La_{0.4}Sr_{0.6}Co_{0.2}Fe_{0.7}Nb_{0.1}O_{3-\delta}$ electrode, J. CO2 Util. 33 (2019) 445–451. https://doi.org/10.1016/j.jcou.2019.07.021.

[271] H. Lv, T. Liu, X. Zhang, Y. Song, H. Matsumoto, N. Ta, C. Zeng, G. Wang, X. Bao, Atomic-Scale Insight into Exsolution of CoFe Alloy Nanoparticles in $La_{0.4}Sr_{0.6}Co_{0.2}Fe_{0.7}Mo_{0.1}O_{3-\delta}$ with Efficient $CO_2$ Electrolysis, Angew. Chemie - Int. Ed. 59 (2020) 15968–15973. https://doi.org/10.1002/anie.202006536.

[272] Z. Yang, N. Wang, C. Ma, X. Jin, Z. Lei, X. Xiong, S. Peng, Co-electrolysis of $H_2O$-$CO_2$ in a solid oxide electrolysis cell with symmetrical $La_{0.4}Sr_{0.6}Co_{0.2}Fe_{0.7}Nb_{0.1}O_{3-\delta}$ electrode, J. Electroanal. Chem. 836 (2019) 107–111. https://doi.org/10.1016/j.jelechem.2019.01.064.

[273] Z. Huang, H. Qi, Z. Zhao, L. Shang, B. Tu, M. Cheng, Efficient $CO_2$ electroreduction on a solid oxide electrolysis cell with $La_{0.6}Sr_{0.4}Co_{0.2}Fe_{0.8}O_{3-\Delta}$-$Gd_{0.2}Ce_{0.8}O_{2-\Delta}$ infiltrated electrode, J. Power Sources. 434 (2019) 226730. https://doi.org/10.1016/j.jpowsour.2019.226730.

[274] X. Peng, Y. Tian, Y. Liu, W. Wang, L. Jia, J. Pu, B. Chi, J. Li, An efficient symmetrical solid oxide electrolysis cell with LSFM-based electrodes for direct electrolysis of pure $CO_2$, J. CO2 Util. 36 (2020) 18–24. https://doi.org/10.1016/j.jcou.2019.10.017.

[275] Z. Cao, B. Wei, J. Miao, Z. Wang, Z. Lü, W. Li, Y. Zhang, X. Huang, X. Zhu, Q. Feng, Y. Sui, Efficient electrolysis of $CO_2$ in symmetrical solid oxide electrolysis cell with highly active $La_{0.3}Sr_{0.7}Fe_{0.7}Ti_{0.3}O_3$ electrode material, Electrochem. Commun. 69 (2016) 80–83. https://doi.org/10.1016/j.elecom.2016.06.008.

[276] Y. Li, S. Zou, J. Ju, C. Xia, Characteristics of nano-structured SFM infiltrated onto YSZ backbone for symmetrical and reversible solid oxide cells, Solid State Ionics. 319 (2018) 98–104. https://doi.org/10.1016/j.ssi.2018.02.003.

[277] Y. Wang, T. Liu, S. Fang, F. Chen, Syngas production on a symmetrical solid oxide $H_2O/CO_2$ co-electrolysis cell with $Sr_2Fe_{1.5}Mo_{0.5}O_6$-$Sm_{0.2}Ce_{0.8}O_{1.9}$ electrodes, J. Power Sources. 305 (2016) 240–248. https://doi.org/10.1016/j.jpowsour.2015.11.097.

[278] S. Hou, K. Xie, Enhancing the performance of high-temperature $H_2O/CO_2$ co-electrolysis process on the solid oxide $Sr_2Fe_{1.6}Mo_{0.5}O_{6-\delta}$-SDC/LSGM/$Sr_2Fe_{1.5}Mo_{0.5}O_{6-\delta}$-SDC, Electrochim. Acta. 301 (2019) 63–68. https://doi.org/10.1016/j.electacta.2019.01.164.

[279] Y. Li, Z. Zhan, C. Xia, Highly efficient electrolysis of pure $CO_2$ with symmetrical nanostructured perovskite electrodes, Catal. Sci. Technol. 8 (2018) 980–984. https://doi.org/10.1039/c7cy02324c.

[280] D. Huan, L. Zhang, S. Zhang, N. Shi, X. Li, K. Zhu, C. Xia, R. Peng, Y. Lu, Ruddlesden-Popper oxide $SrEu_2Fe_2O_7$as a promising symmetrical electrode for pure $CO_2$ electrolysis, J. Mater. Chem. A. 9 (2021) 2706–

2713. https://doi.org/10.1039/d0ta09585k.

[281] L. Zhang, Y. Tian, Y. Liu, L. Jia, J. Yang, B. Chi, J. Pu, J. Li, Direct Electrolysis of $CO_2$ in a Symmetrical Solid Oxide Electrolysis Cell with Spinel $MnCo_2O_4$ as Electrode, ChemElectroChem. 6 (2019) 1359–1364. https://doi.org/10.1002/celc.201801831.